69-19,326

PARK, James Edward, 1935-

A NUMERICAL METHOD OF SOLUTION FOR THE EQUATIONS DESCRIBING THE COMPRESSIBLE, TURBULENT, TIME-DEPENDENT FLOW OF AN IDEAL GAS NEAR A SOLID BOUNDARY.

Rice University, Ph.D., 1969
Engineering, aeronautical

University Microfilms, Inc., Ann Arbor, Michigan

RICE UNIVERSITY

A NUMERICAL METHOD OF SOLUTION FOR THE EQUATIONS DESCRIBING THE COMPRESSIBLE, TURBULENT, TIME-DEPENDENT FLOW OF AN IDEAL GAS NEAR A SOLID BOUNDARY

by

James E. Park

A THESIS SUBMITTED
IN PARTIAL FULFILLMENT OF THE
REQUIREMENTS FOR THE DEGREE OF

DOCTOR OF PHILOSOPHY

Thesis Director's signature:

William F. Walker

Houston, Texas

April, 1969

To Cynthia

ACKNOWLEDGMENTS

It is a paradox of post graduate studies that the independent research performed by an individual student is absolutely dependent on the support, interest and encouragement of so many other people. The debt of this author to several of those people is acknowledged in this section.

The financial support of the Department of Mechanical and Aerospace Engineering and Materials Science, under the chairmanship of Professor A. J. Chapman, was essential during several years of graduate study. In addition, individual grants were made available by Professors F. A. Wierum, J. B. Cheatham and W. F. Walker. Each of these expressions of confidence was and is greatly appreciated by the author.

The generosity of Dr. Kenneth Weston, of the NASA Manned Spacecraft Center*, in arranging for the author to use that installation's computer facility should be recognized.

The continuous patience and confidence of Mr. L. L. Anthony and Mr. N. H. Van Wie, manager and assistant manager respectively of the Applied Science Department of the Computing Technology Center**, have been a source of reassurance and determination for the author during the final months of this research.

---

*Current address: University of Tulsa, Tulsa, Oklahoma.

**Operated for the U.S. Atomic Energy Commission by Union Carbide Nuclear Division, Oak Ridge, Tennessee.

The performances of Miss Margaret Poole, who typed the most difficult equations in perfect fashion, and Mrs. Sarah Sparks, who typed the final form of this work under the pressure of a deadline, are gratefully recognized.

Professors A. J. Chapman and G. D. Fisher are due thanks for serving on the advisory committee for this thesis.

The thanks owed to Professor W. F. Walker, thesis director for this research, cannot be overstated. His financial and moral support, his physical insight and judgment, and his perspective and sense of humor have contributed immeasurably to this work.

NOMENCLATURE

a	Streamwise component of fluid momentum, appendix D
A	Constant in model for effective viscosity, chapter III
A,B,C,D	Coefficients used in stability analysis, appendix F
A,B,C	Fitted coefficients for extrapolation, chapter IX
b	Normal component of fluid momentum, appendix D
C_D	Local drag of friction coefficient, chapter IX
C_0	Acoustic velocity for fluid, equation (D-9)
C_p	Specific heat at constant pressure
C_v	Specific heat at constant volume
c'	Parameter characterizing turbulent fluctuations, appendix C
E	Unspecified constant coefficient in an alternate model for turbulent stress, chapter V
e	Specific flow energy, equation (A-13)
f	Time derivative, $\frac{\partial f}{\partial t}$, chapter IV
f,g,F,G	General dependent variables or functions
g_c	Gravitational constant
K	Knudsen number, chapter II
k	Parameter characterizing turbulent fluctuations, appendix C
L_1, L_2	Scaling lengths for streamwise and normal dimensions, appendix D
$\ell' \ell^*$	Mixing lengths normal to and parallel to the solid boundary, appendix C

ℓ_0 Initial value for q, equation VII-9

ℓ_a, ℓ_b, ℓ_c Spacings between nodes, figure 2

m Fluid momentum vector, equation (A-11)

M, M_∞ Free-stream Mach number, equation (D-9)

M,N Groupings used in stability analysis, appendix F

N_R Reynolds number based on L_2, equation (D-7)

N_δ Reynolds number based on boundary layer thickness, chapter II

P_R Fluid Prandtl number, equation (D-8)

P_{R_T} Turbulent Prandtl number, equation (C-20)

p Fluid pressure

q Coordinate transformation function, equation (VII-9)

$\bar{\bar{S}}$ Viscous stress tensor, equation (B-9)

s Transformed independent variable, equation (E-1)

T Temperature of fluid

t Independent variable time

U, U_0 Free stream fluid velocity, equation (D-6)

U Internal energy of fluid, equation (A-20)

u_t Shear velocity, chapter III

u,v Components of fluid velocity parallel to and normal to the solid boundary, equation (D-5)

v Fluid velocity vector

x,y Distance measured parallel to and normal to the solid boundary

Z Non-dimensional distance measured normal to the solid boundary, equation (E-1)

α Relaxation factor, equation (VIII-1); period of disturbance for stability analysis, appendix F

β Coordinate transformation parameter, equation (E-2)

γ Specific heat ratio for fluid, appendix D

δ Boundary layer thickness, chapter VI

δ^* Displacement thickness, chapter III

$\delta_1, \delta_2, \delta_3$ Spacing between nodes, figure 2

ε Ratio of scaling distances, equation (D-11)

θ Non-dimensional fluid temperature; stability phase angle, appendix F

κ Thermal conductivity for fluid, equation (A-9); constant in effective viscosity, chapter III

λ Non-dimensional effective viscosity, equation (D-6)

μ Dynamic viscosity of fluid, equation (B-9); stability parameter, appendix F

ν_e Effective viscosity due to turbulence, chapter III

ξ, ζ General dependent variables or functions

η, ξ Non-dimensional distances measured normal to and parallel to the solid boundary, equation (D-6)

π Convergence tolerance, equation (VIII-2)

ρ Fluid density

τ Time period over which fluctuating quantities are averaged, appendix B

τ_W Wall shear stress, chapter III

$\overline{\overline{\tau}}$ Turbulent stress tensor, equation (C-27)

$\overline{\overline{\Omega}}$ Combined viscous and turbulent stress tensor, equation (D-3)

$\delta S, \Delta S$ Non-dimensional step size in transformed coordinate system

Δt Size of time step, chapter IV

Δx Nodal spacing in streamwise dimension

SUBSCRIPTS

$(\_)$ Time-averaged quantity, appendix B

$(_0)$ "Standard" or "scaling" value for a variable

$(_\infty)$ Free-stream conditions

$(_{xx}), (_{xy}), (_{yx}), (_{yy})$ Identify components of tensor quantities

SUPERSCRIPTS

$(\bar{})$ Vector quantity

$(\bar{\bar{}})$ Tensor quantity

(') Fluctuating component of a turbulent quantity, equation (B-1); non-dimensional form of a variable, equation (D-6)

TABLE OF CONTENTS

LIST OF TABLES

LIST OF FIGURES

CHAPTER I

INTRODUCTION

The quantitative description of the physical properties of a fluid flowing along a solid boundary is a problem of long-standing interest to engineers working in a variety of fields. It is a fact of nature that the interaction of fluid viscosity and energy transfer between the boundary and the fluid takes place in a narrow region adjacent to that boundary. Thus the fluid properties in this region largely determine the forces which the fluid impresses upon the boundary and the energy transfer between the fluid and the boundary. Not surprisingly, this region is called the boundary layer.

Historically, attempts at the analytic solution of successively more complicated (and more difficult) boundary layer problems have followed the examples of Prandtl in reducing the mathematical expressions of the governing physical laws to their dominant terms and of Blasius in employing a high level of mathematical sophistication to obtain a solution of the simplified equations. These efforts are summarized in [1], [10], [9].

The utility of Prandtl's simplifying approach in attaining analytic solutions to the less complicated problems is unassailable. As solutions to more complex problems have been required, however, even the Prandtl approach does not reduce the equations (a group of coupled,

non-linear partial differential equations in two, three or four independent variables) to a tractable form. Variable transformations can sometimes convert the equations to the appearance of the equation set first solved by Blasius to yield a solution for the transformed variables.

More often, the engineer seeking information about the boundary layer developed in a particular flow application is forced to make a priori assumptions concerning the detailed structure of the boundary layer flow (a technique which was originated by von Karman). At the same time, he must accept less detail in the solution obtained, and answers often consist only of gross parameters which roughly characterize the flow.

The use of digital computers to solve the fundamental equations of fluid mechanics for various fluid flow situations is presently a developing art. As examples of current achievements, problems have been treated involving jet mixing [12], cellular convection [13], laminar separated flows [14] [14], vortex shedding from cylinders [17], shock wave propagation [15], shock wave - shock layer formation around a blunt body [16] and development of a hypersonic wake [19].

The application of numerical techniques to boundary layer problems has been rather cautious. Most (if not all) of the documented effort has been directed toward the solution of slight generalizations of the same simplified equations which Blasius treated (for example [18], [20], [21]). Apparently little effort has been made to utilize the flexibility and calculation speed of the digital computer in exploring the details of boundary layer flow in complex situations.

The problem of describing the flow of an ideal gas in a turbulent boundary layer is an excellent candidate for solution by numerical techniques. The severely nonlinear empirical models required make mathematically sophisticated approaches (such as similarity assumptions) extremely difficult to apply, and more details of the flow may be needed than are available from von Karman integral techniques.

In developing such a numerical technique, a number of separate problems must be considered.

(1) The equations which describe the motion of a fluid must be carefully reviewed.

(2) An empirical physical model to describe the nature of the turbulent "stress" terms encountered must be selected or developed.

(3) Numerical problems relating to numerical stability of the solution algorithm, mathematical boundary conditions and computer program logistics must be recognized and solved.

(4) An actual numerical solution must be obtained and compared to representative experimental data to assure the physical relevance of the numerical solution.

The procedure outlined above has been carried out in developing a numerical technique for describing the flow of an ideal gas in a turbulent boundary layer. The various steps are described in the following chapters of this dissertation. This description is developed within the framework of a general numerical approach to the detailed description of a general class of turbulent boundary layer problems.

CHAPTER II

DEVELOPMENT OF THE FUNDAMENTAL EQUATIONS

In this chapter the derivation of the continuum laws of fluid mechanics are reviewed and the various assumptions are discussed. The normal modification of these equations to describe turbulent flows is reviewed, leading to the form into which the empirical "turbulent stress tensor" model development in chapter III will be introduced.

Fundamental Laws and Assumptions

The idea that physical systems obey a set of fundamental rules, or physical laws, is basic to engineering and science. In this section, the basic physical laws which apply to fluid mechanics problems are stated, and the assumptions introduced in appendix A are discussed. The mathematical expressions for the laws and the notational manipulations are presented in appendix A.

The first basic assumption is that the fluids to be studied can be considered as continuous; that is, the fluid flow must obey the rules of continuum mechanics. This assumption allows the behavior of individual molecules to be averaged and represented by appropriate parameters without introducing significant error. Schaaf and Chambre [22] set a limit for continuum flow in a boundary layer of

$$K \sim \frac{M}{N_\delta} < .01 \quad ,*$$

where K is the Knudsen number, the ratio of molecular mean free path to boundary layer thickness, M is the Mach number and N_δ is the Reynolds number based on the boundary layer thickness. In the present work,

$$.13 < M < .6$$

and

$$.2 \times 10^6 < N_\delta < 1.0 \times 10^6 \quad ,$$

which gives

$$K \sim .6 \times 10^{-6} \quad .$$

Thus the assumption of continuum flow is quite adequate. In appendix A, the equations are developed from the assumption of a continuous fluid.

It has been assumed in appendix A that no chemical reactions are occurring in the flow being studied. That is, the effects of concentration gradients due to chemical reactions and mass diffusion are not considered. In the development of the mathematical expression for the mass conservation law (equation A-16), no further assumptions have been introduced.

The equation of motion (Newton's second law) is developed into the desired form (equation A-17) by defining the momentum and combining with the mass conservation law. The resulting equation allows a convenient transformation to the finite difference approximations later. The momentum rather than the velocity was used as the principal

*This expression has been altered to reflect a turbulent boundary layer thickness.

variable by Burnstein [23], Van Driest [8] and Walker [12]. The body forces (gravitational, electrical and magnetic forces) have been assumed to be negligible. While this assumption is not strictly necessary, the effects of these forces are normally small in the physical cases of interest for this study.

One other assumption has been included in developing equation (A-17). Newton's second law applies in an "inertial coordinate system", a reference system fixed in the center of the sun. Goldstein [25] calculated the centrifugal correction needed when expressing the law in a coordinate system fixed on the surface of the earth to be about 0.36% of the gravitational attraction. Thus, when gravitational and other body forces are ignored, the centrifugal correction due to rotation of the earth is certainly negligible. However, centrifugal effects may be important when analyzing flow in rotating equipment such as centrifuges, turbines or compressors.

The first law of thermodynamics, expressing the conservation of energy, is applied to the case of a moving fluid by assuming that the fluid is in local thermodynamic equilibrium (see [11]). A specific allowance for radiant heat transfer between fluid elements or between the fluid and its surroundings has not been included. Burstein [23] and Walker [12] have chosen to express this law in terms of changes in the specific flow energy (equation A-20) rather than temperature; this approach has been followed in the present work. Equation (A-18) expresses the first law of thermodynamics.

The assumptions described above are among those normally introduced when a boundary layer problem is formulated; thus the equations

listed at the end of appendix A should yield solutions which may be compared to existing solutions.

Modifications Preparatory to Modeling Turbulent Flow

Turbulent fluid flows are characterized by rapid fluctuations in velocity, pressure and the other basic flow properties. Little progress has been made in analyzing the details of these fluctuations and their dependency on the independent time and space variables. In fact, measurements of fluctuations other than those associated with velocity are scarce.

The normal engineering approach to solving the equations of fluid mechanics for turbulent flows is to introduce a separate variable for the turbulent fluctuation of each basic flow property. When the resulting equations are averaged over a suitable period of time, the averaged equations describe the behavior of the non-fluctuating portions of each basic flow property. In this section, the above procedure and the assumptions introduced are discussed. The equations and algebraic details are presented in appendix B.

The traditional approach to laminar boundary layer problems is to simplify the "complete" equations of fluid mechanics (appendix B) through an analysis of the magnitude of each term, retaining only the dominant terms in each equation. The resulting equations are usually referred to as the "boundary layer" equations. When studying turbulent boundary layers, the variables representing turbulent fluctuations are usually substituted into these boundary layer equations rather than into the complete equations. In this work, fluctuations have been

introduced into the full equations, giving rise to turbulent fluctuation averages which are not easily discarded through the normal order-of-magnitude analysis. This doubtful elimination of these terms (which do not appear in the traditional formulation) is not necessary or even desirable when applying the present method of solution to a turbulent boundary layer problem.

The introduction of fluctuating components, the time-averaging and the algebraic reduction of the resulting equations to equations (B-4) through (B-6) are relatively straightforward operations. The requirement of internal consistency among definitions and averaging laws which leads to equations (B-7) and (B-8) is detailed in appendix B. The additional assumption necessary in treating time variation of the mean flow quantities,

$$\underline{\xi}\,\zeta' = \frac{1}{\tau}\int_0^\tau \underline{\xi}(t)\zeta'(t)dt = \frac{\underline{\xi}\,(\bar{\tau})}{\tau}\int_0^\tau \zeta'(t)dt = 0 \ ,$$

is mathematically valid if the function $\underline{\xi}\,(t)$ is analytic (and can thus be expanded in a Taylor series). Intuitively, the assumption is that $\underline{\xi}\,(t)$ is "sufficiently smooth". As a practical matter, the assumption was introduced without comment by Walker [12] and others and apparently caused no complications.

The assumptions concerning the physical nature of the fluid and the turbulent fluctuations are of more interest than those listed above.

The choice of the ideal gas as a working fluid could be designated as a part of the problem statement rather than an assumption. Other

equations of state might have been selected at only a slight cost in computer program complexity.

The assumption that density fluctuations are negligible,

$$\rho' = 0 ,$$

limits the range of applicability of the formulation, but the extent of the limitation is not well defined. Nagamatsu estimated the assumption to be satisfactory for a free-stream Mach number less than 1.5 [26]. Ferrari estimated the Mach number limit to be "about three" [27], while Walz claimed "10 or 5" as the upper limit for the validity of the assumption [28]. The density fluctuation has been modeled by various investigators ([29] and [30] for example) using the mixing length approach discussed in the following chapter. However, there is apparently no method available to measure density fluctuations or velocity-density fluctuation averages. Thus the selection of a density mixing length would require yet another empirical parameter (see [10] for example). A third alternative would be to neglect pressure fluctuations,

$$p' = 0 ,$$

and obtain density fluctuations from temperature fluctuations through the ideal gas law. This approach has no apparent advantage over the alternatives but would require a more complicated computer code.

The assumption that viscosity and thermal conductivity fluctuations are negligible,

$$\mu' = \kappa' = 0 ,$$

is based on the fact that the viscous contribution to shear stress and the molecular contribution to heat transfer are nearly negligible except

very near the boundary in a turbulent boundary layer. In that region, all fluctuations are nearly negligible. Since either the mechanism or fluctuation amplitude is small throughout the boundary layer, significant contributions from the combined effects seem unlikely. In this situation also, the complications of empirical parameter selection for a mixing-length model seem unjustified.

The stress law selected for the fluid (equation B-9) is that normally selected for an ideal gas. Slight inaccuracies in the values for the molecular stresses are probably not significant, since the molecular terms are important only near the solid boundary, and only one term is of substantial size there.

The assumptions discussed above have largely been made for convenience in empirical modeling and ease of computer programming. It should be noted that the assumptions do not introduce fundamental limitations to the usefulness of the calculation method being developed. In the case of the equation of state and the molecular stress law, some specification must always be made; those used here were selected due to their convenience. In the case of assumptions regarding the nature of density and kinetic coefficient fluctuations, the choices were made for convenience and in the light of a shortage of experimental information which might be used to construct models.

One additional assumption should be discussed here although it is first introduced in appendix C. That is the assumption of two-dimensional flow. As introduced in appendices C and D, this is really three assumptions. First, the mean flow variables are assumed to depend upon spatial dimensions parallel and normal to the solid boundary

but not upon the third dimension normal to these two. Second, the components of vector (momentum, velocity, heat flux) and tensor (shear stress) quantities associated with that third dimension are neglected. Third, the velocity fluctuations associated with that third spatial dimension have been neglected in developing and modeling the turbulent fluctuation averages. The first two assumptions are acceptable since they approximate actual fluid flow situations of interest. The third assumption is accepted as a matter of necessity, since adequate information for modeling is not available. It is known that velocity fluctuations are decidedly three-dimensional [6]. This assumption is used widely and has probably influenced the empirical constants specified in the following chapter so that some compensation for errors it might introduce is included in the models developed.

After appropriate models for the averages of products of fluctuating terms have been constructed, the resulting set of equations will be presumed to describe the time-dependent behavior of a turbulent boundary layer flow.

CHAPTER III

EXPIRICAL MODEL FOR AVERAGES OF PRODUCTS OF FLUCTUATING COMPONENTS

Possibly the most important portion of the solution of any fluid mechanics problem involving turbulence is the specification of the model for the turbulent stress tensor. The model functions, which relate the time averages of the products of fluctuating components to the slowly-varying components, vary vastly in form from one class of problem to another. Thus, they are highly empirical and are usually developed from a combination of experimental data, intuition, dimensional analysis and conjecture. In this chapter, some previous modeling approaches for turbulent boundary layers are summarized, the model used in the present work is developed, and the model for temperature-velocity fluctuation products is discussed. The manipulative details associated with model development are reported in appendix C.

Some Approaches to Modeling the Turbulent Stress Tensor

The universal first step in solving a boundary layer problem is to reduce the equations of fluid mechanics to the "boundary layer" equations. This was originally done through a careful order-of-magnitude analysis, such as that reported by Schlichting [1]. The consequence of performing this analysis before introducing the fluctuation variables and time-averaging

(the most common approach) is that only two components of the turbulent stress tensor appear and the equation describing the normal component of momentum is reduced to a single term. Despite these traditional simplifications, the resulting equations present formidable mathematical difficulties. Thus the selection of a model equation for the turbulent shear stress is usually strongly influenced by the need for mathematical simplicity. Several approaches to modeling which appear in this current literature are sketched and discussed below.

One simplification is to specify the functional forms for the velocity and temperature rather than determining them by solving the partial differential equations. These specifications and subsequent integration normal to the boundary reduce the boundary layer equations to coupled ordinary differential equations with the streamwise coordinate as the independent variable. This, of course, is von Karman's integral approach. The solutions obtained from this procedure consist of various "typical" thickness parameters as functions of the streamwise coordinate. Because most of the desired answer is specified, the success of this approach depends upon the accuracy of the functions specified. Various attempts to model the velocity profile are described by Hinze [6].

A less restrictive approach is to specify the turbulent stress as a function of the independent variables (see [42] for example). This approach usually requires a numerical solution, but the velocity profile is calculated from its governing equation rather than being stipulated arbitrarily.

Another less restrictive approach is to specify the turbulent stress as a function of local values of the dependent variables and their

derivatives as well as the independent variables. This places minimum restriction upon the modeling goal and is usually the starting point for attempts to develop the velocity profiles mentioned above. While this technique should allow the most accurate modeling for the shear stress at any point in a given flow by allowing maximum freedom for expression of intuition, it is still highly empirical, and a given model will apply at best only to a class of turbulent boundary layer problems. The probable difficulties in solving the boundary layer equations with such an unrestricted function for the turbulent stress model virtually require the use of numerical solution techniques.

The model described in the next sections allows local specification of the elements of the turbulent stress tensor in terms of local independent variables, dependent variables and derivatives of dependent variables. The additional stress elements arise from the use of the "complete" equations rather than the boundary layer equations, as mentioned in chapter II. The concept adopted is that of the eddy viscosity, due to Boussinesq and described in [7] for example.

Description of the Model

In appendix C, the mixing-length technique is used to establish the elements of the turbulent stress tensor in terms of the eddy viscosity ν_e:

$$\overline{\overline{\tau}} = \frac{1}{g_c}\begin{bmatrix} -\rho\overline{u'^2} & -\rho\overline{u'v'} \\ -\rho\overline{v'u'} & -\rho\overline{v'^2} \end{bmatrix} = \frac{\rho\nu_e}{g_c}\begin{bmatrix} 14.18\,\frac{\partial \overline{\overline{u}}}{\partial x} & \frac{\partial \overline{\overline{u}}}{\partial y} \\ -4.25\,\frac{\partial \overline{\overline{v}}}{\partial x} & -3.33\,\frac{\partial \overline{\overline{v}}}{\partial y} \end{bmatrix} \qquad \text{(C-27)}$$

The development of this expression is discussed in this section. The form and values for ν_e are described in the following section, completing the specification of $\overline{\overline{\tau}}$.

The mixing-length technique was selected as a relatively straightforward approach to expressing all of the fluctuating components of velocity in terms of the slowly-varying components. In appendix C, the representations selected are not unique. Even after arranging the factors so that a common multiplier ν_e could be drawn from each term, the remaining portion of each element could have been expressed in terms of several gradients. For example, using the assumptions introduced in appendix C,

$$-\rho\underline{u'v'} = \rho\nu_e \frac{\partial \bar{u}}{\partial y} = \frac{\rho\nu_e}{k} \frac{\partial \bar{v}}{\partial y} = -\frac{\rho\nu_e}{k^2} \frac{\partial \bar{v}}{\partial x} = -\frac{\rho\nu_e}{k^3} \frac{\partial \bar{u}}{\partial x}$$

are four possible representations for one element of the tensor, depending on the combination of dependent variable and independent variable in the partial derivative in the model equation. The selections were made finally on the basis of a linearized numerical stability analysis, which is discussed in chapter V. Two restrictions imposed by the form of the equation analysed for stability are used to select each element of the turbulent stress tensor.

1. The dependent variable in the model should be the same as that determined by the equation in which the model is used. For example, $-\rho\underline{u'v'}$ appears in the equation which determines the steamwise component of momentum, $\frac{\rho u}{g_c}$. Thus two of the possible choices presented above (those in which the dependent variable is the normal velocity, $\underline{v}$) are discarded, and

$$-\rho\underline{u'v'} = \rho\nu_e \frac{\partial \bar{u}}{\partial y} \quad \text{or} \quad -\frac{\rho\nu_e}{k^3} \frac{\partial \bar{u}}{\partial x} \quad .$$

2. The derivative contained in the model should be with respect to the same independent variable as the derivative of that turbulent stress element in the equation. Continuing the above example, in the streamwise momentum equation,

$$\frac{\partial(-\rho\underline{u'v'})}{\partial y} = \frac{\partial}{\partial y}\left(\rho\nu_e \frac{\partial u}{\partial y}\right) ,$$

which finally establishes the desired form for the stress element.

This particular stress element is of course the only one normally appearing in the boundary layer equations. Its form is routinely established not from stability conditions but through analogy with the major viscous stress term. The remaining elements in equation (C-27) are defined through similar application of the rules from the stability analysis (see chapter IV, following).

An additional stability requirement is imposed on the stress elements

$$-\rho\underline{v'u'} \quad \text{and} \quad -\rho\underline{v'^2}$$

from the normal component of the momentum equation. That requirement is that the sign of the coefficient must be positive. Thus in the numerical work reported in chapter IX, the signs of these two elements are changed so that

$$-\rho\underline{v'u'} = +\,4.25\,\rho\nu_e \frac{\partial u}{\partial x} \quad \text{and} \quad -\rho\underline{v'^2} = +\,3.33\,\rho\nu_e \frac{\partial v}{\partial y} .$$

Obviously the model equation (C-27) contains several rather sweeping approximations and assumptions; in fact the experimental information used to evaluate the correlation coefficients (equations C-25, 26) was

measured in an incompressible fluid. The necessity of changing the sign on two elements to establish numerical stability for an equation which supposedly describes a physical situation suggests that the intuitive mixing length concept for turbulent boundary layer flow has been extended nearly beyond its limit of applicability.

Despite the obvious shortcomings of equation (C-27), it at least provides a first approximation for the remaining elements in the turbulent stress tensor; no previous attempts to model these elements for a turbulent boundary layer have been discovered in the literature. Also, the model as presented provides the mechanism necessary for numerical stability of the finite difference analog to the equation system.

Model for the Eddy Viscosity

In this section the model for the turbulent stress tensor is completed by establishing the functional form for the eddy viscosity. It is convenient to divide the turbulent boundary layer into two regions normal to the boundary, the wall region and the wake region, as sketched in figure 1.

In the wall region, the form for the eddy viscosity results by comparing equations (C-4) and (C-9):

$$\nu_e = \ell'^2 \left| \frac{\partial u}{\partial y} \right| .$$

Van Driest [37] suggested a correction factor,

$$(1 - e^{-y/A})^2$$

where

$$A = \frac{26\ \nu}{u_\tau} ,$$

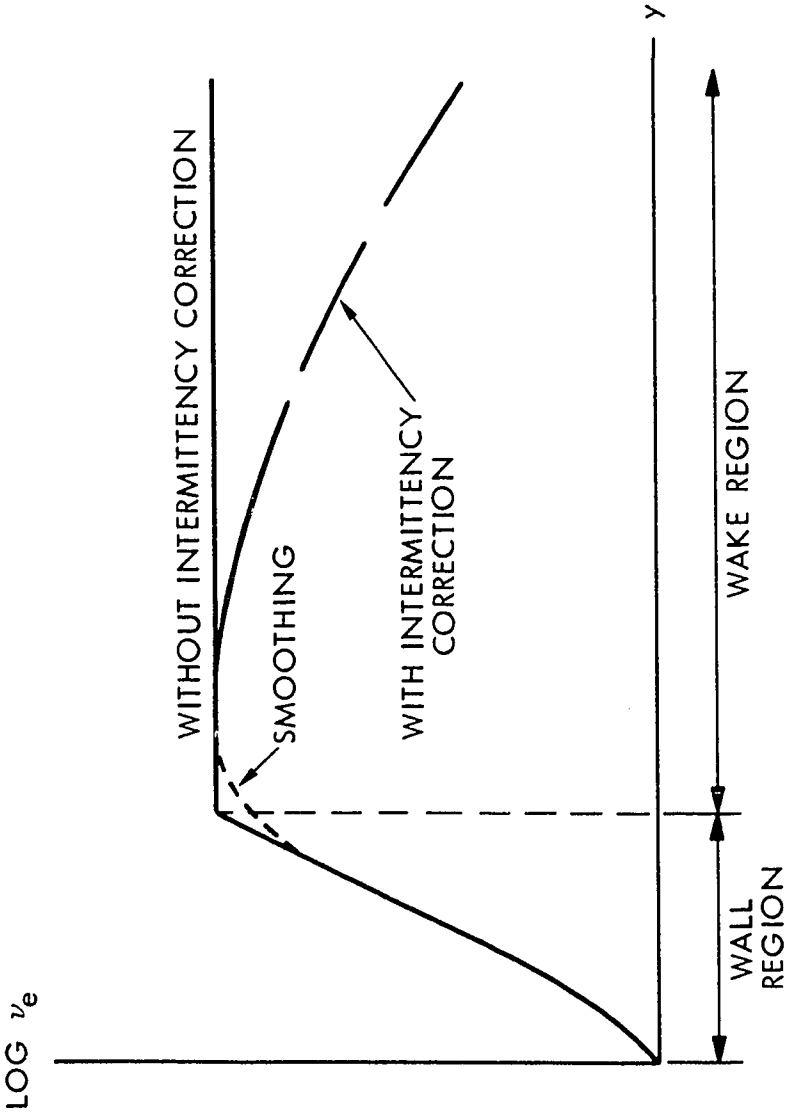

Figure 1
VARIATION OF EDDY VISCOSITY WITH THE NORMAL DIMENSION

ν is the kinematic viscosity for the fluid, u_τ is the shear velocity,

$$u_\tau = \sqrt{g_c \left(\frac{\tau}{\rho}\right)_w} \quad ,$$

and τ_w is the shear stress at the wall,

$$\tau_w = \left(\frac{\rho\nu}{g_c}\frac{\partial u}{\partial y}\right)_w \quad .$$

The inclusion of this factor in the model resulted in more accurate calculation of velocity profiles and is discussed in chapter IX. Prandtl (see [1]) postulated that the mixing length ℓ' should be proportional to the normal variable y for small y (physically near the solid boundary). The proportionality constant is normally taken from the data of Nikuradse for incompressible turbulent flow through smooth pipes (as reported in Schlichting [1]) so that

$$\ell' = .4y \quad .$$

Thus, in the wall region, the eddy viscosity used in this work has the form

$$\nu_e = (.4y)^2(1 - e^{-y/A})^2 \left|\frac{\partial u}{\partial y}\right| \quad . \qquad \text{(III-1)}$$

For the wake region, Clauser [31] established a very simple form for the eddy viscosity,

$$\nu_e = \kappa\, U\, \delta^* \quad ,$$

where U is the free stream velocity and δ^* is the displacement thickness defined by

$$\delta^*(x) = \int_0^\infty \left(1 - \frac{a(x,y)}{a(x,\infty)}\right) dy \quad . \qquad \text{(III-2)}$$

a is the streamwise component of momentum, equation (D-5). Mellor and Gibson [32] have determined the optimum value of κ by comparing numerical and experimental results for a variety of flows, including some negotiating streamwise pressure gradients. Therefore the eddy viscosity used in the wake region is

$$\nu_e = .016\ U\ \delta^* \ . \qquad \text{(III-3)}$$

Many of the models encountered in the literature provide for an overlap region, which allows a smooth mathematical transition between the wall and wake regions. In this work, the results of preliminary numerical studies led to the use of a cubic polynomial to round the corner at the junction of the model eqations.

In applications described in the literature, equation (III-3) is often multiplied by an intermittency factor, introduced in an attempt to describe the fact that turbulent fluctuations tend to occur in "bursts" or pulses alternating with "quiet" flow. These turbulent bursts occur less and less frequently as the free stream is approached. If the bursts are absorbed in the time averaging of the basic equations in the correct manner, the model for the turbulent stress should show a proper reduction as the intermittency factor becomes smaller. Smith, Jaffe and Lind [39] observed negligible effect on numerical results due to this correction, and no correction for intermittency has been used in the present work. Equations (III-1) and (III-3) represent the empirical eddy viscosity selected for a compressible turbulent boundary layer.

Modeling of Temperature — Velocity Fluctuation Averages

The "turbulent heat flux" has been defined by equations (C-20, 21).

The effect of the manipulations detailed in appendix C is to relate the heat flux vector to the turbulent stress tensor through the parameter P_{R_T}, the "Turbulent Prandtl Number."

The virtue of this parameter is that it appears to be nearly constant across the width of the boundary layer ([44], [45]), although a few sources report a variation (see [43] for example). Most references suggest a rough value of

$$P_{R_T} = .8 \ . \tag{3-4}$$

This value has been used in the present work, although a functional variation,

$$P_{R_T} = P_{R_T}(y) \ ,$$

could be easily accommodated in the numerical technique under development if that were found desirable to match available data on temperature profiles.

The developments described in this chapter show the empirical nature of turbulent shear stress models quite well. In addition to gross physical assumptions, the form of the model equations is restricted by the necessity for numerical stability. Within these limits, the proposed numerical procedure is not dependent upon the model actually described and used but could be used to test other proposed models.

CHAPTER IV

NUMERICAL METHOD

GENERAL DISCUSSION AND DIFFERENCE ALGORITHMS

In this chapter, the philosophy of the numerical method being developed is explained and compared with existing numerical methods of solution for the boundary layer equations. The necessity for finite difference forms which make efficient use of computer memory space and time is discussed. The finite difference expansions used in this work are developed within that framework. A coordinate transformation utilized to give a further savings in memory requirements is described.

Background and Philosophy

In chapter III, the prevalent practice of reducing the governing equations of fluid mechanics to the dominant terms was mentioned. If a turbulent boundary layer flow is under study, the mathematical simplifications realized are usually exploited by using one of several specialized numerical techniques, all of which depend on the absence of derivatives higher than first order with respect to the streamwise coordinate (in the "steady-flow" formulation, derivatives with respect to time are absent by definition). Various methods are described by Gilliam [33] and Blottner and Flugge-Lotz [34] for example.

The type of problem in which second derivatives with respect to the streamwise coordinate are absent is known as an "initial value problem" in the streamwise coordinate. The finite difference analogs for the differential equations can be solved for the nodes distributed across the boundary layer at each value of the streamwise coordinate in turn, starting upstream at the initial values and "marching" downstream. This solution is accomplished relatively easily, since the knowledge of the solution at one streamwise location allows either an explicit evaluation at the next or an implicit equation system which is easily inverted to obtain that evaluation.

If the boundary layer assumptions which simplify the equations of fluid mechanics are not justified or not desirable, a situation which seems quite likely in some turbulent boundary layer problems, the simple marching technique can no longer be used. The differential equations in this case contain second derivatives with respect to the streamwise coordinate, so that a solution for the finite difference equations at each node requires solutions from nodes both upstream and downstream of the node. Thus solutions cannot be obtained for all nodes at a streamwise location and then projected to the next group of nodes. The difference analogs for the "complete" equations must be solved simultaneously for every node in the flow field under consideration. This type of problem is known as a "boundary value problem" in the streamwise and normal coordinates.

The solution of such a system is not a trivial matter. Trial-and-error techniques, such as linearization combined with repeated matrix inversion or a systematic relaxation scheme, appear as natural

candidates for the job. However, inversion of very large matrices is required in the former method, and the automatic correction scheme required by relaxation techniques is not available.

One method of solution for a physical boundary value problem is to utilize the "unsteady terms", the temporal derivatives, casting the problem as an initial value problem in the independent variable time. If the steady-state solution is known to exist, then the time-dependent solution of the equations should converge to the steady-state solution.

In this method, a flow field (e.g., values for the dependent variables) at some arbitrary time is assumed, the spatial derivatives are evaluated by finite differences or a related technique, and the derivatives of dependent variables with respect to time are calculated from the spatial derivatives. These temporal derivatives are then replaced by differences for a short increment of time and the dependent variables are evaluated at the new time. This process is repeated until the time derivatives are sufficiently near zero, that is, until the flow field at the current time is sufficiently near steady state.

This approach is used routinely to solve heat conduction problems (see [36], for example). Aziz [13] has used the technique to solve a problem in cellular convection, and Walker [12] has described the flow field of a turbulent, supersonic jet. The technique is sometimes known as the "time-marching technique" or the "unsteady approach".

As a final note on this technique, if the initial flow conditions assumed represent an actual flow field, the numerical solution will mimic the development of the physical flow in time. Thus a time-dependent problem can be solved.

Finite Difference Terminology and Factors Effecting Computer Time Usage

The solution being sought for equations (D-12) — (D-15) consists of values of the mean flow variables (density, two components of fluid momentum, specific flow energy, temperature and pressure) throughout a defined region of space, subject to given mathematical boundary conditions and determined for the steady state (derivatives with respect to time negligible). If a finite difference technique is adopted, the solution is obtained only at specified points within the spatial region of interest; these points are usually called grid or mesh points or nodes. The collection of nodes is known as the finite difference net, mesh or grid. The instantaneous values of the mean flow variables associated with the mesh at any particular time are known as the solution at that time plane.

One requirement determined from the stability analysis presented in appendix F was that the difference equations should be implicit in the variable time. Briefly, this means that spatial derivatives are evaluated at the nearest unsolved time plane; thus the equations at each time plane must be solved by trial-and-error, by iteration.

Mathematical theorems establishing the convergence of the solution of difference equations to the solution for the associated differential equations are not available for systems such as the present coupled, non-linear set. Therefore, a comparison of numerical results to experimental data is desirable to establish convergence to the physical solution. Intuitive assurance of convergence and uniqueness is provided by assuming initial conditions relatively far removed from

the known physical answer and allowing the numerical calculations to proceed to the physical answer. This procedure is needed only once to establish physical relevance; subsequently significant savings in computer time consumption can be realized by selecting initial conditions very near the expected final answer.

In order for a calculation technique to be most useful, its requirements for computer storage space and time should be modest. The time demand and storage demand are each proportional to the number of nodes required on the difference net. Storage demands can usually be reduced by increasing the time requirements. The most efficient approach, however, is to reduce the number of nodes to a minimum. The number of nodes has been reduced by two methods in the present work:

1) The coordinate transformation shown in appendix E has been used to locate most nodes within the region of physical interest; and
2) a non-uniform grid spacing has been devised as described in the next section, placing nodes closer together where the largest errors are expected and spreading nodes elsewhere.

Difference Analogs for Partial Derivatives With Respect to Spatial Coordinates

In chapter V and appendix F, the basic equations to be solved are of the general form

$$\frac{\partial f}{\partial t} = \frac{\partial F}{\partial x} + \frac{\partial G}{\partial y} .$$

To evaluate the right-hand size of this equation, finite difference analogs must be developed for terms of the form

$$\frac{\partial f}{\partial y} \quad , \quad \frac{\partial F}{\partial x} \quad \text{and} \quad \frac{\partial G}{\partial y} \, .$$

The purpose of this section is to develop these difference formulae.

Two approaches are possible in developing these analogs:

1) force a parabola through the values at three points and evaluate the derivative of the parabola at the desired point; or

2) expand the functions in Taylor series about the points where the functions are known and solve the resulting equation set for the desired derivative.

The resulting formulae are identical for computing purposes, but the latter option gives some idea of the magnitude of the truncation error. Thus the Taylor series approach is followed below. The notation is identified on figure 2.

In deriving the expression for $\frac{\partial f}{\partial y}$, the difference analog is derived at the node 3 (or d). The expansions are written around the node 3:

$$f_4 = f_3 + f_3' \, \delta_3 + \frac{f_3''}{2} \delta_3^2 + \frac{f_3'''}{6} \delta_3^3 + \ldots \, ,$$

$$f_2 = f_3 - f_3' \, \delta_2 + \frac{f_3''}{2} \delta_2^2 - \frac{f_3'''}{6} \delta_2^3 + \ldots \, .$$

Solving these to eliminate the term f_3', the result is

$$f_3' = \frac{(f_4 - f_3)\delta_2^2 - (f_2 - f_3)\delta_3^2}{\delta_2 \delta_3 (\delta_2 + \delta_3)} - \frac{f_3'''}{6} \delta_2 \delta_3 + \ldots \, . \qquad \text{(IV-1)}$$

If $\delta_2 = \delta_3$, (IV-1) reduces the usual centered difference formula. The final term,

$$\frac{f'''}{6} \delta_2 \delta_3 \, ,$$

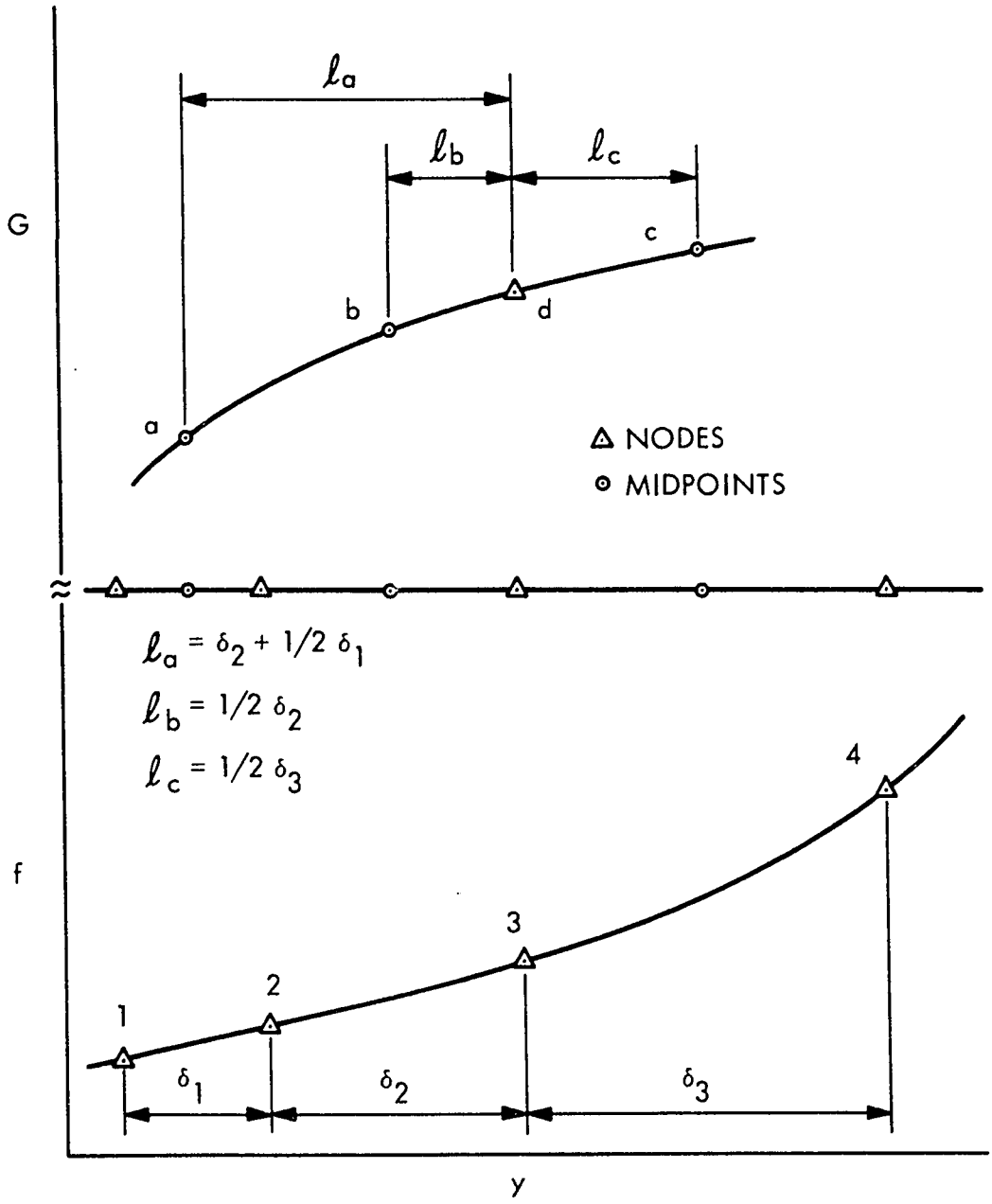

Figure 2

SCHEMATIC DIAGRAM OF NODAL SPACING NORMAL TO THE SOLID BOUNDARY WITH NOTATION IDENTIFIED

is the first term neglected in the expansion and the dominant term of the remainder. It is therefore an indication of the magnitude of the truncation error.

As mentioned in the previous section, the size of the error has been limited without resorting to an enormous number of nodes by closely spacing the nodes (δ_2 and δ_3 small) near the solid boundary where the function f changes rapidly and thus the derivative f''' is presumably large. In regions more remote from the solid boundary where f is known to change slowly and f''' is presumably smaller, nodes have been more widely spaced (δ_2 and δ_3 larger). Brailovskaya and Chudov [38] applied the difference formula (IV-1) by choosing three zones normal to the boundary, each having a unique mesh width. Their technique, using four zones instead of three, has been adopted in the present work. Other techniques involving a constant ratio δ_3/δ_2, to give a continuously growing mesh spacing or a transformation on the independent variable normal to the boundary [39] were available. It was felt that the zonal spacing variation used offered the advantages of programming simplicity and ease of interpretation of the numerical results.

The term $\frac{\partial G}{\partial y}$ is also to be evaluated at the node 3 (or d), but the values of G are known at the midpoints a, b, c. The expansions are written about the node d:

$$G_c = G_d + G'_d \ell_c + \frac{G''_d}{2} \ell_c^2 + \frac{G'''_d}{6} \ell_c^3 + \ldots ,$$

$$G_b = G_d - G'_d \ell_b + \frac{G''_d}{2} \ell_b^2 - \frac{G'''_d}{6} \ell_b^3 + \ldots ,$$

$$G_a = G_d - G'_d \ell_a + \frac{G''_d}{2} \ell_a^2 - \frac{G'''_d}{6} \ell_a^3 + \ldots ,$$

If the terms involving G_d''' are truncated, the equations form a linear set in the unknowns

$$G_d \ , \ G_d' \ , \ G_d'' \ .$$

Inverting the set for G_d', the desired expression is

$$\frac{\partial G_d}{\partial y} =$$

$$G_d' = \frac{G_a(\ell_c^2 - \ell_b^2) - G_b(\ell_c^2 - \ell_a^2) + G_c(\ell_b^2 - \ell_a^2)}{-\ell_a^2(\ell_b + \ell_c) + \ell_b^2(\ell_a + \ell_c) + \ell_c^2(\ell_b - \ell_a)} \ . \quad \text{(IV-2)}$$

As in the case above, the term

$$\frac{G'''}{6} \ell^2$$

is an indication of the magnitude of the error in the difference formula. If $\delta_1 = \delta_2 = \delta_3$, the above expression reduces to the usual centered difference formula,

$$\frac{\partial G_d}{\partial y} = \frac{G_c - G_b}{\delta_1} \ . \quad \text{(IV-3)}$$

For the term

$$\frac{\partial F}{\partial x} \ ,$$

the difference analog used was equation (IV-3),

$$\frac{\partial F}{\partial x} = \frac{F_R - F_L}{\Delta x} \ , \quad \text{(IV-4)}$$

with values of F to the right (R) and left (L) of the node at which the equation is evaluated.

In the present problem, the functions F and G are complicated conglomerates of dependent variables and partial derivatives which represent the strong non-linearities and coupling in the problem.

Expansion for Time Derivatives

A Taylor series expansion in the variable time may be made about the known time plane t_1, or the unknown time t_2:

$$f_2 = f_1 + \dot{f}_1 \Delta t + \frac{\ddot{f}_1}{2} (\Delta t)^2 + \ldots$$

$$f_1 = f_2 - \dot{f}_2 \Delta t + \frac{\ddot{f}_2}{2} (\Delta t)^2 - \ldots .$$

For advancing the solution in time, two formulae are possible,

$$f_2 = f_1 + \dot{f}_1 \Delta t + \frac{\ddot{f}_1}{2} (\Delta t)^2 + \ldots$$

and

$$f_2 = f_1 + \dot{f}_2 \Delta t - \frac{\ddot{f}_2}{2} (\Delta t)^2 + \ldots .$$

where the terms

$$\frac{\ddot{f}_1}{2} (\Delta t)^2 \quad \text{and} \quad - \frac{\ddot{f}_2}{2} (\Delta t)^2$$

are the first terms neglected by the difference schemes.

The explicit form,

$$f_2 = f_1 + \dot{f}_1 \Delta t ,$$

can be evaluated without trial-and-error at each node (the subscripts represent time planes here; $\dot{f}_1$ is evaluated at each node from the fundamental equations) because all conditions at time plane 1 are known. Unfortunately, this form is shown to be unstable in appendix F; that is, the truncated terms tend to accumulate and grow in size, eventually destroying any physical sense in the numbers calculated.

As is shown in appendix F, the implicit form

$$f_2 = f_1 + \dot{f}_2 \Delta t \qquad \text{(IV-5)}$$

is stable if certain rules are obeyed in developing the model equations for the turbulent stress tensor. Since the derivative

$$\dot{f}_2$$

is determined from spatial derivatives evaluated at the time plane 2

where the solution is not yet known, (IV-5) must be solved by trial-and-error. The technique used in this solution is described in chapter VIII.

CHAPTER V

CONSIDERATIONS FOR NUMERICAL STABILITY

The problem of numerical stability is dominant when attempting finite difference solution techniques. If the difference analog is stable, a solution may be possible; if the scheme is unstable, completely meaningless numbers result. In this chapter, the concept of numerical stability is explained, and results of the stability analysis in appendix F are interpreted for this specific boundary layer problem.

Repetitive evaluation of finite difference algorithms introduces perturbations into the numbers calculated to represent the dependent variables at the various nodes. These perturbations may be due to roundoff error (digital computers usually carry the equivalent of eight decimal digits), truncation error in the difference formulae or some other source such as random machine error. The important point is that such numerical disturbances are always present; if the algorithm is such that they accumulate and grow as the calculation progresses, the algorithm is said to be unstable.

The objective of a stability analysis is to determine under what conditions a calculation scheme is stable. To do this, disturbances are introduced into the difference equations for a single node, and the equations which result describe the variation of the disturbance

as the calculation develops. In order to accomplish this, it is usually necessary to linearize the equation for the disturbance and to assume a solution for the resulting equations. When a non-linear equation is linearized, a variety of linear equations may result; therefore, the result of a stability analysis may not be unique. For this reason, the analysis which has proved successful in this work has been presented in some detail in appendix F. Other, unsuccessful, analyses have not been presented; their existence is mentioned here as a warning that the assumptions made during analysis render all conclusions conditional. The results of a stability analysis can be regarded as useful guidelines only after numerical verification for a typical problem.

In appendix F, the four fundamental equations are represented by the general equation,

$$\frac{\partial f}{\partial t} = \frac{\partial F}{\partial x} + \frac{\partial G}{\partial y} \, . \qquad \text{(F-1)}$$

This equation is linearized into the form

$$\frac{\partial f}{\partial t} = A \frac{\partial f}{\partial y} + B \frac{\partial^2 f}{\partial y^2} + C \frac{\partial g}{\partial y} + D \frac{\partial^2 g}{\partial y^2} + \ldots \, . \qquad \text{(F-3)}$$

The implicit difference analog for this equation is analyzed for numerical stability in the interaction between the variables t and y (x considered constant) and the variables t and x (y considered constant). The result of that analysis is that, for numerical stability, the condition

$$\frac{\Delta t}{(\Delta y)^2} (B + D \, g/f) \geq 0 \qquad \text{(F-10)}$$

must be satisfied at every node. The dependent variables g represent coupling between the fundamental equations at any node under consideration.

In the case of the streamwise momentum equation (D-13),

$$B = \frac{\varepsilon}{N_R}(1 + \lambda) \quad \text{and} \quad D = 0 \ .$$

With $B > 0$ no stability problem is anticipated. For the normal component of the momentum equation (D-14),

$$B = \left(\frac{4}{3} - \frac{\lambda}{c'}\right) \frac{\varepsilon}{N_R} \quad \text{and} \quad D = 0 \ .$$

In this case,

$$B < 0$$

for most nodes. Thus the sign on the model used in this equation was changed to give

$$B > 0 \ .$$

When (F-10) is applied to the streamwise difference analogs (x-derivatives instead of y-derivatives), the equation is

$$M = \frac{\Delta t}{(\Delta x)^2}(B + D\ g/f) \geq 0 \ . \qquad \text{(F-10a)}$$

In this case, for the streamwise momentum equation,

$$B = \frac{1}{N_R}\frac{\lambda}{c'k\varepsilon} > 0 \ , \quad D = 0 \ ,$$

which is stable. However, an unsuccessful attempt was made to model this element of the turbulent stress tensor in a form which required

$$B < 0 \ .$$

That model resulted in unstable behavior.

For the normal component of the momentum equation,

$$B = \frac{1}{\varepsilon\ N_R}\left(1 - \frac{\lambda}{k^2}\right) \quad \text{and} \quad D = \frac{1}{N_R} \ .$$

It was necessary to change a sign in this model to allow

$$B > 0$$

and insure stability. The turbulent stress term under consideration here is

$$- \rho \underline{v'u'} \quad .$$

Since physically

$$- \rho \underline{v'u'} = - \rho \underline{u'v'} \quad ,$$

(the turbulent shear stress term encountered in the streamwise momentum equation), an early attempt was made to model the two terms identically. This led to an unstable solution. In retrospect, the explanation is clear from (F-10a).

In that model,

$$B \underset{\sim}{=} 0 \quad , \quad D = \frac{1}{N_R} (1 + \lambda) \quad ,$$

while

$$f \equiv b = \rho v, \; g = a = \rho u \quad .$$

The stability condition (F-10a) is virtually

$$\frac{1}{N_R} (1 + \lambda) \frac{u}{v} \geq 0 \quad .$$

This depends on the sign of u and v. While

$$u > 0$$

generally in a boundary layer and

$$v > 0$$

is the normal steady-state result,

$$v < 0$$

is encountered routinely in the numerical transient solutions. Therefore the normal component of the momentum equation leads to unstable numerical behavior.

Thus it is desirable for numerical stability that models be constructed which minimize the dependence of the condition (F-10) upon the ratio g/f. That is, the equations should be de-coupled as much as is feasible. In terms of the coefficients,

$$B >> D \quad .$$

In the present condition this was done by constructing the model to depend on the variable

$$b = \rho v$$

rather than

$$a = \rho u$$

in the equation used to calculate b.

The third restriction on the model equations for stability was, essentially, to avoid cross derivatives. As an example,

$$\frac{\partial \tau}{\partial y} = \frac{\partial}{\partial y}\left(\rho \nu_e \frac{\partial u}{\partial y}\right)$$

was chosen rather than

$$\frac{\partial \tau}{\partial y} = \frac{\partial}{\partial y}\left(E\rho \nu_e \frac{\partial u}{\partial x}\right) \quad .$$

This rule was imposed due to the difficulty in analyzing cross difference analogs for stability and the more complicated computer codes required to handle the cross terms.

The energy conservation law (D-15) will not be discussed, since

$$B > 0 \quad \text{and} \quad B >> D$$

are implicit in the formulation. Thus no additional restrictions are developed from this equation.

This completes the interpretation of the stability condition developed in appendix F.

CHAPTER VI

BOUNDARY AND INITIAL CONDITIONS

Since a solution is being sought for a problem of interest only within a limited physical region, the boundary layer, provision must be made for treating nodes in the finite difference net which lie on the boundary of that region. In this chapter, the techniques used in obtaining solutions to the equations at the boundary nodes will be discussed and the conditions actually used will be detailed. The initial conditions are discussed briefly.

Boundary Conditions

In this work, the term "boundary" is used to refer to the edges of the region of physical interest, including the actual solid physical boundary, the upstream edge, the free-stream edge and the downstream edge. Figure 3 is a sketch of a typical solution region.

When explicit closed-form functional solutions to partial differential equations are sought (see Wylie [4] for example), the boundary conditions of the problem are used to evaluate the arbitrary constants which appear in the solutions. One boundary (or edge) condition is selected for each undetermined constant in the solution; the selection of these conditions usually specifies the unique physical situation under study.

When the problem under study is to be solved using finite difference techniques, as in the present case, the numerical procedure

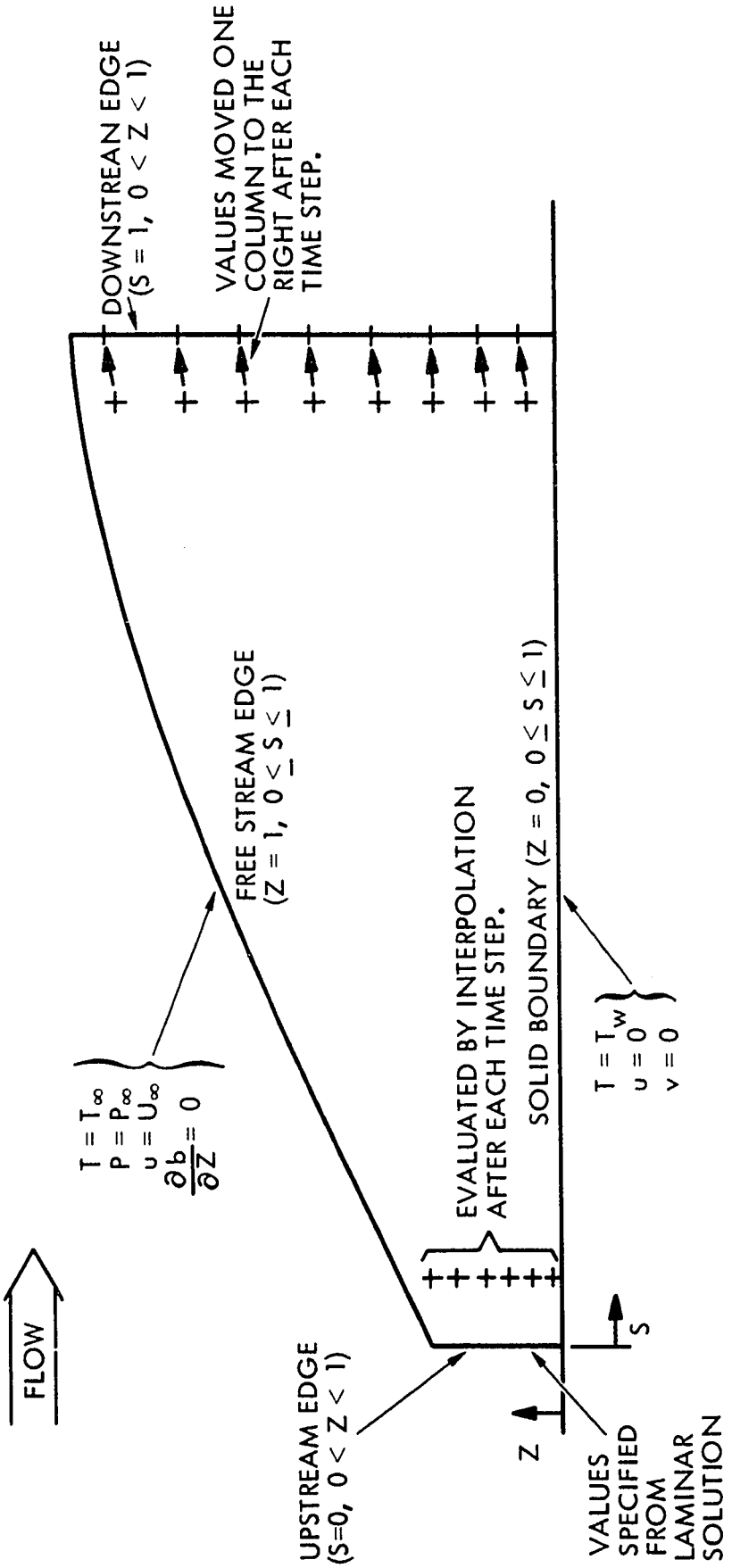

Figure 3
MATHEMATICAL BOUNDARY CONDITIONS APPLIED TO
THE TURBULENT BOUNDARY LAYER PROBLEM

simply requires some method of calculating values for each dependent variable at each boundary node. This is necessary because the difference equations at a particular node depend on values at the surrounding nodes, and the boundary nodes are not "surrounded". As in the case where closed-form solutions are possible, selection of the boundary conditions determines the unique physical situation the solution is to describe. Among possible special techniques are:

1. specification of the values at each boundary node,
2. specification of slopes at each boundary node, and
3. substitution of alternate expressions for the difference equations at each boundary node.

Eight variables,

$$\rho, a, b, e, p, u, v, T,$$

are to be determined (or specified) at each node, including the boundary nodes. To balance the variables, eight equations are available, including the four basic partial differential equations ((D-12) - (D-15)), definitions for momentum and specific flow energy ((D-16), (D-5)), and the ideal gas law (D-17). Each time a value is specified, an equation is discarded.

The specific conditions applied in the numerical work are discussed in the following sections.

Upstream Conditions

The upstream conditions were specified for all nodes along the line

$$S = 0 \ , \ 0 < Z < 1 \ . \qquad \text{(VI-1)}$$

The momentum component a was given as the cubic polynomial

$$a(0,Z) = \varepsilon(\varepsilon^2 - 3\varepsilon + 3),\ \varepsilon = \frac{Z}{\delta} . \qquad \text{(VI-2)}$$

The thickness δ is given in table I.

This polynomial (VI-2) approximates the classical laminar solution. The normal momentum component b was calculated from the continuity equation for steady state:

$$b(0,Z) = b(0,0) - \beta q \{a(0,Z) - a(0,0)\} - q \int_0^Z \left(\frac{\partial a}{\partial s}\right) dZ .$$

The pressure was constant at the free-stream value. The temperature was scaled between the value at the wall and the free-stream value:

$$T(0,Z) = T(0,0) + \{T(0,1) - T(0,0)\} \frac{a(0,Z)}{a(0,1)} . \qquad \text{(VI-3)}$$

The density was then calculated from the ideal gas law, and the velocity components were calculated from the momenta and density. Finally, the specific flow energy e was calculated from its definition (with no turbulent terms included). Once these values were determined, they were frozen for the duration of the calculation.

The idea on this boundary was to approximate a laminar, steady-state solution, with the first few columns of nodes immediately downstream being in the "transition" zone. This was intended as a numerical transition, and the values calculated at those nodes should not be interpreted as valid physical quantities. Some difficulty was encountered in obtaining convergence for the nodes nearest this upstream edge. Therefore, the variables on the second column of nodes were evaluated by interpolation between the first (edge) column and interior columns. The values on the second column were frozen during the interative solution for each time step, and the interpolation was performed before continuing with the next time step.

A turbulent solution (from existing solutions for the boundary layer equations) might have been substituted to simulate further development of an already-turbulent boundary layer.

Solid Boundary (Wall)

The first conditions selected here were the classic set. The velocity was specified as zero (the no-slip condition),

$$u(s,0) = v(s,0) = 0,$$

which implied

$$a(s,0) = b(s,0) = 0 \quad . \tag{VI-4}$$

As suggested above, the wall temperature was specified as constant,

$$T(s,0) = \text{constant} \quad . \tag{VI-5}$$

Alternately, the heat flux or temperature gradient might have been specified,

$$\frac{\partial T}{\partial Z}(s,0) = f(s) \quad . \tag{VI-5a}$$

This would include the special case of an adiabatic wall,

$$f(s) = 0 \cdot$$

The pressure at the wall was replaced by the pressure at the node nearest to the wall after each iteration. The specific flow energy was determined from its definition, equation (D-16), (the turbulent effects were assumed to be zero at the wall). The density was calculated from the ideal gas law, equation (D-17).

On this boundary, only the no-slip condition and the wall temperature were frozen. Values for the other variables were updated as values on the mesh were changed due to iteration and advancing time steps.

Free Stream

The free stream condition is only approached in the physical case. The distance from the solid boundary at which the influence of that boundary upon the local flow properties is negligible is a matter of engineering judgment for a particular problem. In the present work, the numerical boundary ($Z = 1$, $0 \leq S \leq 1$) was located at about

$$L_2 = 1.25 \times \delta \quad ,$$

where δ is the boundary layer "thickness" determined from von Karman integral solutions for the boundary layer equations. L_2 is the scaling factor used for non-dimensionalizing the basic equations (see appendix D).

Along the free stream boundary, the streamwise momentum, pressure and temperature were specified:

$$a(s,1) = a_\infty, \; p(s,1) = p_\infty, \; T(s,1) = T_\infty \quad . \tag{VI-6}$$

The density was calculated from the ideal gas law. The condition

$$\frac{\partial b}{\partial Z}(s,1) = 0 \tag{VI-7}$$

was imposed, and a parabolic extrapolation was substituted for the normal component of the momentum equation to determine $b(s,1)$. The velocities were calculated from the definition of momentum, equation (D-16). The specific flow energy $e(s,1)$ was calculated from its definition. The values of $v(s,1)$ and $e(s,1)$ changed slightly as values on the interior nodes were updated and were re-evaluated after each iteration and each time step.

The model for the turbulent stress tensor described in chapter III has no provision for the effects of free stream turbulence; hence no boundary condition is imposed upon the fluctuation averages.

If the intermittency correction sketched in figure 1 were incorporated into the model, the shape of that curve would reflect an imposed boundary condition upon the value of the free-stream turbulence. An investigation [46] of the effect of free-stream turbulence upon velocity profiles in a boundary layer indicated a negligible effect for values of free-stream turbulence less than those generated within the boundary layer.

Downstream

For the group of nodes along the boundary,

$$s = 1,\ 0 < Z < 1 \quad ,$$

the objective of the boundary conditions was to insure a controlled numerical behavior. It has been established that the techniques used did not effect the solution significantly at the interior nodes (see chapter IX).

During any time step, the values along this boundary were frozen. After the iterations on the interior nodes were completed, the values on the column

$$s = 1\ ,\ 0 < Z < 1$$

were updated by one of two methods:

(1) the values were replaced by values from the column

$$s = 1 - \delta s,\ 0 < Z < 1 \quad ;* \tag{VI-8}$$

(2) new values were calculated by linear extrapolation of values at

$$s = 1 - \delta s\ ,\ s = 1 - 2\delta s;\ \ 0 < Z < 1 \quad . \tag{VI-9}$$

---

*This technique was suggested by Professor W. F. Walker.

Various one-sided difference analogs and extrapolations were attempted at these boundary nodes during preliminary development of the computer program. These algorithms were applied at every iteration over the grid, and all resulted in an interaction between the values at the boundary and those in the interior which rapidly caused the calculation to generate meaningless numbers.

Initial Conditions

The selection of starting values is somewhat arbitrary, the main objective being to assure smooth profiles and compatibility among definitions for the dependent variables.

As a starting point, a momentum profile a(s,Z) was specified which matched those boundary conditions already selected:

$$a(s,0) = 0 \quad , \quad a(s,1) = a_\infty \quad .$$

The remaining momentum component was estimated from steady-state continuity requirements,

$$b(s,Z) = b(s,0) - \beta q \{a(s,z) - a(s,0)\} - q \int_0^Z \left\{ \frac{\partial a}{\partial s}(s,Z) \right\} dZ \quad . \tag{VI-10}$$

The temperature was interpolated between the values in the free stream and at the wall,

$$T(s,Z) = T(s,0) + \{T(s,1) - T(s,0)\} \frac{a(s,Z)}{a(s,1)} \quad . \tag{VI-11}$$

The pressure was initially constant across the boundary layer,

$$p(s,Z) = p(s,1) \quad , \tag{VI-12}$$

and the density was calculated from the ideal gas law. The specific flow energy was then calculated from its definition.

Once the initial profile a(s,Z) is selected to achieve some objective, the other starting values can be generated automatically. For the initial numerical work reported in chapter IX, a cubic profile was selected,

$$a(s,Z) = \left(\frac{Z}{\delta}\right)\left\{\left(\frac{Z}{\delta}\right)^2 - 3\left(\frac{Z}{\delta}\right) + 3\right\} \quad \text{for } Z < \delta$$

and (VI-13)

$$a(s,Z) = a_\infty \quad \text{for } Z \geq \delta$$

$$\delta = \delta(s) = \delta(0) + .8s \quad .$$

This approximates a laminar profile and is quite far removed from the expected turbulent profile. Considerable computer time was consumed in generating a steady-state turbulent solution from this starting profile. However, the accomplishment of the solution (see chapter IX) is solid heuristic evidence of the validity of the time-marching technique in obtaining physically valid solutions to boundary-layer problems. For the remaining demonstration of the time-marching technique, approximate turbulent solutions were used as initial conditions in order to conserve computer time.

As the introduction to this chapter suggests, there appears to be no single accepted technique for selecting or evaluating the boundary conditions needed to complete a numerical solution for partial differential equations. The techniques described above have resulted from extensive development and have been developed with two goals in mind:

1. to obtain algorithms which are "well behaved" numerically so that the evaluation of the boundary conditions does not complicate the task of obtaining solutions within the interior of the mesh; and

2. to select conditions reflecting the experience available from solutions for classical boundary layer problems.

CHAPTER VII

SUMMARY OF EQUATIONS AND SPECIFICATION OF THE PHYSICAL CASE TO BE STUDIED

Ih this chapter, the system of equations to be studied is collected into a single grouping, and the specific physical cases to be studied are presented.

Equation Summary

In appendix F, the general equation

$$\frac{\partial f}{\partial t} = \frac{\partial F}{\partial x} + \frac{\partial G}{\partial y} \qquad \text{(F-1)}$$

is expressed in finite difference form and analyzed for numerical stability. When the non-dimensional form of the equation (appendix D) is treated with the coordinate system transformation developed in appendix E, the resulting form is

$$\frac{\partial f}{\partial t} = \frac{\partial F}{\partial s} + \beta\frac{\partial F}{\partial Z} + \frac{\varepsilon}{q}\frac{\partial G}{\partial Z} \quad . \qquad \text{(VII-1)}$$

By comparison with equations (D-12) — (D-15), f, F, and G are identified as

$$f = \begin{bmatrix} \rho \\ a \\ b \\ e \end{bmatrix}, \tag{7-2}$$

$$F = -\begin{bmatrix} a \\ au + \dfrac{p}{\gamma M^2} - \dfrac{\Omega_{xx}}{N_R} \\ av \qquad\qquad -\dfrac{\Omega_{yx}}{N_R} \\ (e+p)u - \left(\dfrac{\gamma}{\gamma-1}\right)\dfrac{K}{\epsilon N_R P R_0}\left(1+\lambda\dfrac{P_R}{P R_T}\right)\left(\dfrac{\partial\theta}{\partial S}+\beta\dfrac{\partial\theta}{\partial Z}\right) - \dfrac{\gamma M^2}{N_R}(u\Omega_{xx}+v\Omega_{xy}) \end{bmatrix}, \tag{7-3}$$

$$G = -\begin{bmatrix} b \\ bu - \frac{\Omega yx}{N_R} \\ bv + \frac{p}{\gamma M^2} - \frac{\Omega yy}{N_R} \\ (e+p)v - \left(\frac{\gamma}{\gamma-1}\right)\frac{K}{N_R P R_0}\left(1+\lambda\frac{PR}{PR_T}\right)\frac{1}{q}\frac{\partial\theta}{\partial Z} - \frac{\gamma M^2}{N_R}(u\Omega yx + v\Omega yy) \end{bmatrix} \qquad (7-4)$$

ALSO,

$$\Omega = \begin{bmatrix} \Omega xx & \Omega xy \\ \Omega yx & \Omega yy \end{bmatrix} = \mu \begin{bmatrix} \frac{\lambda}{c' k\epsilon}\left(\frac{\partial u}{\partial s} + \beta\frac{\partial u}{\partial z}\right) & (1+\lambda)\frac{1}{q}\frac{\partial u}{\partial z} \\ \left(1+\frac{\lambda}{k^2}\right)\frac{1}{\epsilon}\left(\frac{\partial v}{\partial s} + \beta\frac{\partial v}{\partial z}\right) + \frac{1}{q}\frac{\partial u}{\partial z} & \left(\frac{4}{3}+\frac{\lambda}{c'}\right)\frac{1}{q}\frac{\partial v}{\partial z} \end{bmatrix} \qquad (7-5)$$

and

$$e = \frac{C_v}{R} p + \frac{\gamma M^2}{2} \left\{ au + bv - \frac{\lambda \mu}{\varepsilon N_R} \left(\frac{1}{c' k^2} \frac{\partial u}{\partial s} + \frac{\beta}{c' k^2} \frac{\partial u}{\partial Z} + \frac{\varepsilon}{c' q} \frac{\partial v}{\partial Z} \right) \right\} \quad . \qquad \text{(VII-6)}$$

In equation (VII-5) and (VII-6), the sign change required for numerical stability (chapter V) has been introduced. For completeness,

$$\frac{p}{\rho \theta} = 1 \quad , \qquad \text{(D-17)}$$

$$\varepsilon = \frac{L_1}{L_2} \quad , \qquad \text{(D-11)}$$

$$\lambda = \frac{\rho \nu_e}{g_c \mu} \quad , \qquad \text{(D-6)}$$

$$\beta = - \frac{Z}{q} \frac{\partial q}{\partial s} \quad . \qquad \text{(VII-8)}$$

Details of the model for the effective viscosity are listed in chapter III and will not be repeated here. The function q(s) was

$$q(s) = \ell_0 + (1 - \ell_0)(2s - s^2) \quad , \qquad \text{(VII-9)}$$

where

$$\ell_0 = 1.25 \times \delta(0) \quad ,$$

was selected.

The equations above are the set which was converted to a finite difference system, using equations (IV-1), (IV-2), (IV-4), and (IV-5). The physical parameters which remain to define the boundary conditions and various coefficients which specify the physical problem under study will be defined in the following section. The equations above are written in terms of variables non-dimensionalized according to equations (D-6).

Case to be Studied

The parameters defining the case to be studied are listed in table I. The reasons for selecting this case are discussed below.

The calculations discussed in the following chapter were made with the thermodynamic properties of air (specific heat C_p, thermal conductivity κ and viscosity μ) frozen at their free-stream values. This simplification allowed a slightly less complex computer program and a corresponding savings in computer time.

The value for free-stream Mach number,

$$M_\infty = 0.13 \quad ,$$

was selected as a test of the ability of the numerical method to describe a nearly incompressible flow. The terms in the two momentum equations which involve derivatives of the pressure have a coefficient of

$$\frac{1}{\gamma M_\infty^2} \quad .$$

Thus, for small Mach numbers, the pressure gradient terms will have a very large coefficient. Even though the pressure gradients may be quite small, a certain amount of numerical noise is inevitable. For sufficiently small Mach numbers, the pressure gradient term will dominate the normal component of the momentum conservation law due to the combined effects of the huge coefficient and numerical noise. This limiting Mach number is a function of the digital computer and program used. The Mach number 0.13 led to unanticipated difficulties which are explained in the following chapter. However, the numerical solution was accomplished, and the results have been compared to the extensive experimental data available for incompressible boundary layers.

TABLE I

SUMMARY OF PHYSICAL PARAMETERS

DIMENSIONLESS PARAMETERS	CASE 1
Free Stream Mach Number, $U_0/\sqrt{\gamma g_c R T_0}$	0.13
Reynolds Number/Foot, $(\rho_0 U_0/g_c \mu_0)$	0.96×10^6
Fluid	Air
Wall Temperature, $\theta(s,0)$	0.9
Free Stream Temperature, $\theta(s,1)$	1.0
Free Stream Momentum, $a(s,1)$	1.0
Free Stream Prandtl Number, P_{R_0}	0.694
Turbulent Prandtl Number, P_{R_T}	0.8
Free Stream Pressure, $p(s,1)$	1.0
$\varepsilon = L_1/L_2$	50.
$\delta(0)/L_2$	.0185
SCALE PARAMETERS (see appendix D)	
L_2, ft.	0.2
T_0, ^oR	560.
U_0, ft/sec	150.
ρ_0, lb_m/ft^3	0.08

CHAPTER VIII

NUMERICAL METHOD

PROCEDURE FOR SOLUTION OF THE BOUNDARY LAYER PROBLEM

During development of the numerical procedure used to solve the present turbulent boundary layer problem, several seemingly slight variations in the numerical technique led to unsuccessful results. Therefore the successful technique is described and diagrammed in this chapter. The unsuccessful variations are discussed. A diagram of the program logical flow is included as figures 4a and 4b.

Since the total time needed to run a single case amounted to several hours, the program was designed to allow the calculation to be interrupted and restarted; intermediate results were stored on magnetic tape. Values of the dependent variables

$$\rho, a, b, e$$

were retained at two successive time steps, while the most recent values of temperature and pressure,

$$\theta, p$$

were retained. Storage space was assigned for a grid having fifty nodes normal to the solid boundary and forty-one nodes in the streamwise direction. As listed in table II, only various portions of the grid were used as step sizes were varied.

The difference analogs for the equations

$$\frac{\partial f}{\partial t} = \frac{\partial F}{\partial s} + \beta\frac{\partial F}{\partial Z} + \frac{\varepsilon}{q}\frac{\partial G}{\partial Z} \qquad \text{(F-1)}$$

were solved by a relaxation technique for each time step. The steps followed were:

(1) values at t_2 ($f_0(t_2)$) were estimated;

(2) the right-hand sides of the equations (F-1) were evaluated, using difference equations (IV-1), (IV-2) and (IV-4);

(3) revised predictions of the values at t_0 ($f_1(t_2)$) were calculated from equations (IV-5);

(4) the predictions were "relaxed" according to equation (VIII-1) to give a new estimate for the values at t_2 ($f_1^*(t_2)$),

$$f_1^*(t_2) = f_1(t_2) + \alpha\{f_1(t_2) - f_0(t_2)\} \quad ; \qquad \text{(VIII-1)}$$

(5) the pressure, temperature and velocity components were recalculated based on the new values $f_1^*(t_2)$.

Steps (2) – (5) were performed at each interior node in turn, sweeping the nodal pattern repeatedly until inequality (VIII-2) was satisfied for each equation at every node. The convergence test used for the iterative procedure was

$$\left[\frac{f_1(t_2)}{f_0(t_2)} - 1\right] < \pi \quad , \qquad \text{(VIII-2)}$$

where π was the convergence tolerance. When (VIII-2) had been solved at each node, the solution for time plane t_2 (the set $f^*(t_2)$) was considered complete. As indicated in figures 4a and 4b, the eddy viscosity λ was evaluated for the entire field before each sweep of the nodal pattern. Similarly, boundary conditions were adjusted as has been detailed in chapter VII.

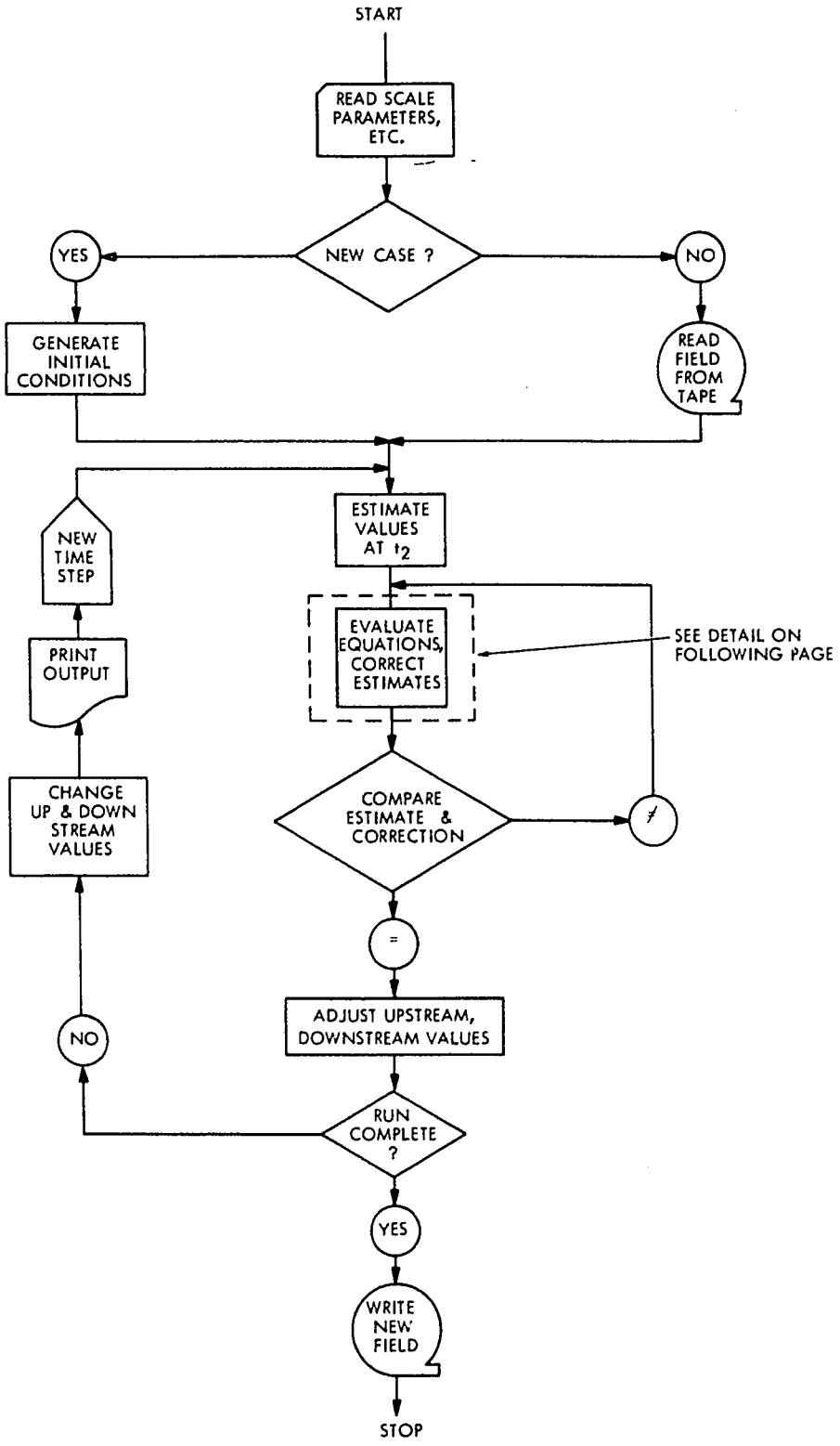

Figure 4a

FLOW CHART OF COMPUTER PROGRAM
ILLUSTRATING SOLUTION TECHNIQUE

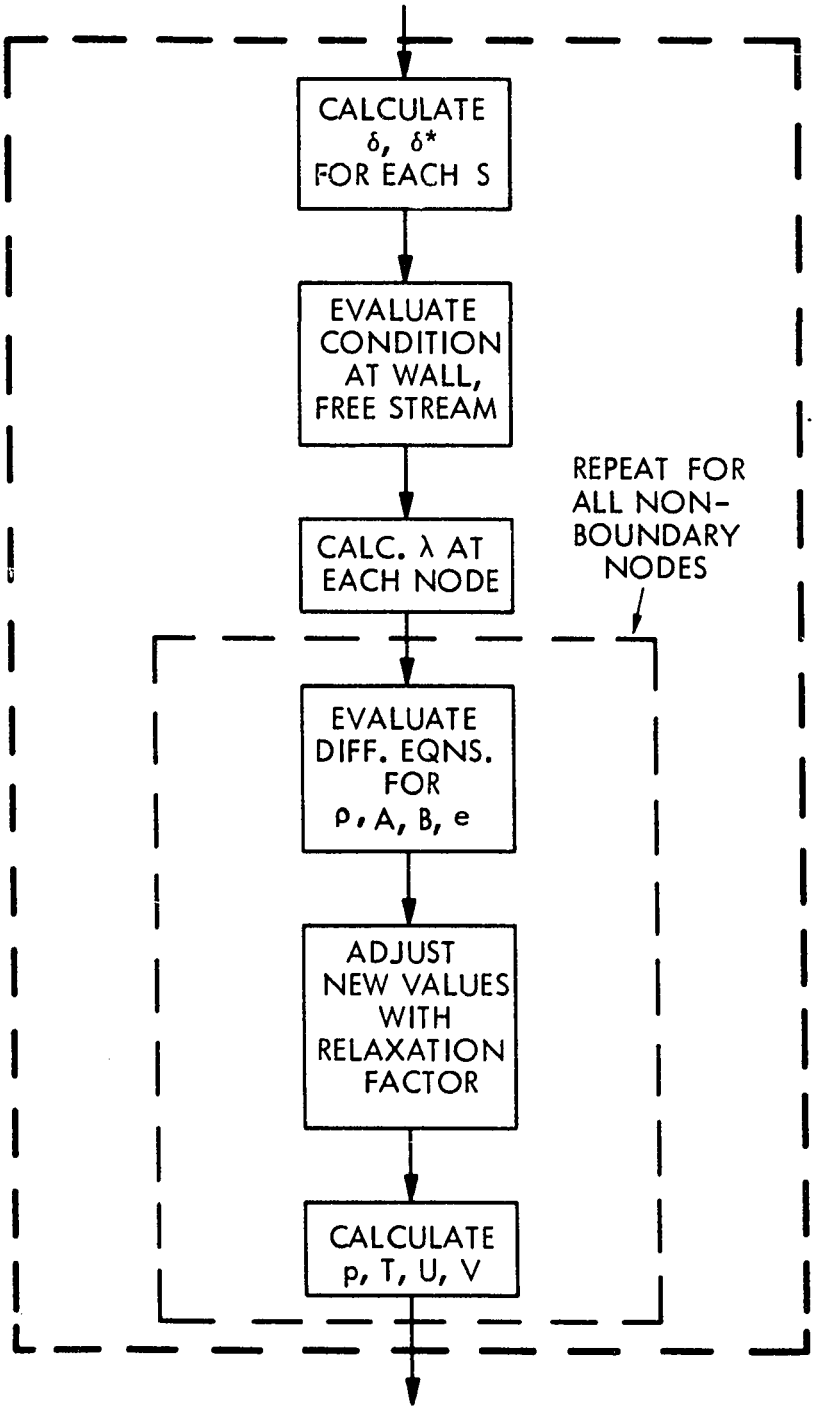

Figure 4b

DETAILS OF SEQUENCE OF CALCULATIONS USED IN ITERATIVE SOLUTION OF EQUATIONS IV-5 FOR EACH TIME STEP

An alternate method was attempted in which steps (4) and (5) were performed for the entire nodal pattern after steps (2) and (3) had been performed for the entire pattern. This scheme led to a divergence of predicted values from the estimates.

One supposedly minor modification which proved undesirable was the evaluation of the eddy viscosity at the time plane t_1, thus removing that calculation from the iterative scheme and avoiding the time loss due to its repetitive calculation. This caused the convergence ratio (left-hand side of inequality (VIII-2)) to grow with successive iterations, leading to the generation of meaningless numbers.

A matrix inversion technique, the highly-regarded ADI* method [40], was programmed as an attempt to obtain a more rapid and efficient solution. No solution was obtained using the ADI method, and successive iterations led to divergence between the estimates and resulting predictions.

In chapter VII, the effect of the pressure gradient term in the normal component of the momentum equation in restricting the study of low Mach number flows was described. Several attempts were made to reduce the random character of that gradient term. Low-order polynomials were fitted to the pressure values at nodes across the boundary layer, and the term

$$\frac{\partial p}{\partial Z}(Z)$$

was evaluated analytically at each node. No improvement in the behavior of calculated values of b (s,Z) was observed. Attempts to smooth the function G(Z) in the normal component of the momentum equation

*Alternating – Direction Implicit

(equation (VII-4)) and b(s,Z) itself were also unsuccessful.

Selection of values for the relaxation factor α in equation (VIII-1) was critical in obtaining a solution. Optimum values of $\alpha > 1$ have been reported for linear difference equations [49]. For most of the current work,

$$\alpha = .08 \qquad \text{(VIII-3)}$$

proved to be a more suitable value. For larger values, successive estimates and the resulting predictions from equation (VIII-1) diverged.

Due to the small relaxation factor required, the selection of the starting estimate $f_0(t_2)$ became important as the time derivatives became small. Three estimates have been employed in various phases of the present work:

$$(1) \quad f_0(t_2) = f(t_1) \quad , \qquad \text{(VIII-4)}$$

$$(2) \quad f_0(t_2) = f(t_1) + [f(t_1) - f(t_0)] \qquad \text{(VIII-5)}$$

and

$$(3) \quad f_0(t_2) = f(t_1) + \frac{1}{2}[f(t_1) - f(t_0)] \quad . \qquad \text{(VIII-6)}$$

Equations (VIII-4) and (VIII-5) bracket the eventual solution; equation (VIII-6) is the arithmetic average of the other predictions.

Briefly, as time derivatives become small (approaching steady state) during the numerical solution, inequality (VIII-2) would be satisfied after only a few (2-4) iterations. Since only a small portion of the predicted change was allowed by equation (VIII-1), a significant error could be introduced unless the tolerances π were made quite small. This error could be reduced by placing the initial estimate $f_0(t_2)$ at each node near the eventual solution. Equations (VIII-5) and (VIII-6) are attempts to refine that initial estimate based on simple assumptions about the derivative

$$\frac{\partial f}{\partial t} \cdot$$

The consequences of these prediction schemes are presented in chapter IX.

In this chapter, details of the relaxation technique used to solve equations (VII-2) — (VII-6) have been presented, and unsuccessful modifications to that technique have been listed. Numerical results are presented in chapter IX.

CHAPTER IX

NUMERICAL SOLUTION FOR THE CASE $M_\infty = 0.13$

The numerical solution for the case characterized by

$$M_\infty = 0.13$$

is presented and discussed in this chapter. The case has been divided into runs, each of which demonstrates a specific point. These runs are described separately and are summarized in table II.

The computer code was developed and exploratory studies were run on the Rice University IBM* 7040 computer system. Runs A-E were generated on the Univac** 1108 computer system at the National Aeronautics and Space Administration — Manned Spacecraft Center (NASA — MSC), Houston, Texas. All other runs were made on the IBM 360/75 computer system at the Oak Ridge National Laboratory (ORNL), Oak Ridge, Tennessee.***

In the discussions which follow, frequent reference is made to figures 5 and 6, which trace the development in time of the streamwise momentum at selected nodal locations.

---

*International Business Machines Incorporated.

**Sperry Rand Corporation.

***Operated for the United States Atomic Energy Commission by Union Carbide Corporation.

TABLE II – SUMMARY OF NUMERICAL PARAMETERS

Run	Time Steps Equiv[1]	Time Steps Actual	Computer Time, Hours[2]	ΔZ[3],	Step	Size	And	Number	Of	Steps		Description
				Inner				Intermediate		Outer		
A	255.6	2556.0	~1.0	.02083	3	.0625	3	.1875	4	-	0	1st Runs on Univac 1108
B	34.0	340.0	~0.3	.02083	6	.0417	3	.0835	9	-	0	New Model; Rescue Run A
C	360.0	360.0	0.5	.02083	6	.0417	3	.0835	9	-	0	Start New Model at Initial Conditions
D	40.0	40.0	0.1	.02083	6	.0417	3	.0835	9	-	0	Remove Artificial Viscosity
E	860.0	860.0	0.8	.02083	6	.0417	3	.0835	9	-	0	Add Exponential Factor to Model
F	40.0	40.0	0.2	.02083	6	.0417	3	.0835	9	-	0	IBM 360/75 – Start at $\frac{1}{7}$ Profile
G	250.0	250.0	0.9	.02083	6	.0417	3	.0835	9	-	0	Continuation of Run E on 360/75
H	170.0	170.0	0.6	.02083	6	.0417	3	.0835	9	-	0	New Procedure for Initial Estimation for Iteration
I	275.0	550.0	2.0	.01042	12	.0313	4	.0939	8	-	0	Halve ΔZ
J	49.0	196.0	5.9	.0051	21	.0156	12	.0469	15	-	0	Halve ΔZ again
K	20.0	1600.0	1.5	.00104	8	.00417	6	.0167	6	.0667	13	Nodes in Laminar Sub-Layer; Start at $\frac{1}{7}$
L	22.0	4400.0	2.9	.00104	8	.00417	6	.0167	6	.0667	13	Continue J, $\Delta Z/5$

[1]One Equivalent Time Step is 2.78×10^{-5} Seconds of Scale Time.
[2]Productive Run Time including Negligible Amounts of Program Compilation. Does not include unproductive and experimental time.
[3]ΔS, Longitudinal Step Size, was 0.10 for all runs (10 Steps).

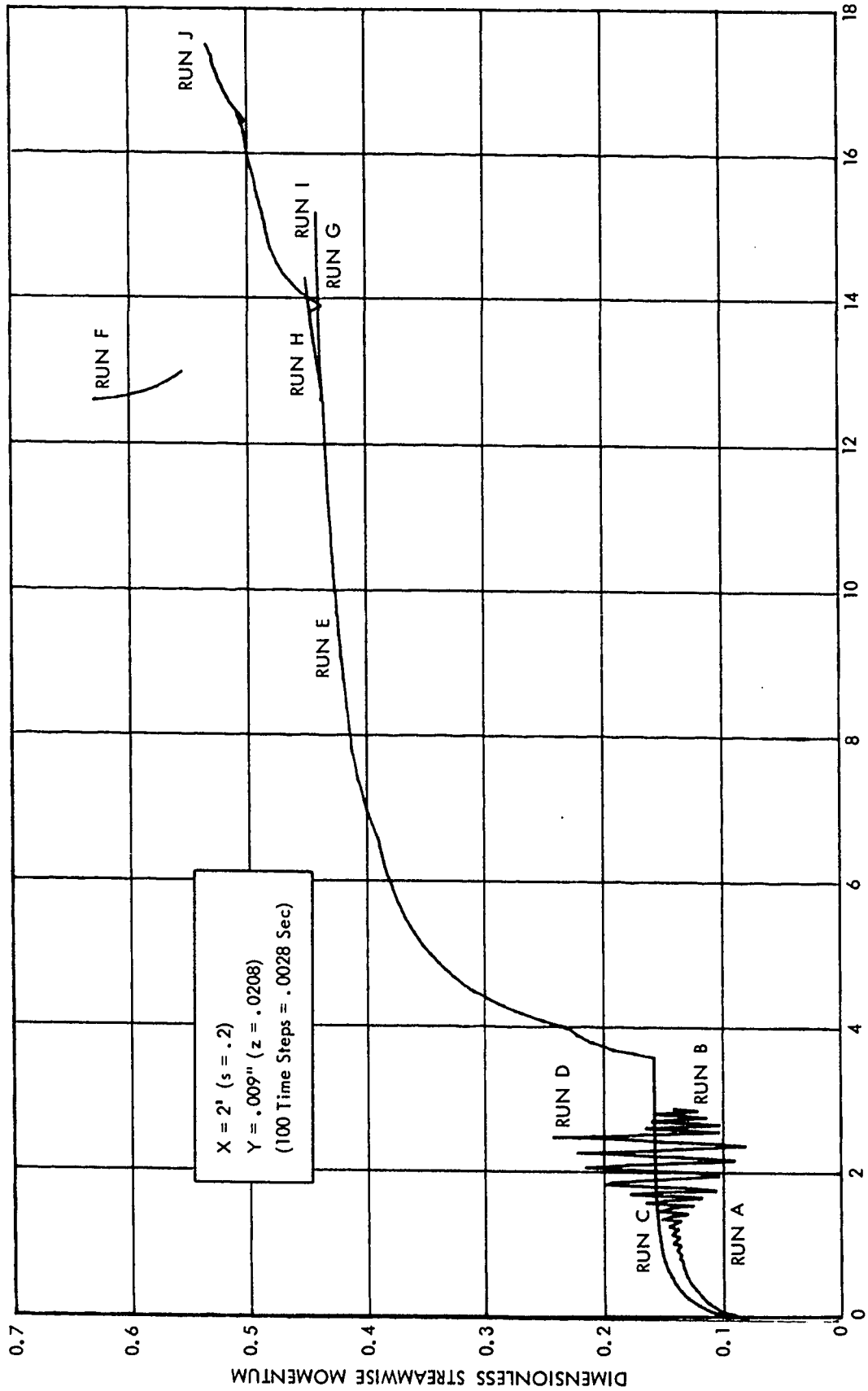

Figure 5

DEVELOPMENT OF STREAMWISE MOMENTUM
AT AN UPSTREAM NODE (NODE 3) WITH INCREASING TIME

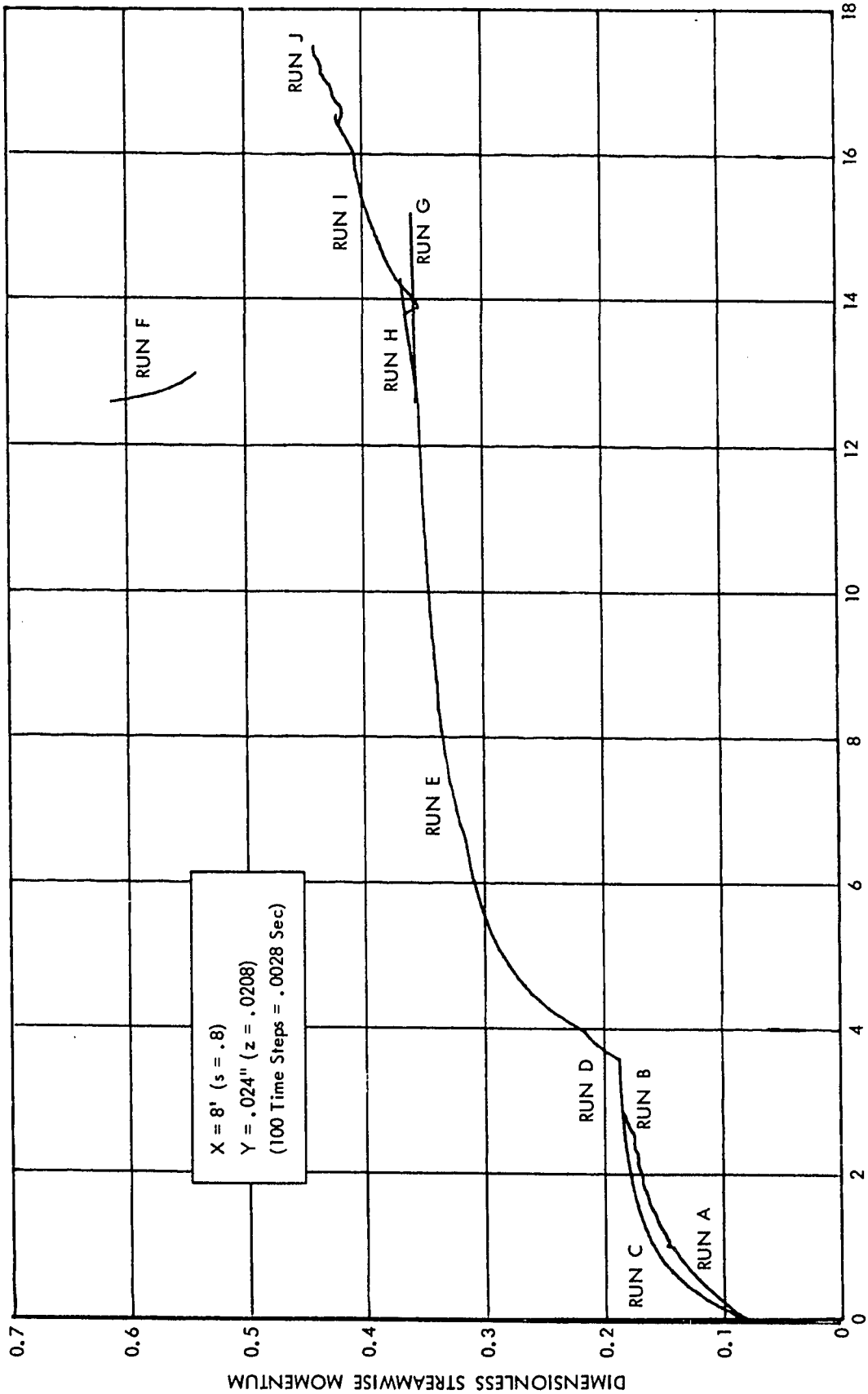

Figure 6
DEVELOPMENT OF STREAMWISE MOMENTUM
AT A DOWNSTREAM NODE (NODE 9) WITH INCREASING TIME

Figure 5 follows the momentum at a node near the solid boundary (node 3) and near the upstream boundary (s = 0.2) of the numerical region.

Figure 6 follows the same component of momentum at a node (node 9) much further downstream (s = 0.8) and removed from the influence of the upstream boundary conditions.

Run A

This exploration run was started with the initial conditions specified in chapter VI. As is seen in figure 5, the values at node 3 began an oscillation at about the one hundredth time step. If a curve similar to figure 5 were plotted for values of normal momentum at node 3, similar oscillations would be visible in the earliest time steps. The oscillations were quite violent, including rapid sign changes, and eventually were transmitted to the specific flow energy and pressure and finally appeared in the streamwise momentum. From figure 6, values of streamwise momentum at node 9 showed no evidence of these oscillations.

This oscillatory behavior of the streamwise momentum during run A led to a careful reexamination of the numerical stability conditions as described in chapter V and appendix F.

Run B

The model for the turbulent stress tensor was revised to assure numerical stability as described in chapter III. Run B was a continuation of run A to demonstrate the stable behavior of the revised model. In figure 5, the immediate reduction in the amplitude of the oscillations can be seen. The value at node 9 remained stable but showed an upward movement which approached the values obtained in run C.

The step size ratio (see chapter IV) was changed from run A to run B. However, various values of the ratio have been used in runs J and K with no indications of instability. Therefore, the oscillatory behavior of the momenta seen in run A is attributed to the model used in that run.

Run C

Run C was started at the initial condition and proceeded to what was virtually a steady-state solution. Although the solution obtained is far from that expected, the results of this run show no evidence of oscillation and demonstrate that, with the model selected, a steady-state solution can be attained. Runs D and E explore improvements in the model which allow closer agreement between the calculated results and solutions for the classical, incompressible boundary layer equations.

Run D

When considering numerical stability, one line of argument led to the addition of a constant term to the value of eddy viscosity, λ, at each node. For run D, this constant was eliminated with the improvement in the calculated values as shown in figures 5 and 6. The marked change in the velocity profile due to the removal of the constant term from λ suggests that the Artificial Viscosity technique, often applied to control numerical stability when using explicit difference schemes (see [12]), would be difficult to apply to a turbulent boundary layer solution.

Run E

In run E, the exponential factor suggested by Van Driest [37] (see chapter III) was added to the eddy viscosity model. The improvement

in the calculated value is again obvious from the upward changes in the traces in figures 5 and 6.

Run F

Examination of the results of run E led to the conclusion that the calculation would not converge to the expected solution. As a check on this conclusion, run F was started at the expected answer, the experimentally-proven one-seventh power law for the velocity profile:

$$a(s,Z) = a(s,\infty)\left(\frac{Zq(s)}{\delta(s)}\right)^{1/7} \quad . \qquad \text{(IX-1)}$$

The thickness profile was based on that velocity profile and a von Karman integral solution for the boundary layer equations:

$$\delta(s) = \frac{0.4L_1 s}{(N_{RS})^{1/5}} \quad . \qquad \text{(IX-2)}$$

As the figures illustrate, the calculated values immediately moved toward those obtained in run E, demonstrating that the steady-state solution to the difference equations with the stated step sizes and model parameters was not equation (IX-1).

Run G

Run G was a continuation of run E. This run established the correctness of the conversion from the Univac 1108 system to the IBM 360/75 system. It was established during this conversion that double precision arithmetic was required to continue this case on the system /360.

Run H

Run H started at the same point as run G, but equation (VIII-6) was used to generate initial estimates for the solution at each time step. In both runs G and H, the relaxation factor α was 0.08, and

only two or three iterations were required to solve the equations at each time step. The difference between runs G and H (seen on both figure 5 and 6) demonstrates the effect of starting estimates for the solution at each time step, as discussed in chapter VIII.

Runs I and J

The results of run H (or G) do not approach the expected solution. In runs I and J, the step size ΔZ was systematically reduced in the region nearest the solid boundary. The step size used in run I was one-half that used in run H, and the step size used in run J was one-half that used in run I. In each case, the initial values for the dependent variables were generated at the newly-added nodes by parabolically interpolating the previous results. Referring to the earlier discussion of run B, the step size ratio was the same as that used in run A, and no instability was evident. This tends to support the conclusion that the damping of oscillations accomplished in run B was due to model changes and not step size ratio adjustments.

It is apparent from the figures that the numerical solution is not approaching the expected solution. In order to formalize this conclusion, the traces for runs H, I and J at nodes 3 and 9 were fitted with an exponentially decaying curve,

$$f = A + B \exp(-Ct) \quad ,$$

which was then extrapolated to infinite time (the steady state). These extrapolated values have been plotted against step size ΔZ in figure 9. Clearly, when these values are extrapolated to zero step size, they do not agree with the expected solution, equation (IX-1).

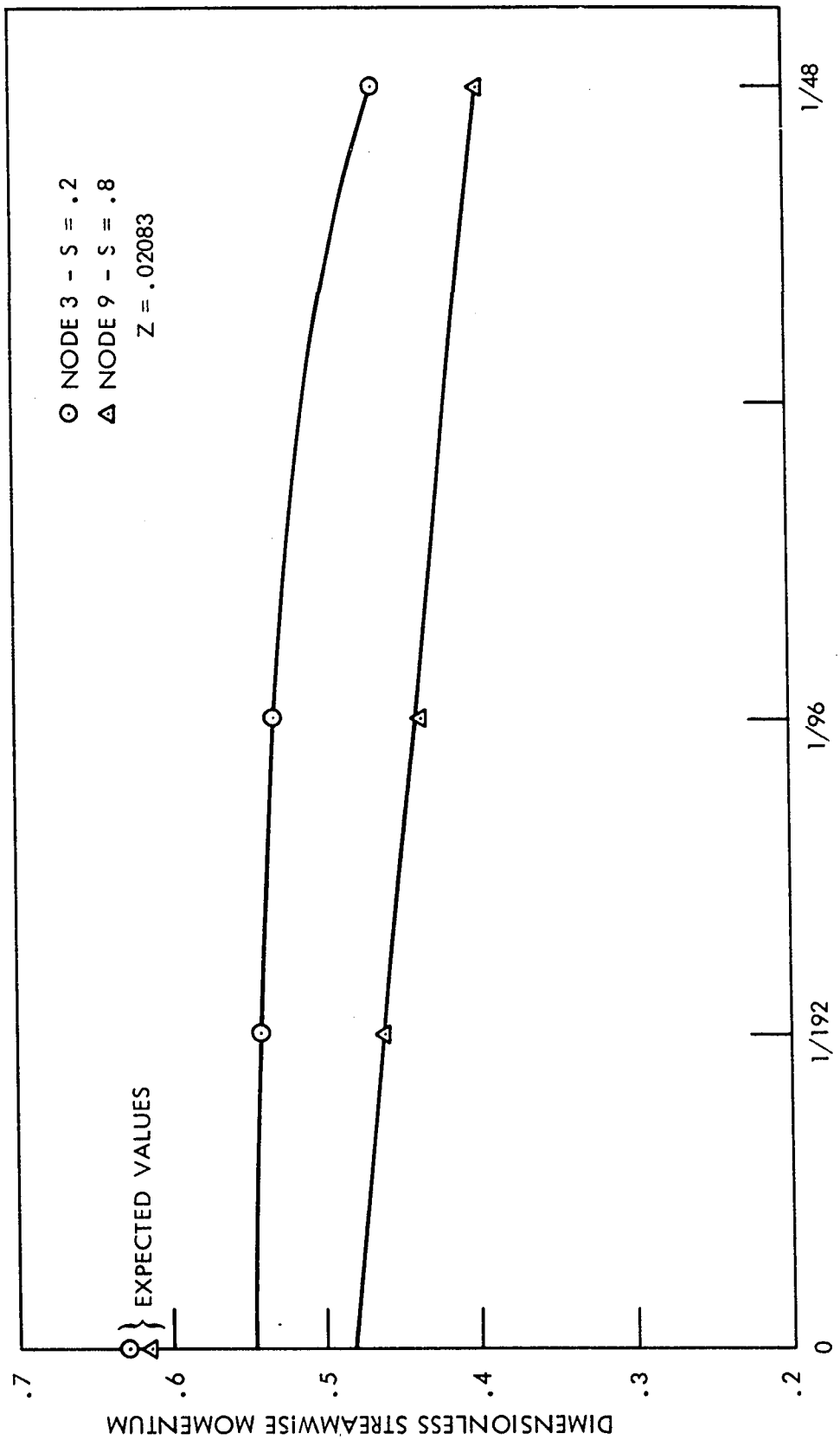

Figure 7
EXTRAPOLATION OF STREAMWISE MOMENTUM AT SELECTED NODES
TO ZERO STEP SIZE IN NORMAL DIMENSION

A careful analysis of the results of run J revealed that values calculated for τ_W, the wall shear stress, were about 50% low when compared to correlations based on data for incompressible flow (figure 9). Since τ_W is calculated from the velocities at nodes immediately adjacent to the solid boundary, the values for those velocities were examined. The viscous sublayer is a thin region in which the effect of the dynamic viscosity of the fluid is of the same magnitude as the eddy viscosity due to the turbulence. For run J (and all previous runs), the node nearest to the solid boundary was located well outside the viscous sublayer. Thus the influence of an entire physical region on the velocity profile was eliminated by the choice of grid spacing near the boundary. Since the wall shear stress τ_W depended strongly upon the velocity profile within that region, erroneous values for the shear stress were inevitable.

When the initial conditions were set up (run C), the velocity profiles which were generated resulted in a value for the displacement thickness of about twice the value predicted by the "one-seventh law" velocity profile. Although the velocity profile resulting from run J was much different from the initial profile, values for the displacement thickness, δ^*, remained at about twice the expected value. The explanation was simply that the momenta at nodes away from the immediate vicinity of the solid boundary were changing very slowly. However, most of the contribution to δ^* (equation (III-2)) was from the more distant nodes, so that marked changes in the velocity profile near the wall caused only slight changes in δ^*.

Run L

The results of run J were parabolically interpolated, placing four additional nodes in the region between the wall and the innermost node used in run J. At least two of those nodes were expected to lie within the viscous sublayer. The values generated by this interpolation were used as initial conditions for run L.

The results of run L are represented on figures 5 and 6 as about the last one-tenth of an inch on the traces labeled "Run J". Run L was terminated due to excessive use of computer time (see table II) without completing sufficient time steps to extrapolate run L and add the result to figure 7. The values of the wall shear stress did increase significantly however.

From the entire span of figures 5 and 6, the momenta are clearly approaching the neighborhood of the expected values (shown by the starting points for run F). This tends to verify the fundamental assertion that the time-marching technique will "automatically" seek the steady state solution if the flow is modeled correctly and the boundary conditions are correct. The indifferent changes in the calculated values for the displacement thickness (ranging from a 25% reduction at $s = 0.3$ to virtually no change for $s > 0.7$) establish that the convergence to steady state is at best very slow for equations representing nodes further removed from the solid boundary. Because this slow convergence would require large blocks (estimated at several hours) of computer time to complete run L, the run was not continued.

Expected Results

To this point, the standard to which the numerical results are being compared has been only vaguely defined. In this section, the

correlations of experimental data which have been termed "expected results" are stated.

Data relating to the turbulent boundary layer, especially velocity profiles, have been compiled and organized by Hinze [6]. Velocity profiles are presented in the form of

$$\frac{u}{u_\tau} = f\left(\frac{u_\tau y}{\nu}\right) \quad ,$$

where u is the streamwise velocity, u_τ is the shear velocity (defined in chapter III of this work), ν is the kinematic viscosity of the fluid and y is the normal distance from the solid boundary. These correlations are presented in table III.

TABLE III

CORRELATIONS OF VELOCITY PROFILES TO BE USED AS STANDARDS FOR COMPARISON TO NUMERICAL RESULTS

Range of $\frac{u_\tau y}{\nu}$	Correlation	
≤ 10	$\frac{u}{u_\tau} = \frac{u_\tau y}{\nu}$	(IX-3)
10-200	$\frac{u}{u_\tau} = 2.44 \ln\left(\frac{u_\tau y}{\nu}\right) + 4.9$	(IX-4)
> 200	$\frac{u}{u_\tau} = 8.3\left(\frac{u_\tau y}{\nu}\right)^{1/7}$	(IX-5)

In order to evaluate u_τ, two further relationships are necessary:

$$C_D = 0.0583 \left(\frac{\rho U x}{g_c \mu}\right)^{-0.2} \qquad \text{(IX-6)}$$

and

$$\frac{u_\tau}{U} = \left(\frac{C_D}{2}\right)^{1/2} . \qquad \text{(IX-7)}$$

In these equations, the group

$$N_x = \left(\frac{\rho U x}{g_c \mu}\right)$$

is the local length Reynolds number and C_D is the local drag of friction coiefficient. As presented in [6], the experimental data show a spread of roughtly ±5% about the correlations.

Run K

The initial conditions specified for run K were approximately the expected results. Specifically, the momenta profiles were generated from equations (IX-1) and (IX-2), using the grid spacing from run L.

Time-momentum traces are shown in figure 8. The momenta at node 3 and node 9 are virtually constant over the entire run. The time derivatives for run K are compared to those for run J in table IV.

TABLE IV

COMPARISON OF TIME DERIVATIVES OF NON-DIMENSIONAL STREAMWISE MOMENTUM

	Time Derivative, Units/Standard Time Step	
	Node 3	Node 9
Run J	0.0057	0.0069
Run K	-0.0002	0.0002

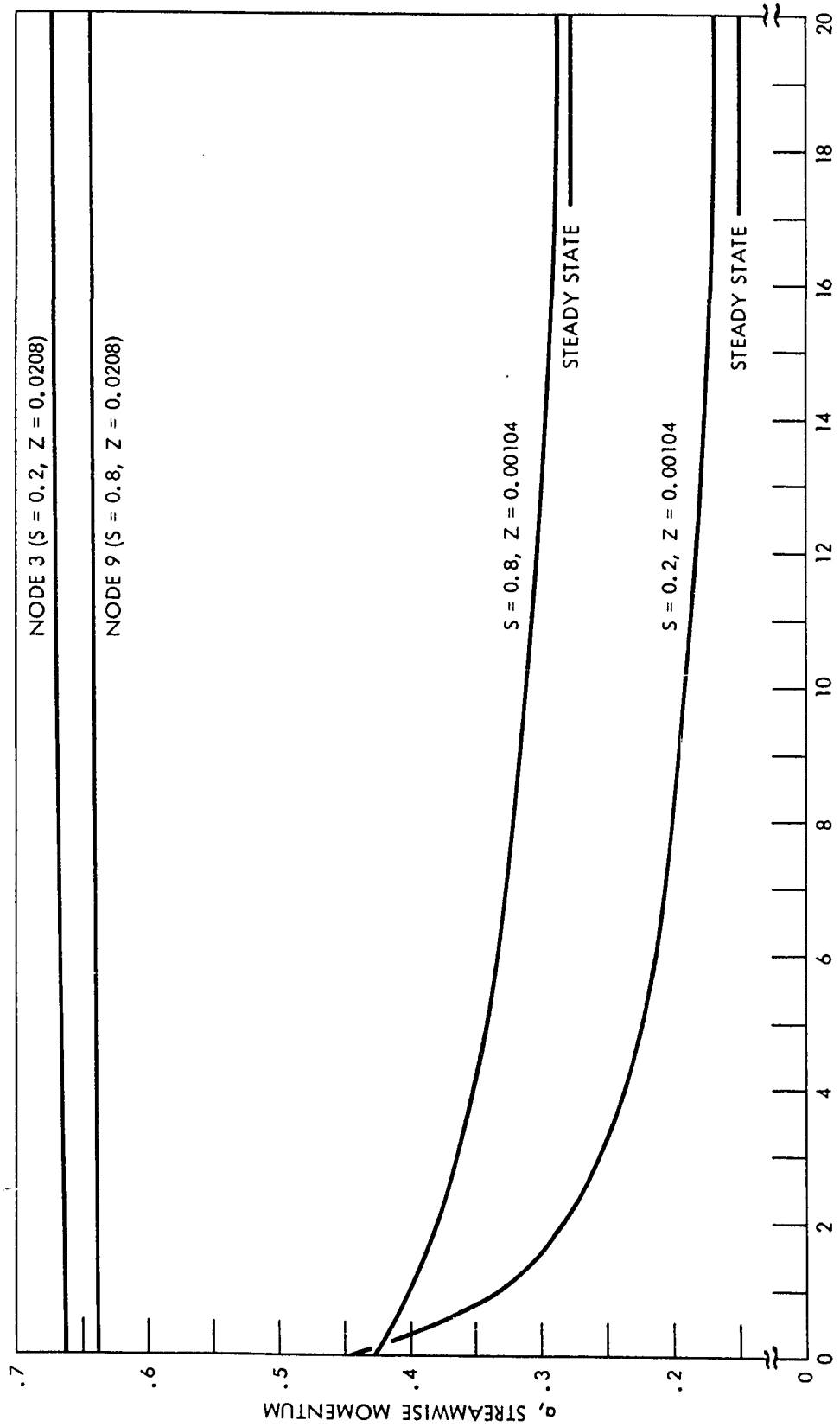

Figure 8

RUN K - TIME HISTORIES FOR NODE 3, NODE 9, AND THE NODES NEAREST THE SOLID BOUNDARY AT THE SAME STREAMWISE LOCATIONS

The small value of time derivatives for run K relative to run J indicate that, at least at these nodes, the difference equations have nearly converged to a steady state. Momenta at the nodes nearest the solid boundary (within the sublayer) show a rapid initial decrease, then approach (apparently assymtotically) values lower than the initial conditions. This is explained by the fact that equation (IX-1) does not apply within the sublayer. A similar trend is illustrated for the momentum at the corresponding node at each streamwise station by figure 9. The drag coefficient profile for run K starts far above the expected profile but has closed to the immediate neighborhood of the profile at the end of the run.

Velocity profiles for runs C, L and K at two streamwise locations (s = 0.2 and s = 0.8) are compared to the expected results in figures 10 and 11. The movement of the momenta from their starting values for run K toward the expected results for the sublayer is evident.

The difference between the velocity profiles from run K and the expected values, as seen in figures 10 and 11, is about 8% for the upstream (s = 0.2) station and 5% for the downstream (s = 0.8) station. This is roughly the amount of spread in the data correlated in [6]. If the profiles from run K were presented as plots of

$$\frac{u}{u_\tau} \text{ vs } \frac{u_\tau y}{\nu}$$

instead of

$$\frac{u}{U} \text{ vs } \frac{y}{L_2} \quad ,$$

the calculated curve would lie much closer to the expected (theory) curve. Conversely, if the data presented in [6] were plotted on figures

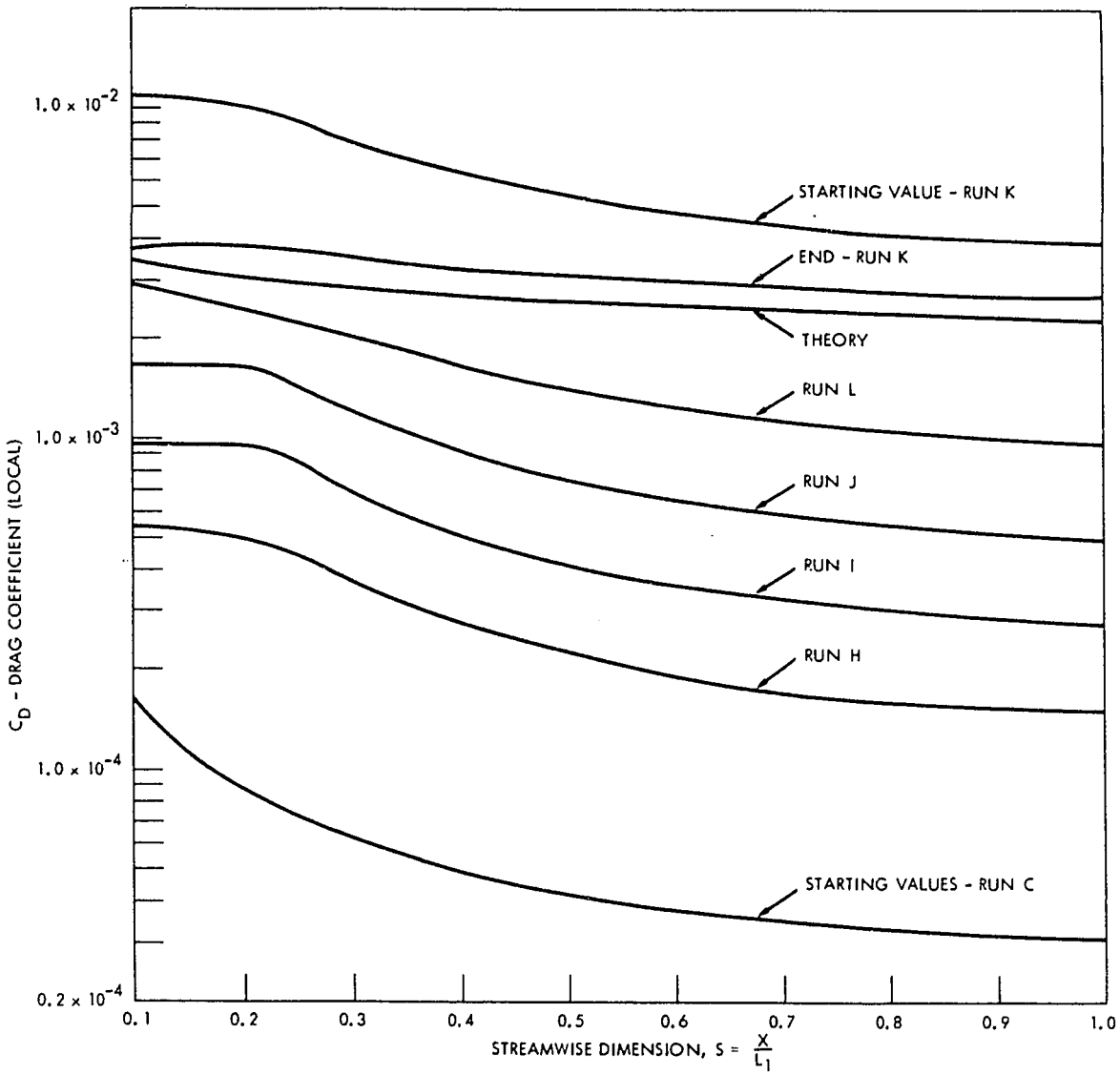

Figure 9

PROFILES OF LOCAL DRAG COEFFICIENT
FOR VARIOUS RUNS

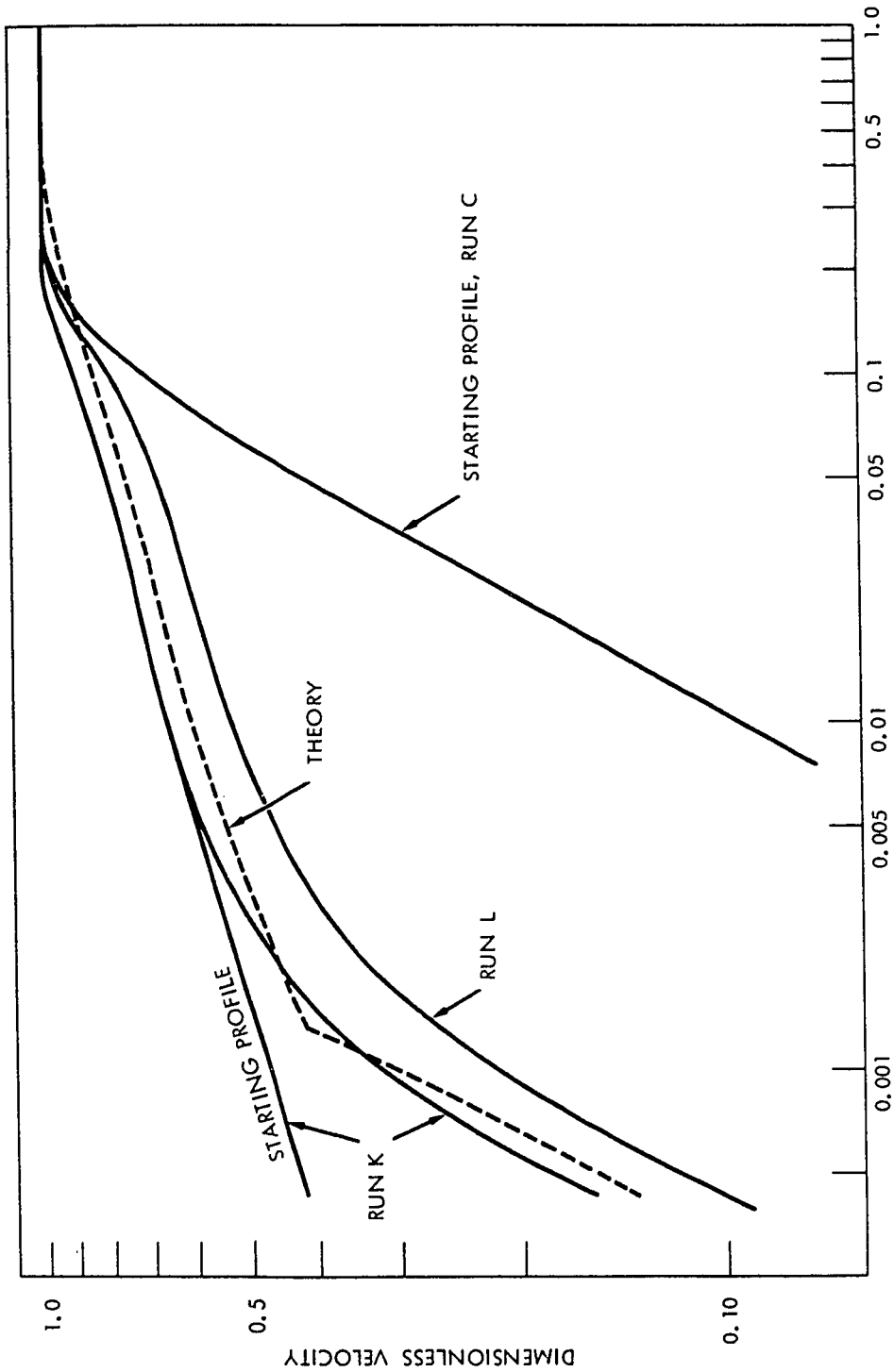

Figure 10
UPSTREAM VELOCITY PROFILES RESULTING
FROM VARIOUS RUNS
(s = 0.2)

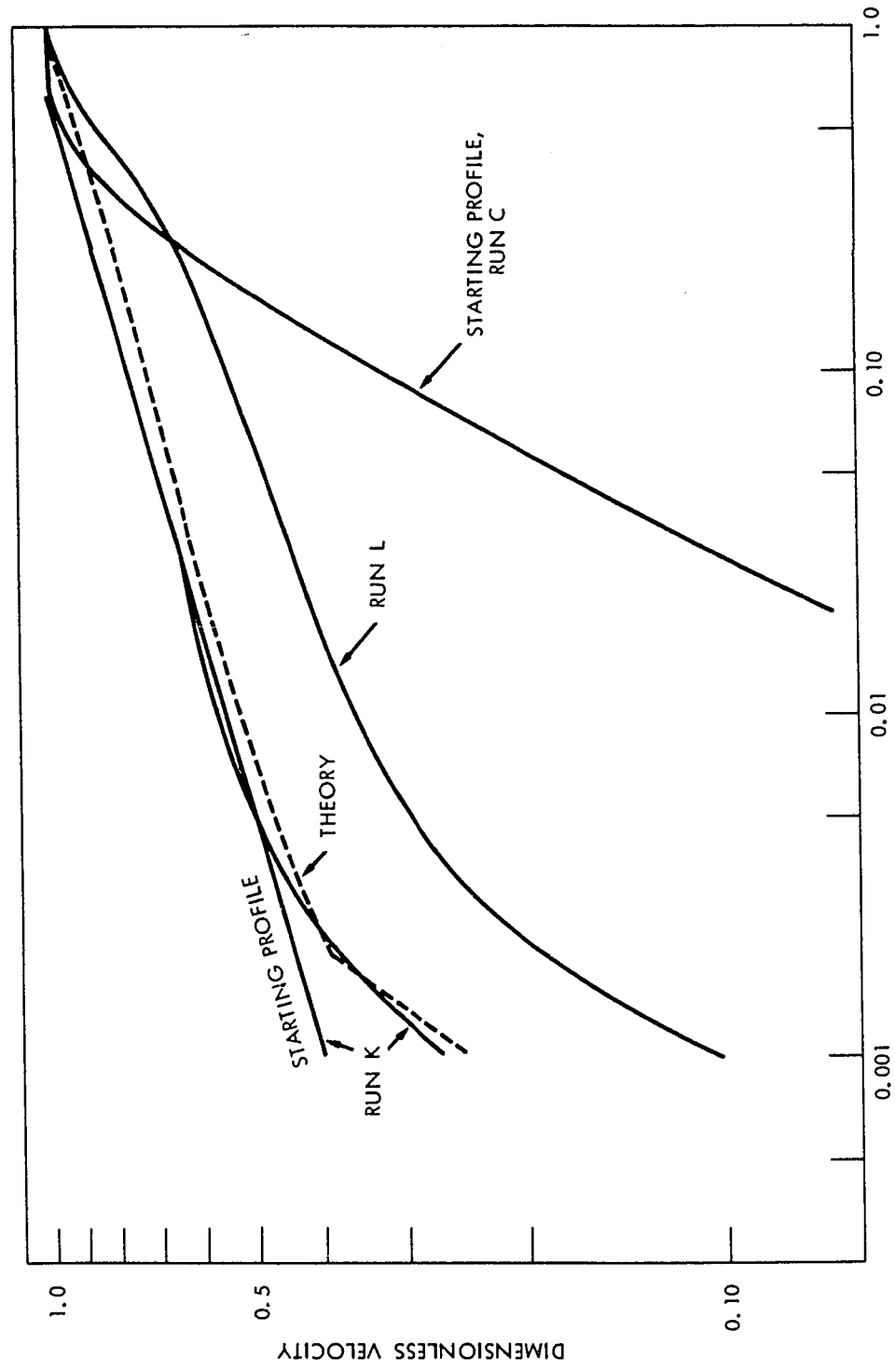

Figure 11
DOWNSTREAM VELOCITY PROFILES RESULTING FROM VARIOUS RUNS
(S = 0.8)

10 and 11, the spread would probably be greater than ±5%.

However, if the difference between the numerical solution and theory were unacceptable, it could be eliminated by judicious adjustment of the seven constants required by the empirical model for the turbulent fluctuation averages (chapter III and appendix C).

ΔS Parametric Study

A number of runs were attempted to investigate the error due to truncation of the series expansion for the streamwise derivatives, equation (IV-4). Those runs were difficult because of the coupling between the laminar profile at the upstream boundary and the first column of nodes downstream. Runs with

$$\Delta S = 0.05$$

(halving the step size used on all other work) were attempted, duplicating the area covered by run G (see figures 5 and 6). The difference equations at the streamwise location S = 0.02 were ill-behaved, but sufficient time steps were taken to establish a trace of node 9 which was essentially identical to that shown for run G on figure 6. The step size

$$\Delta S = 0.10$$

was thus judged to cause negligible truncation error in the difference equations.

Discussion of Limiting Time Step Size

In chapters VII and VIII, the effect of the term

$$\frac{\partial p}{\partial Z}$$

is dominating the equation for the normal component of momentum is

described. That term is actually the factor which determines the maximum time step which may be taken.

The initial conditions as set up for run C (or run K) contain no numerical noise. In table V, the time derivatives at node 3 are listed for the initial conditions for run C and after only a single iteration. The immediate dominance of the term

$$\frac{\partial b}{\partial t}$$

by the noise is obvious, and the non-dimensional time step must be selected sufficiently small to control this noise. Furthermore, since this noise is related to the flow Mach number, it does not diminish as steady state is approached but remains relatively constant. For the case

$$M_\infty = 0.13$$

described in this chapter, the grouping

$$\left(\frac{L_1\ \Delta t}{L_2\ \Delta Z}\right)$$

took a maximum value of 1.0 or less.

TABLE V

COMPARISON OF TIME DERIVATIVES AT NODE 3
CALCULATED FROM INITIAL CONDITIONS USING EQUATIONS (VII-1)
$M_\infty = 0.13$

	$\frac{\partial a}{\partial t}$	$\frac{\partial b}{\partial t}$	$\frac{\partial e}{\partial t}$
From Initial Conditions	-43.	.60	-280.
After One Iteration	-2.8	-3850.	770.

CHAPTER X

CONCLUSIONS AND RECOMMENDATIONS

The conclusions which have been reached regarding the numerical technique under study in this work are collected in this chapter. Recommendations for further work are listed.

It is evident from the numerical results presented in chapter IX that the time-marching technique, when combined with the model for the apparent turbulent stress presented in chapter III, will provide an adequate description of the fluid in the wall region of a compressible, turbulent boundary layer.* A number of qualifications must be stated for this conclusion:

1. A constant term (such as the artificial viscosity often used in explicit time-marching schemes) should not be added to the model for the eddy viscosity.
2. At each streamwise location on the finite difference mesh, at least one node must be within the region nearest the solid boundary in which the dynamic viscosity of the fluid is the same magnitude as the eddy viscosity.

---

*This conclusion was strengthened by the results of a second case, run at $M_\infty = 0.6$, which duplicated the numerical behavior reported for run K in chapter IX. This case roughly duplicated experimental results reported in [48]. The assistance of Dr. Serafini, National Aeronautics and Space Administration, Lewis Research Center, Cleveland, Ohio, in augmenting the published data from his private records is gratefully acknowledged.

3. Any alternate model which might be considered to describe the apparent turbulent stress tensor should be constructed with careful attention to numerical stability.
4. The numerical treatment of mathematical boundary conditions which is described in chapter VI is preferred. In particular, upstream and downstream conditions should be changed only after each time step while solid boundary and free stream conditions may be updated after each iteration.
5. When sweeping the nodal network during an iteration, newly-calculated values for the variables at each node must be used as soon as they are calculated. This was discussed in chapter VIII.

It is obvious that the algorithm as presented in this work requires large amounts of computer time to solve a specific problem. For that reason, the convergence of the numerical solution to a physical solution has not been absolutely verified within the outer portion of the boundary layer.

The large computer times required result from the effects of numerical noise on the normal pressure gradient term and the dominance of the equation for the normal component of momentum by the pressure gradient. After examining the behavior of the other equations (VII-1), it is concluded that control or avoidance of that numerical noise would allow much larger time steps, thus requiring much less computer time for solution of a particular problem. Therefore additional development effort could be profitably directed at a controlled, efficient solution of the equation for the normal momentum.

The time-marching technique requires less a priori knowledge of (or assumptions about) the properties of the turbulent boundary layer. It is recommended that this technique be applied to the study of those boundary layer situations in which the basis for broad assumptions about the nature of the flow is uncertain. A typical (but far from exhaustive) list of these situations includes:

1. Flow negotiating substantial free-stream pressure gradients, including near-separation conditions,
2. Flow along non-uniformly heated or cooled walls,
3. Flow along a boundary with mass injection into or removal from the boundary layer,
4. Flow along a moderately curved boundary.

It is also suggested that the time-marching technique is a useful tool for exploration of the effects of alternate models for the turbulent stress tensor on boundary layer solutions.

BIBLIOGRAPHY

1. Schlichting, H., Boundary Layer Theory, McGraw-Hill, New York, 1960.

2. Shapiro, A. H., The Dynamics and Thermodynamics of Compressible Fluid Flow, Ronald Press, New York, 1953.

3. Lamb, H., Hydrodynamics, Dover, New York, 1945.

4. Wylie, C. R. Jr., Advanced Engineering Mathematics, McGraw-Hill, New York, 1951.

5. Taylor, A. E., Advanced Calculus, Ginn and Co., Boston, 1955.

6. Hinze, J. O., Turbulence, An Introduction to Its Mechanism and Theory, McGraw-Hill, New York, 1959.

7. Chapman, A. J., Heat Transfer, MacMillian, New York, 1960.

8. Van Driest, E. R., "Turbulent Boundary Layer in Compressible Fluids", J. Aero. Sci., Vol. 18, No. 3, 1951, p. 145.

9. Goldstein, S., Modern Developments in Fluid Dynamics, Dover, New York, 1965.

10. Kutateladze, S. S. and Leont'ev, A. I., Turbulent Boundary Layers in Compressible Gases, Academic Press, New York, 1964.

11. McWhirter, R. W. P., "Departure from Local Thermodynamic Equilibrium", United Kingdom Atomic Energy Authority CLM-P150, October, 1967.

12. Walker, W. F., Zumwalt, G. W. and Fila, L. J., "Numerical Solution for the Interaction of a Moving Shock Wave With a Turbulent Mixing Region", Trans. ASME, Series E, 1968, p. 220.

13. Axiz, K., "A Numerical Study of Cellular Convection", Ph. D. Dissertation, Rice University, May, 1966.

14. Roache, Patrick J. and Muller, Thomas J., "Numerical Solution of Compressible and Incompressible Laminar Separated Flows", AIAA Paper No. 68-741, June, 1968.

15. Lax, P., "Weak Solutions of Nonlinear Hyperbolic Equations and Their Numerical Computation", Comm. Pure and Appl. Math., Vol. VIII, 1954, p. 159.

16. Trulio, J. G., "Numerical Solution of the Equations of Continuum Motion:Vortex Formation and Shedding in a Viscous Compressible Fluid", NASA TM-X57779, June, 1966.

17. Fromm, J. E., and Harlow, F. H., "Numerical Solution of the Problem of Vortex Street Development", Phys. Fluids, Vol. 6, No. 7, 1963, p. 975.

18. Steiger, M. H. and Sepri, P., "On the Solution of Initial-Valued Boundary Layer Flows", Polytechnic Institute of Brooklyn PIBAL Report No. 872, May, 1965.

19. Zeiberg, S. L. and Bleich, G. D., "Finite Difference Calculations of Hypersonic Wakes", AIAA J., Vol. 2, 1964, p. 1396.

20. Kramer, R. F. and Lieberstein, H. M., "Numerical Solution of the Boundary-Layer Equations Without Similarity Assumptions", J. Aero. Sci., Vol. 26, 1959, p. 508.

21. Davis, R. T. and Flugge-Lotz, I., "Second-Order Boundary-Layer Effects in Hypersonic Flow Past Axisymmetric Blunt Bodies", J. Fluid Mech., Vol. 20, 1964, p. 593.

22. Schaaf, S. A. and Chambré, P. L., Flow of Rarefied Gases, Princeton University Press, Princeton, New Jersey, 1961.

23. Burstein, S. Z., "Numerical Methods in Multidimensional Shocked Flows", AIAA J., Vol. 2, No. 12, 1964, p. 2111.

24. Fromm, J. E., "Finite Difference Methods of Solution of Nonlinear Flow Processes with Application to the Be'nard Problem", Los Alamos Scientific Laboratory of the University of California LA-3522, January, 1957.

25. Goldstein, H., Classical Mechanics, Addison-Wesley, Reading, Massachusetts, 1959.

26. Personal communication with H. T. Nagamatsu, General Electric Company, September 20, 1966.

27. Personal communication between Carlo Ferrari and W. F. Walker, November, 1966.

28. Walz, A., "Compressible Turbulent Boundary Layers with Heat Transfer and Pressure Gradient in Flow Direction", J. of Research of Nat. Bur. Standards -B- Mathematics and Math. Physics, Vol. 63B, No. 1, 1959, p. 53.

29. Kosterin, S. I. and Koshmarov, Yu. A., "The Turbulent Boundary Layer on a Flat Plate in a Uniform Stream in a Compressible Fluid", Soviet Phys. — Tech. Phys., Vol. 4, 1960, p. 819.

30. Ferrari, Carlo, "Study of the Boundary Layer at Supersonic Speeds in Turbulent Flow: Case of Flow Along a Flate Plate", Qtrly. Appl. Mech., Vol. 8, 1950, p. 33.

31. Clauser, F., "Turbulent Boundary Layers in Adverse Pressure Gradients", J. Aero. Sci., Vol. 21, 1954, p. 91.

32. Mellor, G. L. and Gibson, D. M., "Equilibrium Turbulent Boundary Layers", Mech. Eng'g. Rept. FLD 14, Princeton University, 1963.

33. Gilliam, D. Mc., "Analysis of Pressure Drop and Heat Transfer in the Flow of an Ethylene Glycol Solution Through a Tube Cooled by Radiation from a Rectangular Fin", M. S. Thesis, Rice University, August, 1966.

34. Blottner, F. G. and Flugge-Lotz, "Finite Difference Computation of the Boundary Layer with Displacement Thickness Interaction", Journal de Mechanique, Vol. II, No. 4, 1963, p. 397.

36. Bagwell, D., Toss, An IBM-7090 Code For Computing Transient or Steady State Temperature Distributions, AEC Research and Development Report K-1494, Dec. 1, 1961.

37. Van Driest, E. R., "On Turbulent Flow Near A Wall", J. Aero. Sci., Vol. 3, 1956, p. 1007.

38. Brailovskaya, I. Y. and Chudov, L. A., "The Solution of Boundary Layer Equations by the Difference Method", translated from: Vychislitel'nyye Metody i Programmirovaniye: Izdatel'stvo Moskovskogo Universiteta, I, 1962, p. 167.

39. Smith, A. M. O., Jaffe, N. A. and Lind, R. C., "Progress in Solving the Full Equations of Motion of a Compressible Turbulent Boundary Layer", presented at the Seventh BOWACA Symposium on Aeroballistics, U.S. Naval Missile Center, Point Mugu, California, June, 1966.

40. Douglas, J. Jr., "Alternating Direction Method for Three Space Variables", Numerische Mathematik, Vol. 4, 1963, p. 41.

41. von Neumann, J. and Richtymer, R. D., "A Method for the Numerical Calculation of Hydrodynamic Shocks", J. Appl. Physics, Vol. 21, 1950, p. 232.

42. Spaulding, D. B., "A Simple Formula for the Law of the Wall", Trans. ASME, Series E, 1961, p. 455.

43. Rochelle, W. C., "Prandtl Number Distribution in a Turbulent Boundary Layer With Heat Transfer at Supersonic Speeds", University of Texas Defense Research Laboratory DRL-508, 1963.

44. Spalding, D. B., "Contribution to the Theory of Heat Transfer Across a Turbulent Boundary Layer", Int. J. Ht. Mass Trans., Vol. 7, 1964, p. 743.

45. Van Driest, E. R., "The Problem of Aerodynamic Heating", Aero. Eng'g. Rev., Vol. 15, 1956, p. 26.

46. Kline, S. J., Lisin, A. V. and Waitman, B. A., "Preliminary Experimental Investigation of Effect of Free-Stream Turbulence on Turbulent Boundary-Layer Growth", NASA TND-368, 1960.

47. Baxter, D. C. and Flugge-Lotz, I., "Compressible Laminar Boundary Layer Behavior Studied by a Finite Difference Method", Zeitschrift fur Angewandte Mathem atik und Physik, Vol. 9B, 1958, p. 81.

48. Serafini, J. S., "Wall-Pressure Fluctuations and Pressure-Velocity Correlations in a Turbulent Boundary Layer", NASA Technical Report R-165, 1963.

49. Richtmyer, R. D., Difference Methods for Initial Value Problems, Interscience, New York, 1957.

APPENDIX A

REVIEW OF DERIVATION OF FUNDAMENTAL EQUATIONS

The basic equations of fluid mechanics have been repeatedly derived in the literature ([1], [2] for example). The derivations are outlined below in order to establish the notational system and to introduce the various simplifying assumptions.

The starting point for each derivation is the appropriate physical law, which is applied to the fluid moving through a particular region of space (the control volume) or to the fluid contained within a mathematical envelope (the control volume) which moves with the fluid.

Vector notation has proved useful in improving the clarity and brevity of this and the following appendices.

Conservation of Mass

The law of conservation of mass states that, barring nuclear reactions, mass can be neither created nor destroyed. The assumption of a continuum fluid (... "the properties of the smallest portions into which we can conceive it to be divided are the same as those of the substance in bulk." [3]) is introduced here for convenience. The mass of fluid crossing an element of the control volume surface dA in time Δt is:

$$\rho \bar{v} \cdot \bar{n} \, dA \, \Delta t \quad ,$$

where ρ is the density and $\bar{v}$ the velocity of the fluid crossing dA. The total increase in mass within the control volume is

$$\int_V \Delta\rho \, dV \quad .$$

The basic law implies that the net mass crossing the volume surface must equal the change in mass within the volume:

$$- \int_V \Delta\rho \, dV = \Delta t \int_A \rho\bar{v} \cdot \bar{n} \, dA \quad .$$

The unit vector $\bar{n}$ is normal to the element of area dA and points outward from the control volume.

$$\int_V \frac{\Delta\rho}{\Delta t} \, dV + \int_A \rho\bar{v} \cdot \bar{n} \, dA = 0 \quad . \tag{A-1}$$

The second integral is converted to a volume integral through application of the divergence theorem, (see [4]),

$$\int_A (\rho\bar{v}) \cdot \bar{n} \, dA = \int_V \nabla \cdot (\rho\bar{v}) \, dV \quad ,$$

which gives

$$\int_V \left\{ \frac{\Delta\rho}{\Delta t} + \nabla \cdot (\rho\bar{v}) \right\} dV = 0 \quad . \tag{A-2}$$

In order for the first term to be interpreted as an instantaneous value rather than an average with respect to time, the limit

$$\frac{\Delta\rho}{\Delta t} \to \frac{\partial\rho}{\partial t}$$

is taken. Finally, (A-2) must hold over any arbitrary volume in space. Using the mean value theorem of integral calculus [5], (A-2) becomes

$$\left[\frac{\partial \rho}{\partial t} + \nabla \cdot (\rho \bar{v})\right]_{AV} \int_V dV = 0 \quad .$$

Since the volume V can be of arbitrary size, the equation requires that

$$\left[\frac{\partial \rho}{\partial t} + \nabla \cdot (\rho \bar{v})\right]_{AV} = 0 \quad .$$

If the volume is allowed to shrink about some point P, in the limit the value of the bracketed term at P approaches the average value of the bracketed term, which is zero. Since the location of P is arbitrary, the bracketed term must vanish at every point. The law of conservation of mass is expressed as:

$$\frac{\partial \rho}{\partial t} + \nabla \cdot (\rho \bar{v}) = 0 \quad . \qquad \text{(A-3)}$$

Conservation of Momentum

This law is also known as Newton's second law, and a familiar form is the statement,

"force equals mass times acceleration."

The law is applied to a fluid "particle" of mass $\frac{\rho}{g_c} dV$, surface area dA and velocity $\bar{v}$:

$$\left(\frac{\rho}{g_c} dV\right) \frac{D\bar{v}}{Dt} = \bar{f}_s \, dA + \bar{f}_B \, dV \quad .$$

The forces are divided into surface forces, $\bar{f}_s$, such as pressure and viscous forces and body forces, $\bar{f}_B$, such as gravitational, magnetic or electrostatic forces. If the equation above is summed over the "particles" contained in the control volume V at any particular instant of time, the result is

$$\int_V \left(\frac{\rho}{g_c}\frac{D\bar{v}}{Dt}\right) dV = \int_A \bar{f}_s \, dA + \int_V \bar{f}_B \, dV \quad . \tag{A-4}$$

In equation (A-4), A is the surface area of the control volume V. The surface integral in (A-4) results because surface forces interior to the control volume cancel, leaving only those forces acting on the surface A. If the surface force is interpreted as a tensor-vector product,

$$\bar{f}_s = \bar{\bar{P}} \cdot \bar{n} \quad ,$$

where $\bar{\bar{P}}$ is the pressure tensor, the surface integral can be converted to a volume integral by using the divergence theorem. Then equation (A-4) becomes

$$\int_V \left(\frac{\rho}{g_c}\frac{D\bar{v}}{Dt} - \nabla \cdot \bar{\bar{P}} - \bar{f}_B\right) dV = 0 \quad .$$

Use of the mean value theorem leads to the result that

$$\frac{\rho}{g_c}\frac{D\bar{v}}{Dt} - \nabla \cdot \bar{\bar{P}} - \bar{f}_B = 0 \quad . \tag{A-5}$$

Since the mean value theorem is used to develop a relationship (such as equation (A-3)) at a spatial point, equation (A-5) applies to every point in space. The operator

$$\frac{D}{Dt}$$

is known as the "substantial derivative" following changes in a quantity due both to time dependency and to spatial dependency. It is written as

$$\frac{D\xi}{Dt} = \frac{\partial \xi}{\partial t} + (\bar{v} \cdot \nabla)\xi \quad , \tag{A-6}$$

where ξ may be a scalar or a vector, depending upon the application.

The body force $\bar{f}_B$ is assumed to be negligible in the forced convection situations to be studied. Thus that term will be dropped from the equations.

The momentum conservation law becomes

$$\frac{\rho}{g_c}\frac{\partial \bar{v}}{\partial t} + (\bar{v} \cdot \nabla)\,\bar{v} = \nabla \cdot \bar{\bar{P}} \quad . \tag{A-7}$$

Conservation of energy

The first law of thermodynamics, which states that energy cannot be created or destroyed (again barring nuclear reactions), is applied to a fixed collection of matter, a "closed system." In this case the system is to consist of a fluid particle. It is necessary to assume that the flowing fluid is in local thermodynamic equilibrium. The law will be written in the form:

$$\begin{bmatrix}\text{Rate of Heat Transfer}\\ \text{Into the Particle}\end{bmatrix} - \begin{bmatrix}\text{Rate at Which Work is}\\ \text{Done by the Particle}\end{bmatrix} = \begin{bmatrix}\text{Rate of Change of}\\ \text{Internal Energy}\end{bmatrix} + \begin{bmatrix}\text{Rate of Change of}\\ \text{Kinetic Energy}\end{bmatrix},$$

or

$$\frac{DQ}{Dt} - \frac{DW}{Dt} = \int_V \rho \left[\frac{DU}{Dt} + \frac{D}{Dt}\frac{\bar{v} \cdot \bar{v}}{2g_c}\right] dV \quad . \tag{A-8}$$

In this case V represents the volume of the fluid particle, Q is the heat transfer into the particle, W is the work done by the particle and U is the internal energy associated with the particle. Although the terminology used is different, it is shown in [1] that

$$\frac{DQ}{Dt} = \int_A \bar{n} \cdot (\kappa\, \nabla\, T)\, dA \quad \text{and} \quad \frac{DW}{Dt} = -\int_A \bar{n} \cdot (\bar{\bar{P}} \cdot \bar{v})\, dA \quad . \tag{A-9}$$

κ represents the thermal conductivity and T represents the temperature of the fluid. These terms are converted to volume integrals through the divergence theorem, and (A-8) is rewritten as:

$$\int_V \left[\nabla \cdot (\kappa \nabla T) + \nabla \cdot (\bar{\bar{P}} \cdot \bar{v}) - \rho \frac{D}{Dt}\left(U + \frac{\bar{v} \cdot \bar{v}}{2g_c}\right)\right] dV = 0 \quad .$$

The mean value theorem is applied, as before, to establish the validity of (A-10) at every point in space and for every fluid particle.

$$\nabla \cdot (\kappa \nabla T) + \nabla \cdot (\bar{\bar{P}} \cdot \bar{v}) = \rho \frac{D}{Dt}\left(U + \frac{\bar{v} \cdot \bar{v}}{2g_c}\right) . \qquad \text{(A-10)}$$

The basic equations (A-3), (A-7) and (A-10) can be put into a more convenient form before specializing the problem to turbulent boundary layer forms. The momentum vector is defined:

$$\bar{m} \equiv \frac{\rho \bar{v}}{g_c} \quad . \qquad \text{(A-11)}$$

$$\frac{\partial \bar{m}}{\partial t} = \frac{1}{g_c}\left[\rho \frac{\partial \bar{v}}{\partial t} + \bar{v} \frac{\partial \rho}{\partial t}\right] = \frac{1}{g_c}\left[\rho \frac{\partial \bar{v}}{\partial t} + \bar{v} (-g_c \nabla \cdot \bar{m})\right]$$

from (A-3). This is rearranged as

$$\frac{\rho}{g_c} \frac{\partial \bar{v}}{\partial t} = \frac{\partial \bar{m}}{\partial t} + \bar{v} (\nabla \cdot \bar{m}) \quad .$$

The left side of (A-7) is

$$\frac{\rho}{g_c} \frac{\partial \bar{v}}{\partial t} + (\bar{v} \cdot \nabla)\bar{m} = \frac{\partial \bar{m}}{\partial t} + \bar{v} (\nabla \cdot \bar{m}) + (\bar{v} \cdot \nabla)\bar{m} = \frac{\partial \bar{m}}{\partial t} + \nabla (\bar{m} \cdot \bar{v}) \quad . \text{(A-12)}$$

The term

$$\rho \frac{D}{Dt}\left(U + \frac{\bar{v} \cdot \bar{v}}{2g_c}\right)$$

can be modified somewhat. If a specific flow energy is defined,

$$e \equiv \rho U + \frac{\rho \bar{v} \cdot \bar{v}}{2g_c} = \rho U + \frac{\bar{m} \cdot \bar{v}}{2} \quad , \tag{A-13}$$

$$\rho \frac{D}{Dt}\left(U + \frac{\bar{v} \cdot \bar{v}}{2g_c}\right) = \rho \frac{D}{Dt}\frac{e}{\rho} = \frac{De}{Dt} - \frac{e\rho}{\rho^2}\frac{D\rho}{Dt} \quad .$$

$$\frac{D\rho}{Dt} = \frac{\partial \rho}{\partial t} + \bar{v} \cdot \nabla \rho = -\nabla \cdot (\rho \bar{v}) + \bar{v} \cdot \nabla \rho = -\rho \nabla \cdot \bar{v} \quad ,$$

where the center step is due to (A-3). Continuing,

$$\rho \frac{D}{Dt}\frac{e}{\rho} = \frac{De}{Dt} + \frac{e}{\rho} \rho \nabla \cdot \bar{v} = \frac{De}{Dt} + e \nabla \cdot \bar{v}$$

$$= \frac{\partial e}{\partial t} + \bar{v} \cdot \nabla e + e \nabla \cdot \bar{v} = \frac{\partial e}{\partial t} + \nabla \cdot (e\bar{v}) \quad .$$

In summary,

$$\rho \frac{D}{Dt}\left(U + \frac{\bar{v} \cdot \bar{v}}{2g_c}\right) = \frac{\partial e}{\partial t} + \nabla \cdot (e\bar{v}) \quad . \tag{A-14}$$

The pressure tensor is normally separated into a component attributed to the thermodynamic pressure and a component due to the viscosity of the fluid:

$$\bar{\bar{P}} = - p \bar{\bar{I}} + \bar{\bar{S}} \quad . \tag{A-15}$$

(A-14) and (A-15) are introduced into (A-10), giving (A-18) below.

The notational changes (A-11), (A-12) and (A-15) are incorporated into (A-3) and (A-17), yielding (A-16) and (A-17).

The system of equations (A-16) — (A-20) includes the notational changes desired. This system is not complete in that it lacks an equation of state for the fluid and no defining relation for the stress tensor is given.

$$\frac{\partial \rho}{\partial t} + g_c \nabla \cdot \bar{m} = 0 \tag{A-16}$$

$$\frac{\partial \bar{m}}{\partial t} + \nabla \cdot (\bar{m}, \bar{v}) + \nabla p - \nabla \cdot \bar{\bar{S}} = 0 \qquad \text{(A-17)}$$

$$\frac{\partial e}{\partial t} + \nabla \cdot [(e + p)\bar{v}] - \nabla \cdot (\bar{\bar{S}} \cdot \bar{v}) - \nabla \cdot (\kappa \nabla T) = 0 \qquad \text{(A-18)}$$

$$\bar{m} = \frac{\rho \bar{v}}{g_c} \qquad \text{(A-19)}$$

$$e = \rho U + \frac{\bar{m} \cdot \bar{v}}{2} \quad . \qquad \text{(A-20)} .$$

APPENDIX B

INTRODUCTION OF FLUCTUATING COMPONENTS AND TIME — AVERAGING OF THE EQUATIONS

Experimental observations of turbulent fluid flow have shown that the mechanical and thermodynamic properties of a fluid at a point in space may be separated into two components. One component (underscored) is "slowly varying' with respect to time; the other component (primed) is "fluctuating" with respect to time. For the instantaneous value of a typical fluid property $\xi(t)$,

$$\xi(t) = \underline{\xi}(t) + \xi'(t) \quad . \tag{B-1}$$

Exhaustive definitions and discussions of turbulent motion and the engineering approaches to describing it are given in [1] and [6]. In this appendix, the usual engineering approach is developed to obtain the fundamental equations in terms of "time-averaged" variables and the averages of the products of the "fluctuating" components. In appendix C the products of fluctuating components are related to the "time-averaged" variables through the introduction of an empirical model.

If the instantaneous value $\xi(t)$ is subjected to an averaging process over a period of time, it is observed that

$$\underline{\xi'(t)} = \frac{1}{\tau} \int_0^{\tau} \xi'(t)\, dt = 0 \quad .$$

From this observation, a list of rules for treating the fluctuating

components mathematically has been derived. These rules are developed in [6] and are repeated here for convenience.

$$\xi = \underline{\xi} + \xi' \qquad \zeta = \underline{\zeta} + \zeta'$$

$$\underline{\xi} = \underline{(\xi + \xi')} = \underline{\xi} = \underline{\xi}$$

$$\underline{\xi\,\zeta} = \underline{\xi}\,\underline{\zeta} = \underline{\xi}\,\underline{\zeta}$$

$$\underline{\xi\,\zeta'} = \underline{\xi}\,\underline{\zeta'} = 0 \tag{B-2}$$

$$\underline{\xi\,\zeta} = \underline{\xi}\,\underline{\zeta} + \underline{\xi'\,\zeta'} \quad .$$

Goldstein [9] has pointed out that, if $\underline{\xi}$ happens to be $\underline{\xi}(t)$, the equation

$$\underline{\xi}\,\underline{\zeta'} = \frac{1}{\tau}\int_0^\tau \underline{\xi}\,\zeta'\,dt = \frac{1}{\tau}\,\underline{\xi}\int_0^\tau \zeta'\,dt = 0$$

represents an additional assumption. This observation applies to the present work.

The usual approach to treating turbulent flow problems is to introduce the characteristic fluctuation terminology into equations (A-16) to (A-20). Then the time averages of the equations are taken, resulting in equations which, if they could be solved, would describe the behavior of the mean flow variables.

The following terms are introduced. The underscores represent time averages, while the overscores designate vector or tensor quantities:

$$\rho = \underline{\rho} + \rho' \quad \bar{m} = \underline{\bar{m}} + \bar{m}' \quad \bar{v} = \underline{\bar{v}} + \bar{v}'$$

$$p = \underline{p} = p' \quad T = \underline{T} + T' \quad e = \underline{e} + e'$$

$$\bar{\bar{S}} = \underline{\bar{\bar{S}}} + \bar{\bar{S}}' \quad U = \underline{U} + U' \quad . \tag{B-3}$$

Continuity

$$\frac{\partial}{\partial t}(\rho + \rho') + g_c \nabla \cdot (\bar{\underline{m}} + \bar{m}') = 0 \quad ,$$

$$\frac{\partial}{\partial t}\int \underline{\rho} dt + \frac{\partial}{\partial t}\int \rho' dt + g_c \nabla \cdot \left[\int \bar{\underline{m}} dt + \int \bar{m}' dt\right] = 0 \quad ,$$

or

$$\frac{\partial \underline{\rho}}{\partial t} + g_c \nabla \cdot \bar{\underline{m}} = 0 \quad . \tag{B-4}$$

Momentum

$$\frac{\partial}{\partial t}(\bar{\underline{m}} + \bar{m}) + \nabla \cdot [(\bar{\underline{m}} + \bar{m}') \, , (\bar{\underline{v}} + \bar{v}')] = - \nabla (\underline{p} + p') + \nabla \cdot (\bar{\bar{\underline{S}}} + \bar{\bar{S}}')$$

or

$$\frac{\partial \underline{m}}{\partial t} + \nabla \cdot (\bar{\underline{m}}, \bar{\underline{v}}) + \nabla \cdot \underline{(\bar{m}', \bar{v}')} = - \nabla \underline{p} + \nabla \cdot \bar{\bar{\underline{S}}} \quad . \tag{B-5}$$

Energy

$$\frac{\partial \underline{e}}{\partial t} + \nabla \cdot [(\underline{e} + \underline{p} + e' + p') \cdot (\bar{\underline{v}} + \bar{v}')]$$
$$= \nabla \cdot [(\bar{\bar{\underline{S}}} + \bar{\bar{S}}') \cdot (\bar{\underline{v}} + \bar{v}')] + \nabla \cdot [(\underline{\kappa} + \kappa') \nabla (\underline{T} + T')] \quad .$$

This reduces to

$$\frac{\partial \underline{e}}{\partial t} + \nabla \cdot [(\underline{e} + \underline{p})\bar{\underline{v}} + \underline{(e' + p')\bar{v}'}]$$

$$= \nabla \cdot [(\bar{\bar{\underline{S}}} \cdot \bar{\underline{v}}) + \underline{(\bar{\bar{S}}' \cdot \bar{v}')}] + \nabla \cdot [\underline{\kappa} \nabla \underline{T} + \underline{\kappa' \nabla T'}] \quad . \tag{B-6}$$

In the above equations, the following assumptions were tacitly introduced:

$$\int \bar{m}' dt = \underline{\bar{m}'} = 0 \quad , \qquad \int \bar{\bar{S}}' dt = \underline{\bar{\bar{S}}'} = 0 \quad ,$$

$$\int e' dt = \underline{e'} = 0 \quad , \qquad \int T' dt = \underline{T'} = 0 \quad .$$

The physical validity of these conditions was noted above; mathematically the imposition of these conditions defines the manner in which $\bar{\bar{m}}'$, $\bar{\bar{S}}'$, and T' are related to velocity, pressure and density fluctuations.

As an example, the conditions imposed on the momentum vector $\bar{\bar{m}}'$ will be developed.

(1) The definition (A-19) is to hold:

$$\bar{\bar{m}} = \frac{1}{g_c}\rho\bar{v} = \underline{\bar{m}} + \bar{m}' = \frac{1}{g_c}(\underline{\rho} + \rho')(\underline{\bar{v}} + \bar{v}') \quad . \tag{a}$$

(2) The average of the fluctuating component is to vanish:

$$\int \bar{m}'dt = 0 \quad . \tag{b}$$

(3) The rules established for ρ and $\bar{v}$ must hold:

$$\underline{\rho\ \bar{v}'} = \underline{\rho'\ \bar{v}} = 0 \quad . \tag{c}$$

If the time average of (a) is taken, together with (b) and (c),

$$\underline{\bar{m}} = \frac{1}{g_c}(\underline{\rho}\ \underline{\bar{v}} + \underline{\rho'\ \bar{v}'}) \quad . \tag{d}$$

If (d) is subtracted from (a), the defining equation for $\bar{m}'$ results:

$$\bar{m}' = \frac{1}{g_c}(\rho'\ \underline{\bar{v}} + \rho'\bar{v}' - \underline{\rho'\ \bar{v}'}) \quad . \tag{B-7}$$

Similarly, using (A-20),

$$e' = \rho'\underline{U} + \underline{\rho}U' + \frac{1}{2}(\bar{m}' \cdot \underline{\bar{v}} + \underline{\bar{m}} \cdot \bar{v}') + \rho'U' - \underline{\rho'U'} + \frac{1}{2}(\bar{m}' \cdot \bar{v}' - \underline{\bar{m}'\cdot\bar{v}}) \quad . \tag{B-8}$$

The equivalent expressions for $\bar{\bar{S}}'$ and T' could be developed from the definitions for $\bar{\bar{S}}$ and T.

The stress law selected is that of the Stokesian fluid [2], in which stress is proportional to strain rate:

$$\bar{\bar{S}} = \mu \left\{ (\nabla,\bar{v}) + (\bar{v},\nabla) - \frac{2}{3} (\nabla \cdot \bar{v})\bar{\bar{I}} \right\} \equiv \mu \langle v \rangle \quad . \tag{B-9}$$

The meaning of the operator <> is also defined by (B-9).

The ideal gas law was selected as the equation of state:

$$p = \rho RT \quad . \tag{B-10}$$

The variables are separated into slowly — varying and fluctuating components, as before:

$$\bar{\bar{S}} = \underline{\bar{\bar{S}}} + \bar{\bar{S}}' = (\underline{\mu} + \mu') (\langle \underline{\bar{v}} \rangle + \langle \bar{v}' \rangle)$$

and

$$p = \underline{p} + p' = R(\underline{\rho} + \rho') (\underline{T} + T') \quad .$$

Taking the time average of these gives

$$\underline{\bar{S}} = \underline{\mu} \langle \underline{\bar{v}} \rangle + \underline{\mu' \langle v' \rangle} \quad \text{and} \quad \underline{p} = R(\underline{\rho}\ \underline{T} + \underline{\rho'\ T'}).$$

At this point the assumptions discussed in chapter II are introduced. They are:

$$\rho' \equiv \kappa' \equiv \mu' \equiv 0 \quad . \tag{B-11}$$

The definitions for $\bar{\bar{S}}'$ and T' are developed after introducing these simplifying assumptions:

$$\bar{\bar{S}}' = 0 \quad \text{and} \quad T' = p'/(R\underline{\rho}) \quad . \tag{B-12}$$

The utility of the assumption $\rho' = 0$ is obvious here, since under that assumption the quantities $\underline{p}$ and $\underline{T}$ as well as p and T conform to the ideal gas law. Similarly, the stress law (B-9) is obeyed by time-averaged as well as instantaneous quantities.

The defining equation for the quantity e (A-20) is treated next. The equation of state (B-10) is used to convert the internal energy U into a more convenient form. For an ideal gas,

$$\rho U = \rho C_v T = \frac{C_v}{R} \rho RT = \frac{C_v}{R} p \quad .$$

Then (A-20) becomes

$$e = \frac{C_v}{R} p + \frac{1}{2} \bar{m} \cdot \bar{v} \quad .$$

$$e = \underline{e} + e' = \frac{C_v}{R} (\underline{p} + p') + \frac{1}{2} (\bar{\underline{m}} + \bar{m}') \cdot (\bar{\underline{v}} + \bar{v}')$$

and

$$\underline{e} = \frac{C_v}{R} \underline{p} + \frac{1}{2} (\bar{\underline{m}} \cdot \bar{\underline{v}} + \underline{\bar{m}' \cdot \bar{v}'}) \quad . \tag{B-13}$$

Utilizing the simplifying assumptions, the set of primary and auxiliary equations relating the several flow variables are collected below:

$$\frac{\partial \rho}{\partial t} + g_c \nabla \cdot \bar{\underline{m}} = 0 \tag{B-4}$$

$$\frac{\partial \underline{m}}{\partial t} + \nabla \cdot (\bar{\underline{m}}, \bar{\underline{v}}) + \nabla \cdot (\underline{\bar{m}', \bar{v}'}) = - \nabla \underline{p} + \nabla \cdot \bar{\bar{\underline{S}}} \tag{B-5}$$

$$\frac{\partial \underline{e}}{\partial t} + \nabla \cdot [(\underline{e} + \underline{p})\bar{\underline{v}} + \underline{(e' + p')\bar{v}'}] = \nabla \cdot (\bar{\bar{\underline{S}}} \cdot \bar{\underline{v}}) + \nabla \cdot (\underline{\kappa} \nabla \underline{T}) \tag{B-14}$$

$$\underline{e} = \frac{C_v}{R} \underline{p} + \frac{1}{2} (\bar{\underline{m}} \cdot \bar{\underline{v}} + \underline{\bar{m}' \cdot \bar{v}'}) \tag{B-13}$$

$$\bar{\underline{m}} = \frac{1}{g_c} \underline{\rho} \, \bar{\underline{v}} \tag{B-15}$$

$$\underline{p} = \underline{\rho} \underline{RT} \tag{B-16}$$

$$\bar{\bar{\underline{S}}} = \mu \left\{ (\nabla, \bar{\underline{v}}) + (\bar{\underline{v}}, \nabla) - \frac{2}{3} (\nabla \cdot \bar{\underline{v}}) \bar{\bar{I}} \right\} = \underline{\mu} \, \langle \bar{\underline{v}} \rangle \tag{B-17}$$

$$e' = \frac{C_v}{R} p' + \frac{1}{2} (\bar{m}' \cdot \bar{\underline{v}} + \bar{\underline{m}} \cdot \bar{v}' + \bar{m}' \cdot \bar{v}' - \underline{\bar{m}' \cdot \bar{v}'}) \tag{B-18}$$

$$\bar{m}' = \frac{1}{g_c} \underline{\rho} \, \bar{v}' \quad . \tag{B-19}$$

A careful balance of relationships against variables shows that two additional defining equations for fluctuating components are needed. The arguments leading to the model selected for these quantities are developed in chapter III. The detailed derivations are presented in appendix C following.

APPENDIX C

DEVELOPMENT OF THE MODEL EQUATIONS FOR TURBULENT STRESS AND HEAT FLUX TERMS

In equations (B-5) and (B-14), certain terms can be interpreted as a turbulent stress tensor ($\bar{\bar{\tau}}$) and turbulent heat flux vector ($\bar{q}_T$). These are:

$$\bar{\bar{\tau}} \equiv - \underline{(\bar{m}', \bar{v}')} \tag{C-1}$$

and

$$\underline{(e' + p')\bar{v}'} = \bar{q}_T - \underline{\bar{v}} \cdot \bar{\bar{\tau}} \quad . \tag{C-2}$$

In this section these quantities are related to the mean flow variables $\underline{\rho}$, $\underline{u}$ and $\underline{T}$.

At this point, the assumption of two-dimensional flow (see chapter II) must be applied. It is advantageous to develop the model equations in cartesian spatial coordinates. Figure 12 below relates the symbols in the various equations to the physical flow situation.

In this cartesian system,

$$\bar{\bar{\tau}} = - \frac{\rho}{g_c} \begin{bmatrix} \underline{u'^2} & \underline{u'v'} \\ \underline{v'u'} & \underline{v'^2} \end{bmatrix} , \quad \bar{q}_T = \begin{bmatrix} q_x \\ q_y \end{bmatrix} \quad . \tag{C-3}$$

Specification of Stress Tensor

The component $\underline{u'v'}$ is usually the one measured experimentally in a turbulent boundary layer. It was used by Boussinesq (see [1]) to de-

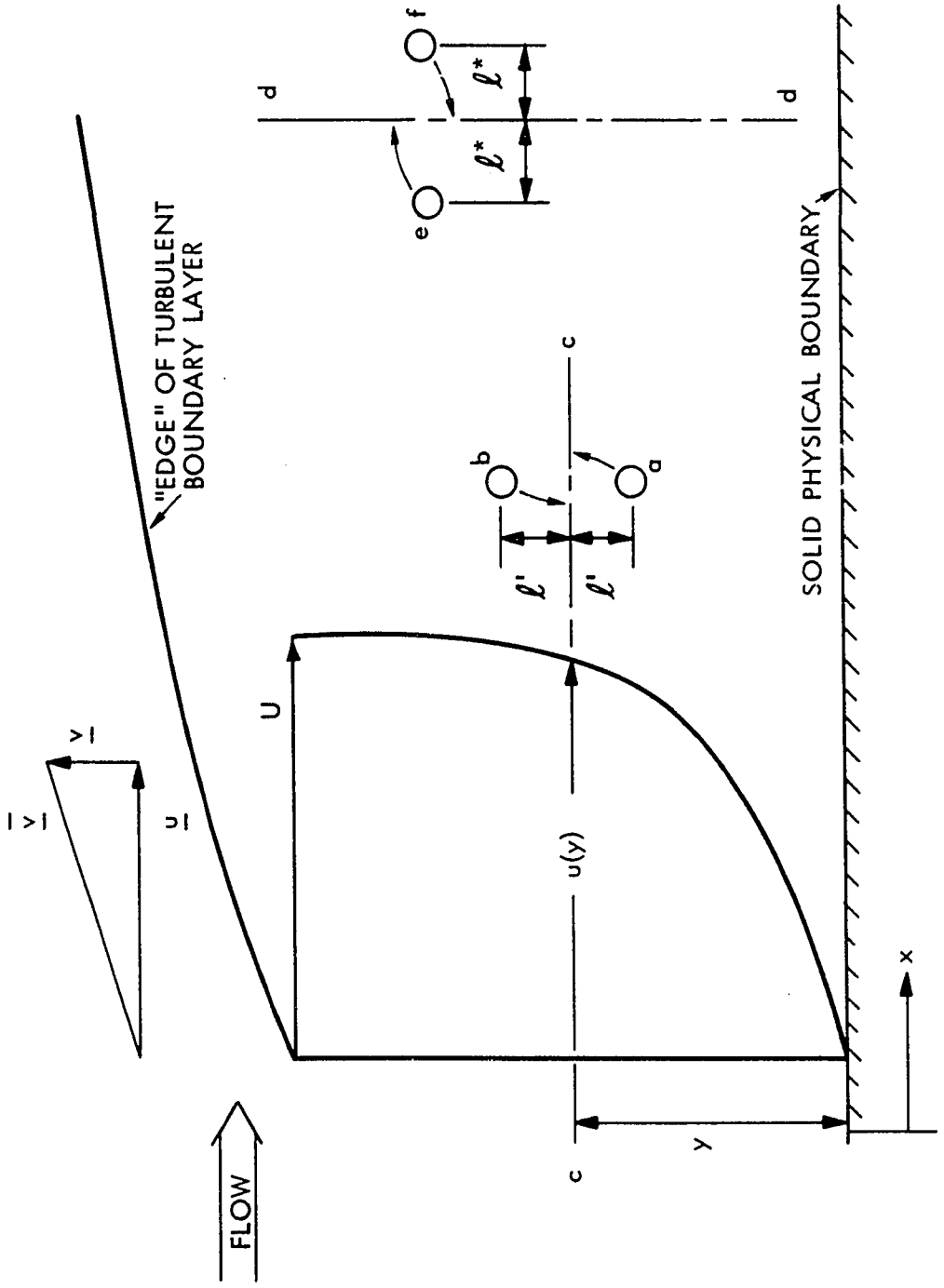

Figure 12
SCHEMATIC OF BOUNDARY LAYER
SHOWING VELOCITY PROFILE AND IDENTIFICATION OF MIXING LENGTHS

fine an "effective viscosity", which becomes a convenient parameter in expressing the remaining elements of the tensor $\overline{\overline{\tau}}$:

$$\underline{u'v'} = - \nu_e \frac{\partial \underline{u}}{\partial y} \quad . \tag{C-4}$$

The intuitive argument used to relate ν_e to the mean flow variables is due to Prandtl and is reported in [1]. The conclusions of that argument will be sketched here for convenience; they will be expanded slightly to connect the components to $\overline{\overline{\tau}}$.

Prandtl's argument is based on the idea (due to Boussinesq) that turbulent momentum and energy transport are analogous to molecular momentum and energy transport, with macroscopic "chunks" of fluid rather than individual molecules being the transport vehicles. The important conclusions of the mixing-length argument are

$$\text{(a)} \quad \underline{|u'|} = \ell \left| \frac{\partial \underline{u}}{\partial y} \right| + \ldots \quad , \tag{C-5}$$

$$\text{(b)} \quad \underline{|v'|} = \ell \left| \frac{\partial \underline{v}}{\partial y} \right| = k \underline{|u'|} = k\ell \left| \frac{\partial \underline{u}}{\partial y} \right| \quad , \tag{C-6}$$

(c) u' and v' are on the average opposite in sign.

Finally, a correlation coefficient is defined:

$$c \equiv - \frac{\underline{u'v'}}{\underline{|u'|}\,\underline{|v'|}} \quad . \tag{C-7}$$

(C-5, 6, 7) are combined to give:

$$- \underline{u'v'} = c \,\underline{|u'|}\,\underline{|v'|} = ck\ell^2 \left| \frac{\partial \underline{u}}{\partial y} \right|^2 \quad .$$

The coefficients c and k are absorbed into a general coefficient,

$$\ell'^2 = ck\ell^2 \quad . \tag{C-8}$$

One additional feature is desirable for the model, that being for the turbulent shear stress to change sign when the derivative of mean velocity changes sign. The resulting form is:

$$- \underline{u'v'} = \ell'^2 \left|\frac{\partial \underline{u}}{\partial y}\right| \left(\frac{\partial \underline{u}}{\partial y}\right) \quad . \tag{C-9}$$

Prandtl's argument (as presented in [1]) is complete at this point. The "mixing length" ℓ' is the link between the empirical model and experimental results.

A similar mixing-length argument applied in the tangential (x) direction gives

$$\underline{|u'|} = \ell^* \left|\frac{\partial \underline{u}}{\partial x}\right| + \ldots \tag{C-10}$$

$$\underline{|v'|} = \ell^* \left|\frac{\partial \underline{v}}{\partial x}\right| + \ldots \tag{C-11}$$

If (C-6) and (C-10) are combined, the length ℓ^* is obtained:

$$\frac{\underline{|u'|}}{\underline{|v'|}} = \frac{1}{k} = \frac{\ell^* \left|\frac{\partial \underline{u}}{\partial x}\right|}{\ell \left|\frac{\partial \underline{v}}{\partial y}\right|} \quad ,$$

and from mass continuity at steady state,

$$\left|\frac{\partial \underline{u}}{\partial x}\right| \approx \left|\frac{\partial \underline{v}}{\partial y}\right|$$

so that

$$\ell^* = \frac{\ell}{k} \quad . \tag{C-12}$$

The remaining elements in the stress tensor (C-3) can now be constructed in the desired form. In estimating the values for the parameters c and k (equations C-20, 22), it was assumed that

$$\frac{\underline{|u'|}}{\underline{u'^2}} = \frac{\underline{|v'|}}{\underline{v'^2}} = f \quad . \tag{C-13}$$

From this,

$$\underline{u'^2} = \frac{1}{f^2}\,\underline{|u'|}\,\underline{|u'|} \quad ,$$

and

$$-\rho\,\underline{u'^2} = -\frac{\rho}{f^2}\,\ell\,\left|\frac{\partial \underline{u}}{\partial y}\right|\,\ell^*\,\left|\frac{\partial \underline{u}}{\partial x}\right| = -\frac{\rho}{f^2}\,\frac{\ell^2}{k}\,\left|\frac{\partial \underline{u}}{\partial y}\right|\left|\frac{\partial \underline{u}}{\partial x}\right|$$

$$= -\frac{\rho}{f^2}\,\frac{\ell'^2}{ck^2}\left|\frac{\partial \underline{u}}{\partial y}\right|\,\left|\frac{\partial \underline{u}}{\partial x}\right| = -\frac{\rho\,\nu_e}{ck^2f^2}\,\left|\frac{\partial \underline{u}}{\partial x}\right| \quad .$$

Finally, since

$$\frac{\partial \underline{u}}{\partial x} < 0$$

in a boundary layer,

$$-\rho\,\underline{u'^2} = \frac{\rho\,\nu_e}{ck^2f^2}\left(\frac{\partial \underline{u}}{\partial x}\right) \quad . \tag{C-14}$$

Next,

$$-\rho\,\underline{v'u'} = \rho c\ell^*\,\left|\frac{\partial \underline{v}}{\partial x}\right|\,\ell\,\left|\frac{\partial \underline{u}}{\partial y}\right| = \frac{\rho c\ell^2}{k}\,\left|\frac{\partial \underline{u}}{\partial y}\right|\,\left|\frac{\partial \underline{v}}{\partial x}\right|$$

$$= \frac{\rho\ell'^2}{k^2}\,\left|\frac{\partial \underline{u}}{\partial y}\right|\,\left|\frac{\partial \underline{v}}{\partial x}\right| = \frac{\rho\,\nu_e}{k^2}\,\left|\frac{\partial \underline{v}}{\partial x}\right| \quad .$$

Again,

$$\frac{\partial \underline{v}}{\partial x} < 0$$

is expected in a turbulent boundary layer, but the term

$$\underline{v'u'} < 0$$

also (see Prandl's conclusions above). Thus:

$$-\underline{\rho\ v'u'} = -\frac{\rho\ \nu_e}{k^2}\left(\frac{\partial \underline{v}}{\partial x}\right) \quad . \tag{C-15}$$

For the last component of the stress tensor,

$$-\underline{\rho\ v'^2} = -\rho\ \frac{1}{f^2}\ \underline{|v'|\ |v'|} = -\frac{\rho}{f^2}\ k\ell\ \left|\frac{\partial \underline{u}}{\partial y}\right|\left|\frac{\partial \underline{v}}{\partial y}\right|$$

$$= -\frac{\rho k}{f^2}\ \frac{\ell'^2}{ck}\ \left|\frac{\partial \underline{u}}{\partial y}\right|\ \left|\frac{\partial \underline{v}}{\partial y}\right| = -\frac{\rho}{cf^2}\ \nu_e\ \left|\frac{\partial \underline{v}}{\partial y}\right| \quad .$$

Since

$$\underline{v'^2} > 0\ ,\ -\underline{\rho\ v'^2} < 0$$

so that

$$-\underline{\rho\ v'^2} = -\frac{\rho}{cf^2}\ \nu_e\ \left(\left|\frac{\partial \underline{v}}{\partial y}\right|\right) \quad . \tag{C-16}$$

Summarizing,

$$\overline{\overline{\tau}} = \frac{\rho\ \nu_e}{g_c}\begin{bmatrix} \frac{1}{ck^2f^2}\ \frac{\partial \underline{u}}{\partial x} & \frac{\partial \underline{u}}{\partial y} \\ -\frac{1}{k^2}\ \frac{\partial \underline{v}}{\partial x} & -\frac{1}{cf^2}\ \frac{\partial \underline{v}}{\partial y} \end{bmatrix} \quad . \tag{C-17}$$

Specification of the Heat Flux Vector

Experimentally a similarity has been observed between the turbulent transfer of energy and momentum. This is known as Reynolds Analogy (see, for example, [1], [7] or [9]).

It is convenient to perform some simplifying manipulations on (C-2) before dealing with the heat flux vector. From (B-18),

$$(e' + p')\bar{v}' = \left(\frac{R + C_v}{R}\right)p'\bar{v}'$$

$$+ \frac{1}{2}\left[(\bar{m}' \cdot \underline{\bar{v}})\bar{v} + (\underline{\bar{m}} \cdot \bar{v}')\bar{v}' + (\bar{m}' \cdot \bar{v}')\bar{v}' - (\underline{\bar{m}' \cdot \bar{v}'})\bar{v}'\right] .$$

Introducing (B-19) and taking the time average gives

$$\underline{(e' + p')\bar{v}'} = \frac{R + C_v}{R}\,\underline{p'\bar{v}'} + \frac{1}{2}\frac{\rho}{g_c}\left[\underline{(\bar{v}' \cdot \bar{v})\bar{v}'} + \underline{(\bar{v} \cdot \bar{v}')\bar{v}'} + \underline{(\bar{v} \cdot \bar{v}')\bar{v}'}\right] .$$

According to [8], the triple product of fluctuating components may be neglected, and for an ideal gas

$$R + C_v = C_P .$$

The equation becomes

$$\underline{(e' + p')\bar{v}'} = \frac{C_P}{R}\,\underline{p'\bar{v}'} + \frac{\rho\,\bar{v}}{g_c}\,\underline{(\bar{v}', \bar{v}')} . \qquad \text{(C-18)}$$

From (B-12),

$$\frac{C_P}{R}\,\underline{p'\bar{v}'} = (\underline{\rho}\,C_P)\,\underline{T'\bar{v}'} . \qquad \text{(C-19)}$$

A "Turbulent Prandtl Number" is defined in [1], which in the present notation becomes

$$P_{R_T} = \frac{\rho\,\nu_e\,C_P}{\kappa_e} , \qquad \text{(C-20)}$$

where κ_e is an eddy thermal conductivity. [1] further relates κ_e to $\bar{q}_T$ by

$$\bar{q}_T = -\kappa_e\,\nabla\,\underline{T} , \qquad \text{(C-21)}$$

which is written (after Boussinesq) in analogy with the case of molecular energy transport.

(C-22) results from a comparison of (C-2, 18, 19, 21):

$$\bar{q}_T = - \kappa_e \nabla \underline{T} = (\underline{\rho}\, C_p)\, \underline{T'\bar{v}'} \quad . \tag{C-22}$$

This equation might also be developed by an extension of Prandtl's intuitive approach which was used to obtain (C-17).

Finally, (C-2, 20, 22) are combined to give:

$$\underline{(e' + p')\bar{v}'} = - \frac{\underline{\rho}\, \nu_e}{P_{R_T}} \nabla \underline{T} - \underline{\bar{v}} \cdot \bar{\bar{\tau}} \quad . \tag{C-23}$$

The advantage of this expression is that the turbulent Prandtl number is nearly constant through a turbulent boundary layer, reflecting the similarity between momentum and energy transfer mentioned previously. The utility of the turbulent Prandtl number and the selection of a proper value are discussed further in chapter III.

Estimation of Numerical Values for Coefficients in (C-13)

It is necessary to estimate values for the coefficients c, k and f.

Correlation coefficients are usually defined as

$$c' \equiv \frac{\underline{-u'v'}}{\sqrt{\underline{u'^2}\ \underline{v'^2}}} ,$$

which should be compared to (C-7). By assuming a simple wave form for the fluctuation components,

$$u' = v' = \sin \Omega t \quad ,$$

the averages are formed to give

$$\frac{1}{f^2} = \frac{c}{c'} = 1.24 \quad . \tag{C-24}$$

From [1] (p. 466) or [9] (p. 194), a value for c' was selected,

$$c' = .3 \quad . \tag{C-25}$$

This value is rather arbitrary due to the scale of curves being interpreted, but it is compatible with the approximate wave form chosen.

A value for

$$k = \frac{|v'|}{|u'|}$$

can be estimated from data reported in [6] (p. 488). It is observed that the value for k changes only a slight amount over most of the thickness of the boundary layer. From this, the value of k has been selected as

$$k = .485 \quad . \tag{C-26}$$

The (C-17) becomes

$$\overline{\overline{\tau}} = \frac{\rho\, \nu_e}{g_c} \begin{bmatrix} 14.18 \dfrac{\partial u}{\partial x} & \dfrac{\partial u}{\partial y} \\ -4.25 \dfrac{\partial v}{\partial x} & -3.33 \dfrac{\partial v}{\partial y} \end{bmatrix} \quad . \tag{C-27}$$

This equation and (C-22) represent the model equations for turbulent fluctuation averages. The form for ν_e is justified in chapter III.

APPENDIX D

NON-DIMENSIONAL FORM OF THE EQUATIONS

In this appendix, the equations developed in appendices B and C will be combined, expressed in their cartesian components and non-dimensionalized with respect to suitable "representative" scaling quantities.

Equations in Cartesian Components

(B-5) and (C-1) are combined to give

$$\frac{\partial \bar{\underline{m}}}{\partial t} = - \nabla \cdot (\bar{\underline{m}}, \bar{\underline{v}}) - \nabla \underline{p} + \nabla \cdot (\bar{\underline{\underline{S}}} + \bar{\underline{\underline{\tau}}}) \quad . \tag{D-1}$$

(B-14) and (C-2) are combined to give

$$\frac{\partial \underline{e}}{\partial t} = - \nabla \cdot [(\underline{e} + \underline{p})\bar{\underline{v}} - \bar{\underline{v}} \cdot (\bar{\underline{\underline{S}}} + \bar{\underline{\underline{\tau}}}) - \kappa \nabla \underline{T} + \bar{q}_T] \quad . \tag{D-2}$$

Also

$$\bar{\underline{\underline{\Omega}}} \equiv \bar{\underline{\underline{S}}} + \bar{\underline{\underline{\tau}}} \quad , \tag{D-3}$$

which is written in cartesian components as*

*The smallest viscous stress terms have been neglected to simplify the computer code. The negligible size of these terms is demonstrated in [1].

$$\bar{\bar{\Omega}} = \mu \begin{bmatrix} \frac{1}{c'k^2}\frac{\rho\nu_e}{g_c\mu}\frac{\partial \underline{u}}{\partial x} & \left(1 + \frac{\rho\nu_e}{g_c\mu}\right)\frac{\partial \underline{u}}{\partial y} \\ \left(1 - \frac{1}{\kappa^2}\frac{\rho\nu_e}{g_c\mu}\right)\frac{\partial \underline{u}}{\partial x} + \frac{\partial \underline{u}}{\partial y} & \left(\frac{4}{3} - \frac{1}{c'}\frac{\rho\nu_e}{g_c\mu}\right)\frac{\partial \underline{v}}{\partial y} \end{bmatrix} .$$

If (B-4), (B-13), (B-15), (D-1) and (D-2) are written in cartesian coordinates, the results are:

$$\frac{\partial \underline{\rho}}{\partial t} = -g_c\left(\frac{\partial \underline{a}}{\partial x} + \frac{\partial \underline{b}}{\partial y}\right)$$

$$\frac{\partial \underline{a}}{\partial t} = -\frac{\partial}{\partial x}\left[\underline{a}\,\underline{u} + \underline{p} - \Omega_{xx}\right] - \frac{\partial}{\partial y}\left[\underline{b}\,\underline{u} - \Omega_{xy}\right]$$

$$\frac{\partial \underline{b}}{\partial t} = -\frac{\partial}{\partial x}\left[\underline{a}\,\underline{v} - \Omega_{yx}\right] - \frac{\partial}{\partial y}\left[\underline{b}\,\underline{v} + \underline{p} - \Omega_{yy}\right] \qquad \text{(D-4)}$$

$$\frac{\partial \underline{e}}{\partial t} = -\frac{\partial}{\partial x}\left[(\underline{e} + \underline{p})\underline{u} - \left(\kappa + \frac{\rho\nu_e C_P}{P_{R_T}}\right)\frac{\partial \underline{T}}{\partial x} - \underline{u}\,\Omega_{xx} - \underline{v}\,\Omega_{xy}\right]$$

$$- \frac{\partial}{\partial y}\left[(\underline{e} + \underline{p})\underline{v} - \left(\kappa + \frac{\rho\nu_e C_P}{P_{R_T}}\right)\frac{\partial \underline{T}}{\partial y} - \underline{u}\,\Omega_{yx} - \underline{v}\,\Omega_{yy}\right]$$

$$\underline{e} = \frac{C_V}{R}\underline{p} + \frac{1}{2}\left[\underline{a}\,\underline{u} + \underline{b}\,\underline{v} - \frac{\rho\nu_e}{g_c}\left(\frac{1}{c'k^2}\frac{\partial \underline{u}}{\partial x} - \frac{1}{c'}\frac{\partial \underline{v}}{\partial y}\right)\right] .$$

The components of (B-15) are

$$\bar{\underline{m}} = \underline{a}\,\bar{i} + \underline{b}\,\bar{j} = \frac{\rho}{g_c}(\underline{u}\,\bar{i} + \underline{v}\,\bar{j}) \quad , \qquad \text{(C-5)}$$

where $\bar{i}$ and $\bar{j}$ are the unit vectors in the x and y directions, respectively (related to the physical situation by figure 12 in appendix C).

Non-Dimensionalization

The physical quantities in equations (D-4) will be non-dimensionalized with respect to combinations of the selected "typical" flow quantities, which are assumed to characterize the problem under study.

The non-dimensional form of the variables are primed (') in the development below. The relationships between non-dimensional and the equivalent dimensional variables are:

$$\begin{aligned}
&\underline{\rho} = \rho'\rho_0 && \underline{u} = u'U_0 && \underline{v} = v'U_0 \\
&\underline{e} = e'(\rho_0 RT_0) && \underline{p} = p'(\rho_0 RT_0) && \underline{T} = \theta T_0 \\
&\underline{a} = a' \frac{\rho_0 U_0}{g_c} && \underline{b} = b' \frac{\rho_0 U_0}{g_c} && \underline{t} = t' \frac{L_1}{U_0} \\
&x = \xi L_1 && y = \eta L_2 && \lambda = \frac{\rho \nu_e}{g_c \mu} \\
&\kappa = \kappa' \kappa_0 && \mu = \mu' \mu_0 && \underline{\underline{\Omega}} = \underline{\underline{\Omega}}' \frac{\mu_0 U_0}{L_2} \quad .
\end{aligned} \tag{D-6}$$

When the relations (D-6) are substituted into (D-4), the equations listed below result:

$$\frac{\partial \rho'}{\partial t'} = - \frac{g_c L_1}{U_0 \rho_0} \left(\frac{\rho_0 U_0}{g_c L_1} \frac{\partial a'}{\partial \xi} + \frac{\rho_0 U_0}{g_c L_2} \frac{\partial b'}{\partial \eta} \right)$$

$$\frac{\partial a'}{\partial t'} = - \frac{L_1 g_c}{\rho_0 U_0^{\,2} L_1} \frac{\partial}{\partial \xi} \left[\frac{\rho_0 U_0^{\,2}}{g_c} a'u' + \rho_0 R T_0 p' - \frac{\mu_0 U_0}{L_2} \Omega_{xx}' \right]$$

$$- \frac{L_1 g_c}{\rho_0 U_0^{\,2} L_2} \frac{\partial}{\partial \eta} \left[\frac{\rho_0 U_0^{\,2}}{g_c} b'u' - \frac{\mu_0 U_0}{L_2} \Omega_{xy}' \right]$$

$$\frac{\partial b'}{\partial t'} = - \frac{L_1 g_c}{\rho_0 U_0^{\,2} L_1} \frac{\partial}{\partial \xi} \left[\frac{\rho_0 U_0^{\,2}}{g_c} a'v' - \frac{\mu_0 U_0}{L_2} \Omega_{yx}' \right]$$

$$- \frac{L_1 g_c}{\rho_0 U_0^{\,2} L_2} \frac{\partial}{\partial \eta} \left[\frac{\rho_0 U_0^{\,2}}{g_c} b'v' + \rho_0 R T_0 p' - \frac{\mu_0 U_0}{L_2} \Omega_{yy}' \right]$$

$$\frac{\partial e'}{\partial t'} = -\frac{L_1}{\rho_0 R T_0 U_0 L_1}\frac{\partial}{\partial \xi}\left[\rho_0 R T_0 U_0 (e' + p')u' - \frac{T_0}{L_1}\left(\kappa + \frac{\lambda C_P \mu g_c}{P_{R_T}}\right)\frac{\partial \theta}{\partial \xi}\right.$$

$$\left. - \frac{\mu_0 U_0^2}{L_2}(u'\Omega_{xx}' + v'\Omega_{xy}')\right]$$

$$- \frac{L_1}{\rho_0 R T_0 U_0 L_2}\frac{\partial}{\partial \eta}\left[\rho_0 R T_0 U_0 (e' + p')v' - \frac{T_0}{L_2}\left(\kappa + \frac{\lambda C_P \mu g_c}{P_{R_T}}\right)\frac{\partial \theta}{\partial \eta}\right.$$

$$\left. - \frac{\mu_0 U_0^2}{L_2}(u'\Omega_{yx}' + v'\Omega_{yy}')\right]$$

$$e' = \frac{C_V}{R}p' + \frac{1}{2\rho_0 R T_0}\left[\frac{\rho_0 U_0^2}{g_c}(a'u' + b'v')\right.$$

$$\left. - \frac{\lambda \mu U_0}{g_c}\left(\frac{1}{c'k^2}\frac{\partial u'}{\partial \xi} - \frac{1}{c'}\frac{L_1}{L_2}\frac{\partial v'}{\partial \eta}\right)\right] \quad .$$

This can be simplified some by recognition of and substitution for several standard groupings:

The Reynolds number,

$$N_R = \frac{\rho_0 U_0 L_2}{g_c \mu_0} \quad , \tag{D-7}$$

the Prandtl number,

$$P_R = \frac{g_c \mu C_P}{\kappa} \quad \text{and} \quad P_{R_0} = \frac{g_c \mu_0 C_{P0}}{\kappa_0} \quad , \tag{D-8}$$

and, interpreting the temperature scale T_0 as a representative absolute temperature, the Mach number,

$$M^2 = \frac{U_0^2}{C_0^2} = \frac{U_0^2}{\gamma g_c R T_0} \quad . \tag{D-9}$$

If the temperature scale T_0 were interpreted as a representative temperature difference, the Eckert number would result:

$$N_{EK} = \frac{U_0^2}{g_c C_{P_0} T_0} = \frac{U_0}{g_c R T_0}\left(\frac{\gamma - 1}{\gamma}\right). \tag{D-10}$$

It is convenient to define

$$\epsilon = \frac{L_1}{L_2} \quad . \tag{D-11}$$

Also

$$\frac{T_0}{L_2}\left(\kappa + \lambda \frac{g_c \mu C_P}{P_{R_T}}\right) = \frac{T_0}{L_2}\kappa\left(1 + \lambda \frac{P_R}{P_{R_T}}\right) \quad .$$

Combining this with (D-7, 8, 9, 11) and the basic equations just above yields the equation set below. The primes are dropped with the understanding that all symbols represent the dimensionless forms of the appropriate variables.

$$\frac{\partial \rho}{\partial t} = -\left(\frac{\partial a}{\partial \xi} + \epsilon \frac{\partial b}{\partial \eta}\right) \tag{D-12}$$

$$\frac{\partial a}{\partial t} = -\frac{\partial}{\partial \xi}\left[au + \frac{p}{\gamma M^2} - \frac{\Omega_{xx}}{N_R}\right] - \epsilon \frac{\partial}{\partial \eta}\left[bu - \frac{\Omega_{xy}}{N_R}\right] \tag{D-13}$$

$$\frac{\partial b}{\partial t} = -\frac{\partial}{\partial \xi}\left[av - \frac{\Omega_{yx}}{N_R}\right] - \epsilon \frac{\partial}{\partial \eta}\left[bv + \frac{p}{\gamma M^2} - \frac{\Omega_{yy}}{N_R}\right] \tag{D-14}$$

$$\frac{\partial e}{\partial t} = -\frac{\partial}{\partial \xi}\left[(e + p)u - \left(\frac{\gamma}{\gamma - 1}\right)\frac{\kappa}{\epsilon N_R P_{R_0}}\left(1 + \lambda \frac{P_R}{P_{R_T}}\right)\frac{\partial \theta}{\partial \xi}\right.$$

$$\left. - \frac{\gamma M^2}{N_R}(u\Omega_{xx} + v\Omega_{xy})\right]$$

$$- \epsilon \frac{\partial}{\partial \eta}\left[(e + p)v - \left(\frac{\gamma}{\gamma - 1}\right)\frac{\kappa}{N_R P_{R_0}}\left(1 + \lambda \frac{P_R}{P_{R_T}}\right)\frac{\partial \theta}{\partial \eta}\right.$$

$$- \frac{\gamma M^2}{N_R} (u\Omega_{yx} + v\Omega_{yy}) \Bigg] \qquad \text{(D-15)}$$

$$e = \frac{C_V}{R} p + \frac{\gamma M^2}{2} \left[au + bv - \frac{\lambda\mu}{\epsilon N_R} \left(\frac{1}{c'k^2} \frac{\partial u}{\partial \xi} - \frac{\epsilon}{c'} \frac{\partial v}{\partial \eta} \right) \right] . \qquad \text{(D-16)}$$

The ideal gas law (B-16) becomes

$$\frac{p}{\rho\theta} = 1 . \qquad \text{(D-17)}$$

Finally, (D-3) becomes

$$\overline{\overline{\Omega}} = \mu \begin{bmatrix} \frac{\lambda}{c'k\epsilon} \frac{\partial u}{\partial \xi} & (1 + \lambda) \frac{\partial u}{\partial \eta} \\ \left(1 - \frac{\lambda}{k^2}\right) \frac{1}{\epsilon} \frac{\partial v}{\partial \xi} + \frac{\partial u}{\partial \eta} & \left(\frac{4}{3} - \frac{\lambda}{c'}\right) \frac{\partial v}{\partial \eta} \end{bmatrix} . \qquad \text{(D-18)}$$

It should be noted once again that all the variables in equations (D-12) — (D-16) are dimensionless and that the primes have been dropped.

APPENDIX E

COORDINATE TRANSFORMATION FROM A NON-RECTANGULAR PHYSICAL REGION INTO A RECTANGULAR REGION

In this appendix the coordinate transformations necessary to locate most of the nodes used in the difference net within the physical region of interest is specified.

The equations (D-12) through (D-18) and (C-12) are expressed in terms of the independent variables ξ and η (and t, which will not be involved in the present transformations). A transformation which will expand a region shaped roughly like that sketched in figure 13 into a rectangular region is

$$s(\xi,\eta) = \xi, \; Z(\xi,\eta) = \frac{\eta}{q(\xi)} \; . \qquad \text{(E-1)}$$

The function $q(\xi)$ specifies the shape of the "edge" of the boundary region as indicated in the figure. It is assumed to be real, continuous, positive, finite and differentiable on the range

$$0 \leq \xi \leq 1 \; .$$

The purpose of this appendix, expressed mathematically, is to develop expressions for

$$\frac{\partial \Phi}{\partial \xi} \text{ and } \frac{\partial \Phi}{\partial \eta}$$

in terms of the new independent variables s and Z. In these and the following expressions, Φ is to represent an arbitrary dependent variable, a function of ξ and η.

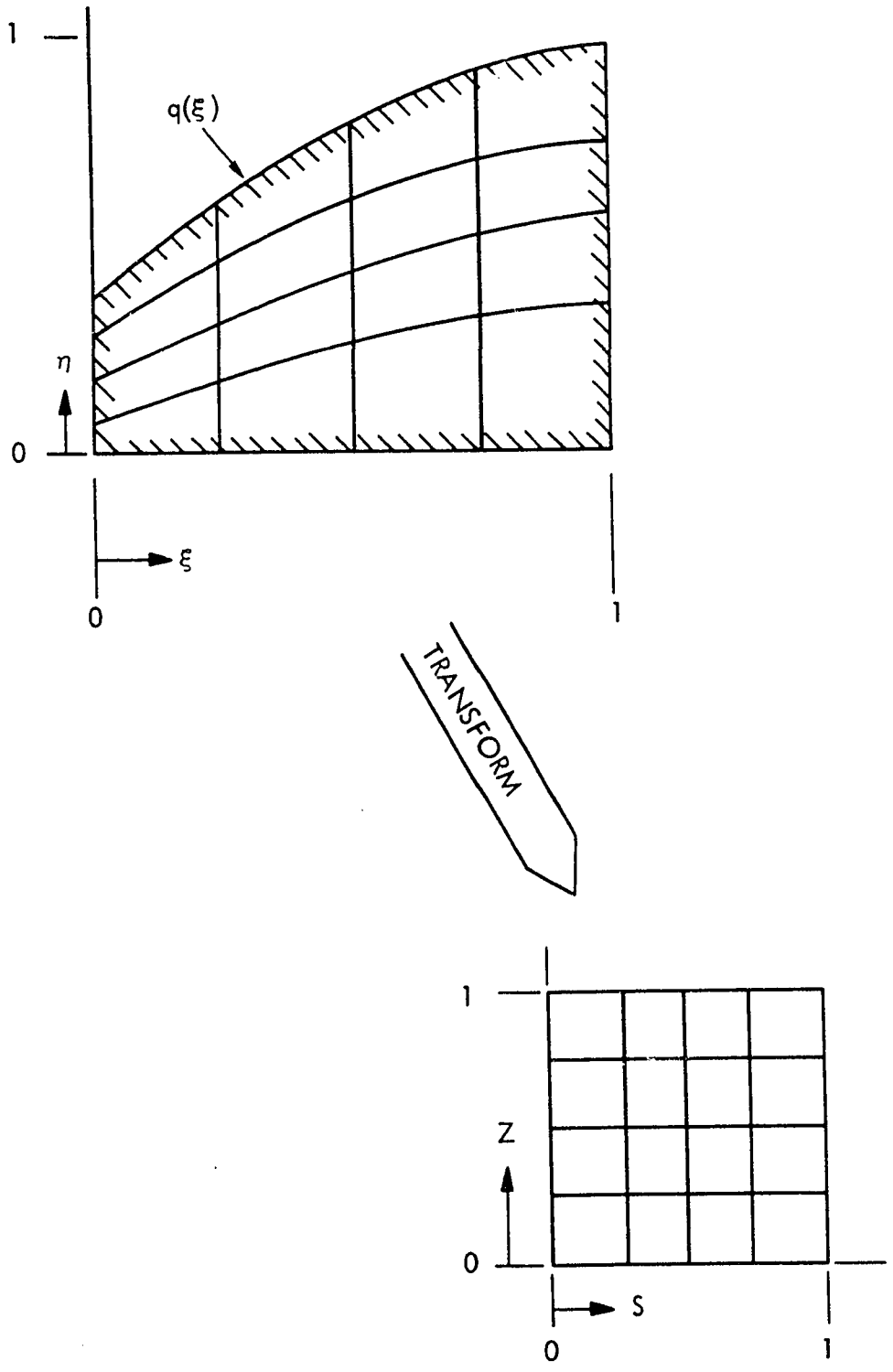

Figure 13

MAPPING OF PHYSICAL REGION INTO
A RECTANGULAR REGION

The expression for the differential of Φ is:

$$d\Phi = \frac{\partial \Phi}{\partial s} ds + \frac{\partial \Phi}{\partial Z} dZ \quad .$$

From this,

$$\left.\frac{d\Phi}{d\xi}\right|_{\eta} = \left.\frac{\partial \Phi}{\partial s} \frac{ds}{d\xi}\right|_{\eta} + \left.\frac{\partial \Phi}{\partial Z} \frac{dZ}{d\xi}\right|_{\eta} \quad .$$

Similarly,

$$\left.\frac{d\Phi}{d\eta}\right|_{\xi} = \left.\frac{\partial \Phi}{\partial s} \frac{ds}{d\eta}\right|_{\xi} + \left.\frac{\partial \Phi}{\partial Z} \frac{dZ}{d\eta}\right|_{\xi} \quad .$$

Forming the indicated partial derivatives from (E-1) gives:

$$\left.\frac{ds}{d\xi}\right|_{\eta} = 1, \left.\frac{dZ}{d\xi}\right|_{\eta} = \frac{\eta}{q^2} \frac{\partial q}{\partial \xi} = - \frac{Z}{q} \frac{\partial q}{\partial \xi} \quad ,$$

$$\left.\frac{ds}{d\eta}\right|_{\xi} = 0 \quad \text{and} \quad \left.\frac{dZ}{d\eta}\right|_{\xi} = \frac{1}{q} \quad .$$

Defining

$$\beta \equiv - \frac{Z}{q} \frac{\partial q}{\partial \xi} \quad ,$$

the transformations become

$$\frac{\partial \Phi}{\partial \xi} = \frac{\partial \Phi}{\partial s} + \beta \frac{\partial \Phi}{\partial Z}$$

and (E-2)

$$\frac{\partial \Phi}{\partial \eta} = \frac{1}{q} \frac{\partial \Phi}{\partial Z} \quad .$$

The factor $\frac{\partial q}{\partial \xi}$ can be expressed alternately as

$$\frac{\partial q}{\partial \xi} = \frac{\partial q}{\partial s} + \beta \frac{\partial q}{\partial Z} = \frac{\partial q}{\partial s} \quad ,$$

since q is not a function of Z. The operators (E-2) are to be applied whenever the partial derivatives

$$\frac{\partial \Phi}{\partial \xi} \quad \text{and} \quad \frac{\partial \Phi}{\partial \eta}$$

are encountered in evaluating equations or boundary conditions. The finite difference approximations introduced in chapter IV are expressed in terms of differences in the dependent coordinates s and Z.

APPENDIX F

ANALYSIS OF NUMERICAL STABILITY

In this appendix, an analysis of the numerical stability of the system of difference analogs for the equations (D-12) — (D-15) is presented. The approach used is due to von Neumann [41].

Two simplifying assumptions are introduced at the outset. First, only a uniform grid spacing ($\delta_1 = \delta_2$ in equation (IV-1)) is analyzed. Second, the representative equation has been analyzed considering the effect of only two independent variables, either the pair x,t or the pair y,t. The conclusions can then be applied separately to the x and y dimensions. This procedure is justified by the convenience of relatively concise results and the sweeping nature of other necessary assumptions.

Each of the partial differential equations (not difference equations) takes the form

$$\frac{\partial f}{\partial t} = \frac{\partial F}{\partial x} + \frac{\partial G}{\partial y} , \qquad \text{(F-1)}$$

where F and G are complicated functions which incorporate coupling and non-linear terms. In the following development, the equation

$$\frac{\partial f}{\partial t} = \frac{\partial G}{\partial y} \qquad \text{(F-2)}$$

will be treated.

The function G has the general form

$$G = fg + B\frac{\partial f}{\partial y} + D\frac{\partial g}{\partial y} + \ldots ,$$

where g represents dependent variables determined from the other basic equations. Then the right-hand side of equation (F-2) can be expanded into equation (F-3) (see (D-12) — (D-15) to identify the coefficients A, B, C, D):

$$\frac{\partial G}{\partial y} = A\frac{\partial f}{\partial y} + B\frac{\partial^2 f}{\partial y^2} + C\frac{\partial g}{\partial y} + D\frac{\partial^2 g}{\partial y^2} + \ldots \qquad \text{(F-3)}$$

The coefficients A, B, C, D, . . . will themselves be functions of both dependent and independent variables and contribute to the non-linearity and the coupling between equations. At this point, these coefficients are assumed to be "locally constant"; that is, their functional dependence will be ignored so that (F-3) can be termed a "locally linear" equation.

Each dependent variable is separated into a "smooth solution" and a perturbation:

$$f = \bar{f} + f',\ g = \bar{g} + g',\ \text{etc.} \qquad \text{(F-4)}$$

Combining (F-2) — (F-4) and reorganizing yields

$$\frac{\partial \bar{f}}{\partial t} + \frac{\partial f'}{\partial t} = A\frac{\partial \bar{f}}{\partial y} + B\frac{\partial^2 \bar{f}}{\partial y^2} + C\frac{\partial \bar{g}}{\partial y} + D\frac{\partial^2 \bar{g}}{\partial y^2} + \ldots$$

$$+ A\frac{\partial f'}{\partial y} + B\frac{\partial^2 f'}{\partial y^2} + C\frac{\partial g'}{\partial y} + D\frac{\partial^2 g'}{\partial y^2} + \ldots .$$

The terms containing the "smooth solutions" ($\bar{f}$, $\bar{g}$) can be eliminated as a valid solution for (F-2). The equation remaining describes the development of the perturbation f':

$$\frac{\partial f'}{\partial t} = A\frac{\partial f'}{\partial y} + B\frac{\partial^2 f'}{\partial y^2} + C\frac{\partial g'}{\partial y} + D\frac{\partial^2 g'}{\partial y^2} + \ldots . \qquad \text{(F-5)}$$

In writing the difference analog for this equation, the following notational shorthand is useful (the equation is written for the node at $y = y_0$, the time plane t_1 is "known" and the time plane t_2 is unknown):

$$f'(t_1,y_0) = f'_{10} \ , \quad f'(t_1 + \Delta t, y_0 + \delta) = f'_{2_p} \ ,$$

$$f'(t_1 + \Delta t, y_0 - \delta) = f'_{2_m} \ , \quad f'(t_1 + \Delta t, y_0) = f'_{20} \ ,$$

with similar expressions for g'. Then the implicit difference analog for (F-5) becomes

$$f'_{20} - f'_{10} = \frac{\Delta t}{2\Delta y}\left[A(f'_{2_p} - f'_{2_m}) + C(g'_{2_p} - g'_{2_m})\right]$$

$$+ \frac{\Delta t}{(\Delta y)^2}\left[B(f'_{2_p} - 2f'_{20} + f'_{2_m}) + D(g'_{2_p} - 2g'_{20} + g'_{2_m})\right]$$

$$+ \ . \ . \ . \ . \qquad \text{(F-6)}$$

The particular solution assumed for f' (and g', etc.) is a periodic function in y with an exponential factor which may grow or decay with time:

$$f'(t_2,y_0 + \delta) = f_{10}\, e^{\alpha t_2}\, e^{\bar{i}k\delta} \ . \qquad \text{(F-7)}$$

The constant k is some real number associated with the wave length of the particular disturbance under study; the constant α may be complex. With the convenient substitutions

$$\xi = e^{\alpha t2} \text{ and } \Phi = e^{\bar{i}k\delta} \ ,$$

$$f'_{20} = f_{10}\xi, \ f'_{2_p} = f_{10}\xi\Phi, \ f'_{2_m} = f_{10}\xi/\Phi \ ,$$

$$g'_{20} = g_{10}\xi, \ g'_{2_p} = g_{10}\xi\Phi, \ g'_{2_m} = g_{10}\xi/\Phi \ .$$

When these are substituted into (F-6), the resulting equation is:

$$f_{10}(\xi - 1) = \frac{\xi\Delta t}{2\Delta y}(Af_{10} + Cg_{10})(\Phi - \frac{1}{\Phi})$$

$$+ \frac{\xi\Delta t}{(\Delta y)^2}(Bf'_{10} + Dg_{10})(\Phi - 2 + \frac{1}{\Phi}) \ ,$$

or

$$\frac{1}{\xi} = 1 - M(\Phi - 2 + \frac{1}{\Phi}) - N(\Phi - \frac{1}{\Phi}) \quad . \tag{F-8}$$

The constants M and N are

$$M = \frac{\Delta t}{(\Delta y)^2} B + D \frac{g_{10}}{f_{10}}$$

and

$$N = \frac{\Delta t}{2\Delta y} A + C \frac{g_{10}}{f_{10}} \quad .$$

From (F-7), the value of f_0' will decrease as t increases if

$$|e^{\alpha t_2}| = |\xi| < 1 \quad .$$

That is, the perturbation will be damped and the difference scheme will be stable if

$$|\xi| < 1 \quad \text{or} \quad \left|\frac{1}{\xi}\right| > 1 \quad .$$

The absolute value of (F-8) can be determined, noting that

$$\text{Im}\,(\Phi - 2 + \frac{1}{\Phi}) = 0$$

$$\text{Re}\,(\Phi - \frac{1}{\Phi}) = 0$$

$$\text{Re}\,(\Phi - 2 + \frac{1}{\Phi}) = 2\,(\cos k\,\delta - 1)$$

$$\text{Im}\,(\Phi - \frac{1}{\Phi}) = 2 \sin k\,\delta \quad .$$

Defining

$$\theta = k\,\delta \quad \text{and} \quad \mu = \cos\theta \quad ,$$

$$\left|\frac{1}{\xi}\right|^2 = [1 - 2M(\cos\theta - 1)]^2 + 4N^2 \sin^2\theta \quad ,$$

or

$$\left|\frac{1}{\xi}\right|^2 = [1 - 2M(\mu - 1)]^2 + 4N^2(1 - \mu^2) \quad . \tag{F-9}$$

Since a difference scheme should be stable with respect to a disturbance of any wave length, the stability requirement must hold for the entire range

$$-1 \leq \mu \leq 1 \quad .$$

Some manipulation of (F-9) gives

$$\left|\frac{1}{\xi}\right|^2 - 1 = -2M(\mu - 1) + 4[M^2(\mu - 1)^2 + N^2(1 - \mu^2)] \quad .$$

The term on the right is positive or zero for all values of M and N for $|\mu| \leq 1$. Therefore, if the term

$$-2M(\mu - 1) \geq 0 \quad ,$$

stability is assured. For

$$|\mu| \leq 1 \quad , \quad M > 0$$

is sufficient to make that term positive. Thus, under the assumptions listed,

$$M \equiv \frac{\Delta t}{(\Delta y)^2} B + D \frac{g_{10}}{f_{10}} \geq 0 \tag{F-10}$$

insures numerical stability. The specific stability requirements listed in chapter III are derived from the condition (F-10).

If the difference equation (F-6) is written in explicit form and the above manipulations repeated, the equation equivalent to (F-9) is

$$|\xi|^2 = [1 + 2M(\mu - 1)]^2 + 4N^2(1 - \mu^2) \quad .$$

This can further be rearranged to the form

$$|\xi|^2 - 1 = 4(\mu - 1)\,[M - M^2(1 - \mu) - N^2(1 + \mu)] \quad .$$

In this case, the stability condition is

$$|\xi|^2 < 1 \quad ,$$

or that the right-hand side of the above equation be negative for all $|\mu| \leq 1$. Since

$$\mu - 1 \leq 0 \quad \text{for} \quad |\mu| \leq 1 \quad ,$$

this requirement becomes

$$M > M^2(1 - \mu) + N^2(1 + \mu) \quad .$$

Incorporating the definitions of M and N and dropping the subscripts, a maximum permissible time step is determined,

$$\Delta t_{max} = \frac{(B + D\, g/f)}{\left(\frac{B + D\, g/f}{\Delta y}\right)^2 (1 - \mu) + \left(\frac{A + C\, g/f}{2}\right)^2 (1 + \mu)} \quad . \qquad \text{(F-11)}$$

Equation (F-11) is a "local" stability limitation on the size of the time step Δt; that is, each node has a separate stability criterion (as does each equation at each node). Since the calculation technique requires the field to be advanced through a uniform Δt at every node, the minimum value of Δt_{max} for the entire field (every equation at every node) is the largest acceptable value that can be used in calculations.

The explicit difference scheme can be eliminated from consideration rather quickly, since

$$B = D \equiv 0$$

for the mass conservation equation (D-12). Thus

$$\Delta t_{max} \equiv 0$$

for that equation and there is <u>no</u> range of stability for the explicit difference representation of the mass conservation equation. In the

parallel case for an implicit difference form, equation (F-10) gives

$$M = 0$$

for

$$B = D \equiv 0 \quad .$$

This is a case of "neutral" stability. The numerical evidence is that this equation will remain stable, perhaps due to the influence of coupling with the other, more stable, equations.

The condition (F-10) does not depend on the value of the coefficients A and C. This is a result of the assumption made above to consider the independent variables in pairs, t and x or t and y.